ANALYTICAL AND STATISTICAL ANALYSIS OF WAVE-CYLINDER INTERACTIONS

A Dissertation

by

JIANGNAN LU

Submitted to the Office of Graduate and Professional Studies of
Texas A&M University
in partial fulfillment of the requirements for the degree of

DOCTOR OF PHILOSOPHY

Chair of Committee,	John M. Niedzwecki
Committee Members,	Hamn-Ching Chen H. Joseph Newton Luciana Barroso
Head of Department,	Sharath Girimaji

December 2020

Major Subject: Ocean Engineering

ABSTRACT

Arrays of closely spaced slender cylindrical-shaped structural elements such as marine risers, TLP tendons, and horizontal pipelines are widely used in many offshore applications. Their response behavior subjected to random waves and current loadings is very complicated and remains an important area for further research. The goal of this research study is two-fold. First it seeks to investigate the possibility of using analytical models as a simple design approach to bound drag force coefficients referred to in design practice, and secondly it pursues a general extremal statistical methodology for the analysis and characterization of industrial-scale model basin test data and field measurements.

Initially, this research investigated the Huse-Muren wake flow model that addressed the interaction of a slender vertical cylinder subject to a harmonically oscillatory flow in the drag-dominated force regime. Analysis of their model led to the formulation of a dimensionless drag coefficient correction ratio. Unfortunately, investigation based on published guidelines and measured data indicated that their model seemed to bound the data for a limited range of applications. For the crossflow formulation, new dimensionless parameters were formulated to better illustrate the impact of the transverse current on the drag coefficient correction ratio. A numerical simulation was subsequently performed, and the results were presented and discussed.

In the second phase of the research, a statistical methodology was formulated based on the generalized extreme value family of distributions for the characterization of in-line interactions of closely spaced two- and three- deep-water cylinder arrays. The most appropriate block size and the corresponding statistical models were selected by an iterative process that utilized Anderson-Darling test criterion, quantile plots, and histograms. The models were found to fit the data excellently, and the roles of spacings and top tensions on the risk of collision were characterized. An unexpected phenomenon in the observed data was successfully identified.

Finally, the flow-induced vibration response behavior of a flexible horizontal cylinder subject to both random waves and constant current conditions was investigated. The measured mid-span displacement was initially analyzed using standard spectral analyses to relate the cylinder's response behavior to traditional deterministic parameters, whose values illustrated significant scatter. Further analyses were performed using the general statistical methodology, which was observed to provide good to excellent results for the random wave cases and at least moderately good results for the combined random wave and constant current cases.

DEDICATION

This dissertation is dedicated to:

My mother and my father, Chao Xiang and Kewu Lu,

for all their caring, love, and support in my life.

And to my teachers and professors at

Texas A&M University, U.S.A.

ACKNOWLEDGEMENTS

I would like to thank my academic advisor and my committee chair, Dr. John M. Niedzwecki during my doctoral endeavors at Texas A&M University at College Station. I am grateful for his insightful guidance on developing ideas in a logical manner and practicing critical thinking in my research, for his encouragement when I met setbacks, and for his patience and advice on improving my communication and writing skills to become a good researcher. I would also like to thank my advisory committee members Dr. H. Joseph Newton, Dr. Hamn-Ching Chen and Dr. Luciana Barroso for their input and guidance throughout the course of this study. I would also like to extend my gratitude to Dr. Michael Longnecker and Dr. Edward Jones for the coursework I learned from them on statistical methods and data analysis methodologies.

I gratefully acknowledge the financial support for my doctoral research by the Cain Senior Chair endowment for Offshore Technology.

I would also like to thank my friends at Texas A&M University. I enjoyed discussing my research topic with Dr. Maopeng Fang, Dr. Yanbin Bai, Dr. Shanran Tang, Dr. Hao Wang, Dr. Yujie Liu, Dr. Yuanzhe Zhi, Dr. Shu Dai, Mr. Yicong Cai, Mr. Tiancong Hou, Mr. Han Huang, Mr. Yu Wang, Mr. Haoyuan Gu, Mr. Maokun Ye, Mr. Haoran Ma, and Mrs. He Jin.

Finally, I am deeply grateful to my mother and father for their financial support, encouragement, patience and love over the years.

TABLE OF CONTENTS

LIST OF FIGURES

LIST OF TABLES

Page

1 . INTRODUCTION

1.1. Research Background

Arrays of closely spaced slender cylindrical-shaped structural elements such as marine risers, TLP tendons, and horizontal pipelines can be found in many offshore applications. These structures are often exposed to random waves and current loadings and it is a challenge for engineering designs to accurately estimate this complicated fluid-cylinder interactive response behavior. Traditionally, the wave force on a slender cylinder is estimated using various forms of the Morison's equation where the empirical values of force transfer coefficients depend on the particular application. This approach requires that the wavelength be at least five times larger than the cylinder diameter so the cylinder can be assumed to be "transparent" to the incident flow field. This traditional approach is widely used in the offshore industry due to its simplicity in calculation. However, when the cylinder is subjected to an oscillatory flow, the wake velocity profiles generated in previous oscillation cycles could be carried to the upstream side of the cylinder as the flow reverse direction. Published API guidelines (1998) indicated that these reversed wake profiles could contaminate the flow incident on the cylinder. As a result, the drag coefficient in the Morison's equation needs to be corrected. Based on Schlichting's (1979) studies on the two-dimensional wake flow problem Huse and Muren (1987) derived the analytical expression of the modified drag coefficient that accounted for the wake effects and they found good agreement with the available data in the open literature (Sarpkaya, 1976, Bushnell, 1977). Their research findings could potentially provide insight to the more complicated cylinder clashing phenomena.

The fluid-cylinder interactive response behavior becomes more complex when the vertical cylinders are densely spaced in an array. Huse (1993) and Blevins (2005) developed numerous analytical models to investigate the influence of wake effects on the interaction of cylinder arrays placed in-line with a steady current. Instead of modeling the whole cylinder array, they focused their attention on the interaction of two cylinders placed in tandem and it was reported from calculation experience that collision in a riser array usually first occurs between the two most upstream elements (Huse, 1993). They compared their models to some of the experimental data published in the open literature and found good agreement in certain ranges of the parameters. However, these analytical formulations did not address the much more complicated phenomena of cylinder array's response behavior when subjected to random waves.

Duggal and Niedzwecki (1992, 1994) took an alternative statistical approach to investigate the interaction of a pair of closely spaced long flexible risers subjected to JONSWAP random waves in a model basin test program. They assumed that the measured time series of the relative displacement between the two risers is a stationary random process and they treated the occurrence of collision as a "barrier-crossing" event. To assess the cylinders' collision probabilities, they formulated a probabilistic model based on Hermite transformation techniques (Winterstein, 1988) to interpret the measured data and they observed good agreement between the model and the measurements. However, they also noted deviances in the upper tail of the probability distributions that is related to the extreme statistical events such as cylinder collisions. Leira et al. (2001, 2002) also incorporated probabilistic methodologies into their CFD and FEM simulations on the collision between two risers subjected to a steady current and floater motions. They did not assess the probability of collisions, but they reported the predicted distribution of the impact stress, the accumulated damage, and the result of reliability analysis, which was found to be consistent with the experimental data published by Herfjord and Bryndum (2001). More recently, Ping Fu et al. (2017) utilized a probabilistic approach in their numerical time domain simulations to investigate the wake-induced collision between two flexible risers in tandem when subject to a current. They utilized Blevins' wake model (2005) to calculate the hydrodynamic drag coefficient of each segment along the downstream riser in their Riflex (Fylling et al., 1995) FEM simulations. The minimum distance between the two risers was fitted by the Gumbel distribution. When this distance decreases below a defined threshold value, a collision occurrence would be recorded. They observed that their model showed an excellent agreement with the results produced by Riflex.

Another phenomenon of significant interest to both academic researches and engineering designs is the flow-induced vibrations of slender horizontal pipelines. To investigate the response behavior of the cylindrical structures under this scenario, traditional research efforts were mostly spent on utilizing a set of deterministic parameters to describe the vibration behavior of the cylinder. Griffin et al. (1975) were the first to introduce a mass-damping parameter to predict the maximum response amplitude of flexible structures and cables in water, but this parameter was found to have limited applicability as reported by Sarpkaya (1979, 2004) and Zdravkovich (1990). Sometime later, Vandiver (1993) identified the important dimensionless parameters for the prediction of vortex-induced vibrations (VIV) of long flexible cylinders based on a series of field experiments, and he (2012) formulated a revised damping parameter to describe the observed response behavior. More recently, Klamo et al. (2005) reported the correlation between the Reynolds number and the cylinder's VIV peak response amplitude, but Resvanis and Vandiver et al. (2012) also observed significant scatter between the predicted trends and the measured data (Klamo (2005), Govardhan and Williamson (2006), and Shell's model basin test program (2011).). However, few of these deterministic parameters were able to capture the essential characteristics of the variability in the observed flexible cylinder's VIV response behavior. Unfortunately, few relevant studies could be found in the open literature that have addressed the stochastic nature of cylinder's VIV response while most of the current popular VIV prediction programs in the industry were deterministic (Resvanis and Vandiver, 2017). To investigate the statistical characteristics of the observed VIV data, Resvanis and Vandiver (2017) introduced a short duration moving window to the observed time series and they were able to describe the data in terms of the mean and standard deviation of the RMS response amplitude within each window. Based on their observations, they (2017) called for more research effort to investigate the stochastic characteristics of the flexible cylinder's VIV response behavior .

1.2. Overview of the Research Study

The purpose of this research study is to investigate analytical and statistical approaches to bound and characterize the interactive wave-cylinder response behavior. As presented in chapter 2, the research initially started with the examination of the assumptions and approximations in Huse and Muren's analytical wake flow model (1987) that addressed the interaction of a slender cylinder and a harmonically oscillatory flow in the drag-dominated force regime. Based on a better understanding of Huse and Muren's mathematical formulations, further research was performed to investigate the wake flow model's ability to provide upper and lower bounds on the dimensionless drag coefficient correction ratio for Sarpkaya's U-tube experimental data considering DNV practice guidelines. For the crossflow formulation when a steady current coming from the transverse direction was superposed to the in-line oscillatory flow, a family of design curves on the drag coefficient correction ratio was also formulated by introducing Blevin's analytical formulations (1977) but future experimental data is required for validation. The focus of the analytical investigation is to determine the parameter ranges within which this wake flow model could be reasonably used as a simple design approach that is easy to apply.

However, it was observed in chapter 2 that the wake flow models developed by Huse and Muren appeared to have limited range of applications for a single cylinder subject to an in-line harmonically oscillatory flow. Unfortunately, no measured data was found available in the open literature for validation of Huse and Muren's model in the crossflow formulation with an additional transverse steady current. Thus, it is perhaps beyond the ability of direct analytical formulations to capture the more complicated interactive response behavior of closely spaced cylinder arrays in random waves. Based upon examination of relevant previous studies (Duggal, 1992, Leira et al., 2001), it was anticipated that a statistical approach will be more suitable.

In chapter 3, the focus of the research was shifted to investigate the ability of extremal statistical models to capture important phenomena observed in industrial scale Offshore Technology Research Center (OTRC) model basin experimental data (Rijken and Niezwecki, 1998). A general statistical methodology was formulated for the characterization of recorded time series of in-line interactive response behavior of closely spaced deep-water cylinder array in random waves. The initial processing of the time series data involved the sequencing of block maxima that represented the maximum observed values of the target variable within a specified duration. This sequenced data was then fitted using the generalized extreme value (GEV) family of distributions. An iterative process was utilized to determine the most appropriate block size and the corresponding statistical models by assessing their performance in fitting the data using the Ander-Darling (AD) test criterion (Anderson and Darling, 1954) concurrently with quantile plots and histograms, where special attention was paid to the quality of the fit in the upper tail of the distribution. The selected models were found to provide an excellent fit to the data, and they could be used to predict the probabilities of collisions between adjacent cylinders. The predicted threshold-crossing probabilities for the in-line relative displacement between adjacent cylinders were found useful to characterize cylinder array configurations and top tensions, and their roles related to the risk of cylinder collisions. A noteworthy finding of the predicted results is that they successfully captured the unexpected phenomenon in the observed data. Based on these observations, it was inferred that this general statistical methodology might also prove useful for other offshore applications. Thus, in the following chapter, the applicability of the methodology was further examined under an entirely different application scenario for the flow-induced vibrations of a flexible horizontal cylinder subject to both random waves and strong current loadings.

In chapter 4, it was investigated if the general methodology could also capture the statistical characteristics of the extreme values in the flexible horizontal cylinder's flow-induced response amplitudes in-line with the flow direction. The experimental data was obtained in another OTRC model basin test program (Chitwood, 1998) and the test cylinder was also of industrial scale. In this experiment the horizontal cylinder model was pretensioned on both ends and was tested under a combination of random waves and strong constant currents. Initially, spectral analysis was performed to examine the measured cylinder's mid-span displacement and relate the observed results to traditional deterministic parameters. Then, the general statistical methodology was utilized to investigate the statistical characteristics of the measured data. The statistical models corresponding to the selected optimal block sizes were found to provide a good to excellent fit when the cylinder was only subject to random waves, and they could also provide an at least moderately good even with a strong current superposed to the random waves. The predicted probabilities could be used to characterize the variance in the observed horizontal cylinder's flow-induced vibration response behavior, which is stochastic in nature and merits further investigation as addressed by Resvanis and Vandier (2017).

In chapter 5, the results of this research investigation were summarized and perspectives on future research studies were discussed. Appendix A presents the detailed derivation of the mathematical expressions of the wake velocities in various wake flow models. Appendix B provides the formula of the Weibull, Fréchet, and Gumbel distributions that could be represented by the generalized extreme value (GEV) distribution.

2 . WAKE INTERACTION WITH VERTICAL CYLINDERS

There are many offshore applications that incorporate vertical cylindrical-shaped structural elements such as marine risers, TLP tendons and near shore pier designs. A better understanding of complex wake flows on the drag dominated force predictions is very much of interest for offshore design problems. This chapter investigates the Huse-Muren analytical wake model, whose mathematical formulation was founded on the earlier definitive studies of Prandtl and Schlichting. Developing a deeper understanding of their key findings that were based upon central assumptions and key approximations is central to the research of this chapter. Analysis of their model leads to the development of dimensionless expressions for the drag coefficient correction ratio. Both the DNV-RP recommended drag force coefficients and some of Sarpkaya's U-tube measurements are used to investigate whether their analytical model could be used to bound the experimental data. The Keulegan-Carpenter number, A_0/D ratios, Sarpkaya's Beta parameter and Reynold's number are used to interpret the range of model applicability. For the current cross flow case, variables identified in Huse and Muren's formulation lead to a dimensionless expression involving the period of in-line oscillation and the velocity of the cross-current resulting in a parameter similar to the Keulegan-Carpenter number. The ratio of this parameter to the Keulegan-Carpenter number allows one to address the drag coefficient correction ratio where a cylinder is simultaneously subjected to in-line oscillatory flow and a steady cross current coming from the transverse direction. A numerical simulation is also performed to investigate the behavior of the correction ratio in this flow condition, and the results are presented and discussed.

2.1 Background

The use of slender cylindrical structural elements can be observed in both coastal and deepwater offshore structural designs. The hydrodynamic forces acting on these various structures and their components remain the subject of numerous research studies (Huse & Muren, 1987, Huse, 1993, Duggal & Niedzwecki, 1994 and Fu et al., 2017) reported in the open literature. To improve the modeling of complex fluid-structure interactions research attention in some studies (Huse & Muren, 1987 and Huse, 1993) has turned to earlier seminal fluid mechanic research results for inspiration, while others (Duggal & Niedzwecki, 1994 and Fu et al., 2017) have focused on statistical characterizations that address only the global phenomena and the observed response behaviors. The research of this chapter is performed to explore the opportunities whether the analytical wake flow models could capture enough the response behaviors of wave-cylinder interactions.

In 1935 Prandtl published his research on the motions of the fluid particles in a turbulent boundary layer on a flat plate. He first derived his initial mixing length theory using a classical fluid mechanic approach, and he later corrected his previous assumptions and formulated the turbulent shearing stress hypothesis based upon the experimental findings of Reichardt (1942). Sometime later, Schlichting (1979) studied the two-dimensional wake flow problem of a steady fluid flow past a vertical cylinder and solved for the downstream wake velocity using Prandtl's mixing length theory. Goertler and Reichardt solved the same problem with Prandtl's turbulent shearing stress hypothesis but they found that the difference between the two solutions was quite small.

Clusters of vertical risers and conductor pipes are widely used in offshore oil and gas production for both fixed and floating offshore platforms. When a cylinder is subjected to an oscillatory flow, the wake generated in previous oscillation cycles could be carried to the upstream side of the cylinder as the flow reverse direction. Published API guidelines (1998) indicated that these reversed wake profiles could contaminate the flow incident on the cylinder. To investigate this phenomenon, Huse and Muren (1987) developed a method based on Schlichting's studies to account the effect of the wake generated in the previous oscillations on the drag force for a single vertical cylinder, which potentially could provide insight into the clashing phenomena of closely spaced marine risers. They compared their model with data available in the open literature (Sarpkaya, 1976 and Bushnell, 1977) and found good agreement. Huse (1993) later noticed that the wake velocity predicted by their original model would falsely approach infinity very close to the cylinder, so he modified his model. An alternate approach to study the cylinder clashing was reported by Duggal and Niedzwecki (1994). They investigated the collision of a pair of closely spaced long flexible risers using a probabilistic approach to interpret model basin experimental data. The wake effects were not explicitly considered in their riser collision formulation but were implicit in the measured data. Fu et al. (2017) also proposed a probabilistic approach to estimate the collision probability between two flexible risers due to wake effects by a time domain simulation. The participating mass in colliding risers can be estimated by the method proposed by Sagatun et al. (1999), who formulated their models by combining experimental investigation, system control theory, and analytical derivations.

A related problem of significant interest to offshore engineers is pipelines laid on or in close proximity to the seafloor. Lambrakos (1987) investigated this problem and incorporated both the wake effects and the time dependence of force coefficients in his Wake Force Model, based on which he and Soedigdo (1997) later developed the Wake II Model by introducing an oscillatory-flow wake velocity correction. They found good agreements with measured data for a horizontal pipeline lying on the seafloor, but both two models contain several coefficients that need to be determined by experimental measurements. Consequently, their model predictions will be specific to each case investigated.

The focus of this chapter is to investigate and gain insight into an interesting analytical approach that could be used to estimate the influence of the wake effects on the drag coefficients with the potential to analytically bound experimental data. A detailed discussion of the mathematical formulations developed by Prandtl (1935), Schlichting (1979), and Huse and Muren (1987) is presented in order to better understand their underlying assumptions, approximations and sources of error. Several dimensionless ratios result that allow one to investigate the drag coefficient correction ratio and its application to provide upper and lower bounds using DNV-RP (2014) together with data from Sarpkaya's U-tube experiments (1976). The objective here is to gain a better understanding of the practical range where the analytical expressions can be used to estimate the drag coefficient amplification. For the case where a cylinder is also subjected to a steady cross current Blevins' model (1977) is used to study the behavior of the drag coefficient correction ratio predicted by Huse-Muren's crossflow formulation.

2.2 Mathematical Formulation

2.2.1 Classical fluid mechanics models

A schematic top view of a vertical flexible cylinder of diameter D, in a constant water depth h, subjected to a steady flow, and the idealized wake profile in the control volume (A, A_1, B_1, B) is depicted in Fig. 2.1. In Fig. 2.1, x is the distance in the flow direction and y is the distance transverse to the flow direction. It is assumed that the flow is two-dimensional, and the fluid is incompressible. The drag force per unit length F_D on the cylinder in the wake flow can be derived using the continuity equation and Euler's momentum law without using the traditional Morison equation, and can be expressed as

$$F_D = \rho \int_{-\infty}^{\infty} u\,(V - u)\,dy = \rho \int_{-\infty}^{\infty} u_1\,(V - u_1)\,dy \qquad (2.1)$$

where, ρ is the fluid mass density, V is the magnitude of the incoming free-stream flow velocity, u is the in-line fluid velocity behind the cylinder, and $u_1 = (V - u)$ is the wake velocity with respect to the seafloor. By assuming that the wake velocity u_1 is small, Schlichting (1979) obtained the following expression

$$F_D = \rho\, V \int_{-\infty}^{\infty} u_1\,dy \qquad (2.2)$$

Schlichting (1979) developed a solution of the governing Navier-Stokes equations by restricting his solution to regions far downstream of the cylinder ($x > 50\, C_{ds}\, D$)

where, C_{ds} is the drag coefficient in the stationary flow and D is the diameter of the cylinder. Consequently, the pressure contribution is negligible, and the governing equation can be expressed as

$$\frac{\partial u}{\partial t}+u\frac{\partial u}{\partial x}+\mathrm{v}\frac{\partial u}{\partial y}=\frac{1}{\rho}\frac{\partial \tau_t}{\partial y} \tag{2.3}$$

where, u and v are the in-line and transverse fluid velocity components, respectively, and τ_t is the turbulent shearing stress.

Schlichting next introduced Prandtl's mixing length assumption of the form

$$\tau_t=\rho\, l^2\left|\frac{\partial u}{\partial y}\right|\frac{\partial u}{\partial y} \tag{2.4}$$

where, τ_t is the turbulent shearing stress, and l is Prandtl's mixing length parameter. The resulting solution yields the following equation for the wake velocity

$$u_1=u_m\left[1-\left(\frac{y}{b}\right)^{\frac{3}{2}}\right]^2=u_m\left[1-\left(\frac{0.441y}{b_{1/2}}\right)^{\frac{3}{2}}\right]^2 \tag{2.5}$$

where,

$$b_{1/2}=\frac{1}{4}\sqrt{C_{ds}\,D\,x} \tag{2.6}$$

where, u_m is the maximum wake velocity, y is the transverse coordinate as illustrated in Fig. 2.1, $b=b(x)$ is the wake width and $b_{1/2}$ is the wake width where the local velocity is half the maximum wake velocity. Measurements reported by Schlichting and Reichardt suggest that $b_{1/2} = 0.441\, b$ is a better estimate for the actual location of this wake velocity as depicted in Fig. 2.1.

To solve the same problem raised by Schlichting, Reichardt and Goertler later utilized Prandtl's turbulent shearing stress hypothesis expressed as

$$\tau_t = \rho \ \kappa_1 \ \mathcal{B} \ (u_{max} - u_{min}) \ \frac{\partial u}{\partial y} \tag{2.7}$$

where, $\mathcal{B}$ is the width of the mixing zone, κ_1 is an experimentally-determined non-dimensional number which reflects the proportionality between the mixing length l and the width of the mixing zone $\mathcal{B}$, and u_{max} and u_{min} are the local mean of the maximum and minimum velocities, respectively. Then solving for the wake velocity based on Schlichting and Reichardt's experimental measurements yields the following equation

$$u_1 = \ u_m \ e^{-0.7014\left(\frac{y}{b_{1/2}}\right)^2} \tag{2.8}$$

2.2.2 Huse and Muren's wake flow model for a single vertical cylinder

In their analysis motivated by their interest in riser cluster collisions Huse and Muren (1987) began by considering the wake behavior with a single vertical cylinder in mind. They assumed that Schlichting's solution was also valid for a cylinder traveling at a constant speed in calm water and they took a simplified form of the solution based on Prandtl's mixing theories. In fact, their expression of the wake velocity was similar to Reichardt and Goertler's solution noted later in Table 2.1. Huse and Muren, considering the simplicity for their analytical formulations, made approximations on the classical solutions of the maximum wake velocity u_m shown in Table 2.1 and they obtained

$$u_m(x) \approx V \sqrt{\frac{C_{ds}\ D}{x}} \tag{2.9}$$

where, C_{ds} is the usual drag coefficient in the stationary flow based upon the magnitude of the incoming free-stream velocity V (or the magnitude of the cylinder's velocity in calm water), and the wake velocity has the form

$$u_1 = u_m\ (x)\ e^{-0.693\left(\frac{y}{b_{1/2}}\right)^2} \tag{2.10}$$

Huse (1993) observed that the above formula will approach infinity and produce a high, narrow peak very close to the cylinder where x is reduced to zero, which might cause error in the calculation of the forces on a second body in the wake. To correct this false peak, he modified the wake velocity as follows

$$u_1 = V \sqrt{\frac{C_{ds}\ D}{x_s}}\ e^{-0.693\left(\frac{y}{b_{1/2}}\right)^2} \tag{2.11}$$

where, x_s is defined as

$$x_s = x + \frac{4D}{C_{ds}} \tag{2.12}$$

Single cylinder subject to unidirectional oscillatory flow

Huse and Muren (1987) assumed that the flow condition of a stationary cylinder subjected to an oscillatory flow is similar to the case that a cylinder is oscillating in calm water. Their focus was to estimate the maximum drag force when the cylinder passes the midpoint of its in-line oscillatory path. Further, as illustrated in Fig. 2.2, they assumed that a wake velocity profile is created with alternating directions each time when the cylinder passes the midpoint at a time interval of one half the oscillation period. They also assumed that u_{mi}, the maximum wake velocity of the i^{th} profile, would decay by $1/\sqrt{i}$ at a fixed x coordinate as reflected in the following equation

$$u_{mi} = V \sqrt{\frac{C_{ds}\ D}{x}}\ \frac{1}{\sqrt{i}} \tag{2.13}$$

Fig. 2.2 also illustrates the summation of individual wake profiles. Huse and Muren only took the maximum wake velocity of each wake profile in the summation, which would yield a conservative estimate on the maximum drag force. They obtained the additional velocity contributions from the previous wake profiles at location x as follows

$$U_w = -\sum_{i=1}^{\infty} (-1)^i\, u_{mi} \tag{2.14}$$

where, U_w is the wake velocity correction affecting the cylinder. For a cylinder experiencing an in-line sinusoidal oscillatory motion of amplitude a_0 one can derive an expression for the maximum velocity. Huse and Muren (1987) indicated that the value of the in-line coordinate x was within the range of a_0 and πa_0, but they found it sufficient to set $x = 2a_0$ and they defined a Keulegan-Carpenter number as $N_{\mathrm{KC}} = 2\pi a_0/D$. An alternate interpretation is possible that considers $A_0 = 2a_0$ and then $N_{\mathrm{KC}} = \pi A_0/D$. It follows that

$$U_w = \left\{ -\sum_{i=1}^{\infty} (-1)^i \, \frac{1}{\sqrt{i}} \right\} \, V \sqrt{\frac{C_{ds}}{\left(\frac{x}{D}\right)}}$$

$$\approx \frac{1}{\sqrt{e}} \quad V \sqrt{\frac{C_{ds}\,\pi}{\left(\frac{2\pi a_0}{D}\right)}} \tag{2.15}$$

$$= V \sqrt{\frac{C_{ds}\,\pi}{e\,N_{KC}}} = V \sqrt{\frac{C_{ds}}{e\,\left(\frac{A_0}{D}\right)}}$$

where, e is the natural logarithm that has a value of $e \approx 2.7183$.

Introducing this expression to account for the wake velocity to the incident flow velocity, the "true" relative velocity V_r between the cylinder and the fluid can be expressed as

$$V_r = V + U_w = V \left(1 + \sqrt{\frac{\pi\, C_{ds}}{e\, N_{\mathrm{KC}}}} \right) = V \left(1 + \sqrt{\frac{C_{ds}}{e\,\left(\frac{A_0}{D}\right)}} \right) \tag{2.16}$$

Then substituting this expression for the relative velocity into the Morison equation and associating the correction with the standard drag coefficient in stationary flow one obtains

$$F_D = \frac{1}{2}\,\rho\, D\, C_{ds}\, V_r^2 = \frac{1}{2}\,\rho\, D\, C_{ds} \left(1 + \sqrt{\frac{\pi\, C_{ds}}{e\, N_{\mathrm{KC}}}} \right)^2 V^2 \tag{2.17}$$

where, F_D is the drag force per unit length on the cylinder. Huse and Muren (1987) introduced a modified drag coefficient C_{dd} to account for the wake effects based on the magnitude of the free-stream velocity V (or the magnitude of the oscillating cylinder's velocity in calm water). Thus, the above equation can also be expressed as

$$F_D = \frac{1}{2} \rho D C_{dd} V^2 \tag{2.18}$$

where, C_{dd} is the modified drag coefficient in the in-line oscillatory flow. Associating Eq. (2.20) with Eq. (2.21), one can obtain the expression

$$C_{dd} = C_{ds}\left(1 + \sqrt{\frac{\pi\ C_{ds}}{e\ N_{\mathrm{KC}}}}\right)^2 = C_{ds}\left(1 + \sqrt{\frac{C_{ds}}{e\left(\frac{A_0}{D}\right)}}\right)^2 \tag{2.19}$$

where, C_{dd} is the modified drag coefficient in the in-line oscillatory flow.

Given these analytical expressions it is possible for one to study the dimensionless drag coefficient correction ratio in relation to the Keulegan-Carpenter number or A_0/D, the ratio of the total amplitude of the in-line oscillation with respect to the cylinder diameter. More specifically, the correction ratio defined as a function of N_{KC} or A_0/D for a given value of C_{ds} forms the following equation

$$\frac{C_{dd}}{C_{ds}} = \left(1 + \sqrt{\frac{\pi\ C_{ds}}{e\ N_{\mathrm{KC}}}}\right)^2 = \left(1 + \sqrt{\frac{C_{ds}}{e\left(\frac{A_0}{D}\right)}}\right)^2 \tag{2.20}$$

In a similar approach, the drag coefficient correction ratio in Huse's modified wake flow model (1993) can be obtained as follows

$$\frac{C_{dd}}{C_{ds}} = \left(1 + \sqrt{\frac{C_{ds}}{e\left(\frac{A_0}{D} + \frac{4}{C_{ds}}\right)}} \right)^2 \tag{2.21}$$

Single cylinder subject to in-line oscillatory flow and steady cross current

The second practical flow situation analyzed by Huse and Muren (1987) was the case when the in-line oscillatory flow previously considered was subjected to an additional steady current approaching from the transverse direction. Their original illustration of the wake velocity profiles in this cross-flow formulation is reproduced in Fig. 2.3. They postulated that the wake profile generated in the previous i^{th} half-periods would be washed away in the direction of the steady current by a distance y normal to the oscillation direction

$$y = \frac{1}{2} V_C \; T \; i \tag{2.22}$$

where, V_C is the magnitude of the cross current velocity and T is the period of the in-line oscillation. Introducing the above equation into Eq. (2.11) and substituting $u_m(x)$ with u_{mi}, the maximum velocity of the i^{th} wake profile, one obtains

$$\begin{aligned} u_{1i} &= V \sqrt{\frac{C_{ds} \; D}{x}} \; \frac{1}{\sqrt{i}} \; e^{-0.693\left(\frac{\frac{1}{2} V_C \; T \; i}{b_{1/2}}\right)^2} \\ &= V \sqrt{\frac{\pi \; C_{ds}}{N_{KC}}} \; \frac{1}{\sqrt{i}} \; e^{-\frac{8.7085 \, N_{KC}}{C_{ds}} \left(\frac{N_{CF}}{N_{KC}}\right)^2 i^2} \end{aligned} \tag{2.23}$$

where, $x = 2a_0$, $b_{1/2} = \frac{1}{4}\sqrt{C_{ds}\, D\, x}$, and u_{1i} is a new parameter defined in this study to represent the magnitude of the i^{th} wake velocity profile in-line with the cylinder where the transverse coordinate with respect to the x axis is zero. In a similar fashion to the in-line case, Huse and Muren (1987) took the summation of both positive and negative wake velocity profiles in-line with the x axis as shown in Fig. 2.3. After some effort, the wake velocity correction can be expressed as

$$U_W = V\sqrt{\frac{\pi\ C_{ds}}{N_{\mathrm{KC}}}} \sum_{i=1}^{\infty} -(-1)^i \ \frac{1}{\sqrt{i}}\ e^{-\frac{8.7085\, N_{KC}}{C_{ds}} \left(\frac{N_{CF}}{N_{KC}}\right)^2 i^2}$$

$$\approx V\sqrt{\frac{\pi\ C_{ds}}{e\ N_{\mathrm{KC}}}} \left(\frac{2\, e^{-\frac{8.7\ N_{KC}}{C_{ds}}\left(\frac{N_{CF}}{N_{KC}}\right)^2}}{1 + e^{-\frac{8.7\ N_{KC}}{C_{ds}}\left(\frac{N_{CF}}{N_{KC}}\right)^2}}\right)^{1.2} = V\, k_n \tag{2.24}$$

where,

$$k_n = \sqrt{\frac{\pi\ C_{ds}}{e\ N_{\mathrm{KC}}}}\ \left(\frac{2k_p}{1 + k_p}\right)^{1.2} \tag{2.25}$$

$$k_p = e^{-\frac{8.7\ N_{KC}}{C_{ds}}\left(\frac{N_{CF}}{N_{KC}}\right)^2} \tag{2.26}$$

where, $N_{CF} = V_C T/D$ is a new dimensionless parameter defined to simplify the interpretation. It is interesting to note that the ratio of the current velocity times the period of the in-line oscillation divided by the cylinder diameter bears a similar form to the standard Keulegan-Carpenter number. The result of including the cross-current then is a modifier to the original in-line wake flow expression. Note that when $N_{CF} = 0$, the coefficient k_n becomes $k_n = \sqrt{\frac{\pi\ C_{ds}}{e\ N_{KC}}}$ and Eq. (2.24) simply reduces to the wake velocity correction in the in-line oscillatory flow formulation.

The relative velocity between the cylinder and the flow in the in-line direction can be expressed as

$$V_{r\_L} = V + U_w = V\ (1 + k_n) \tag{2.27}$$

The evaluation of the magnitude of the in-line and crossflow velocities leads to the expression

$$V_{r\_LC} = \sqrt{V^2(1+k_n)^2 + V_C^2} = V\sqrt{(1+k_n)^2 + \left(\frac{N_{CF}}{N_{KC}}\right)^2} \tag{2.28}$$

Huse and Muren (1987) approximated the “true” relative velocity between the cylinder and the flow as the square root of the product of the above in-line velocity and the magnitude of the in-line and crossflow velocities, specifically

$$V_r = \sqrt{V_{r\_L}\ V_{r\_LC}} = V\sqrt{(1+k_n)\left[(1+k_n)^2 + \left(\frac{N_{CF}}{N_{KC}}\right)^2\right]^{\frac{1}{2}}} \tag{2.29}$$

This approximation for the “true” relative velocity in Eq. (2.29) was introduced by Huse and Muren (1987) into their derivation without any elaboration regarding their rationale. Substituting the above expression for the relative velocity into the Morison’s equation, and associating the correction with the standard drag coefficient Huse and Muren (1987) obtained the following correction to the in-line drag coefficient.

$$C_{dc} = C_{ds}\,(1+k_n)\left[(1+k_n)^2+\left(\frac{N_{CF}}{N_{KC}}\right)^2\right]^{\frac{1}{2}} \tag{2.30}$$

where, C_{dc} is the drag coefficient in the in-line oscillatory flow direction for a cylinder subject to a cross current V_C. However, it should be noted that the "true" relative velocity V_r they defined for this crossflow condition does not necessarily lie in the in-line direction, which could be a source of error. The original forms of the equations published by Huse and Muren (1987) are presented here and they can easily be converted to address the cylinder oscillation amplitude noting as before that $N_{KC} = \pi A_0/D$.

Thus, the dimensionless drag coefficient correction ratio can now be expressed as

$$\frac{C_{dc}}{C_{ds}} = (1+k_n)\left[(1+k_n)^2+\left(\frac{N_{CF}}{N_{KC}}\right)^2\right]^{\frac{1}{2}} \tag{2.31}$$

In Huse's (1993) modified flow model the crossflow formulation was not addressed, however following his earlier rationale the drag coefficient correction ratio for his modified model can be derived and expressed as

$$\frac{C_{dc}}{C_{ds}} = (1+k_n')\left[(1+k_n')^2+\left(\frac{N_{CF}}{N_{KC}}\right)^2\right]^{\frac{1}{2}} \tag{2.32}$$

where,

$$k_n' = \sqrt{\frac{\pi\ C_{ds}}{e\left(N_{KC}+\frac{4\pi}{C_{ds}}\right)}}\ \left(\frac{2k_p'}{1+k_p'}\right)^{1.2} \tag{2.33}$$

$$k_p' = e^{-\frac{8.7\,N_{KC}}{C_{ds}\,(1+\frac{4\pi}{C_{ds}\,N_{KC}})}\ \left(\frac{N_{CF}}{N_{KC}}\right)^2} \tag{2.34}$$

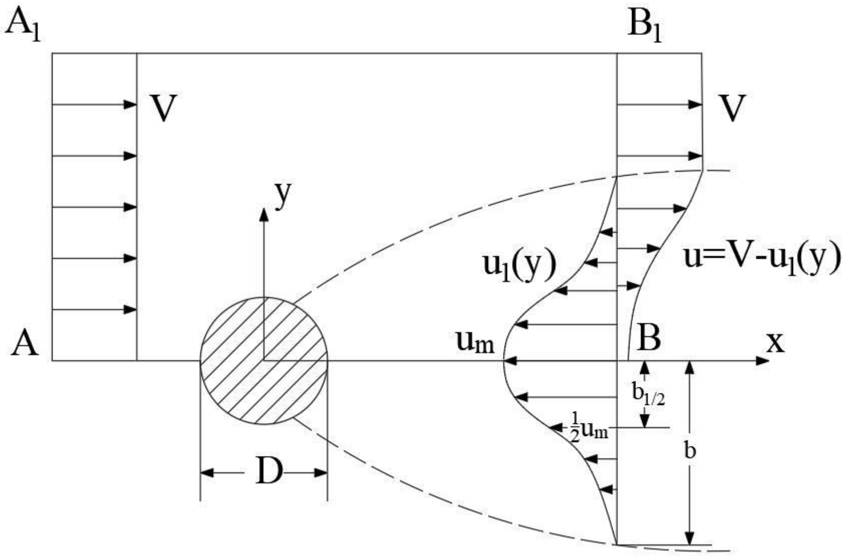

Fig. 2.1. Definition sketch of wake flow downstream of a vertical cylinder (adapted after Schlichting, 1979).

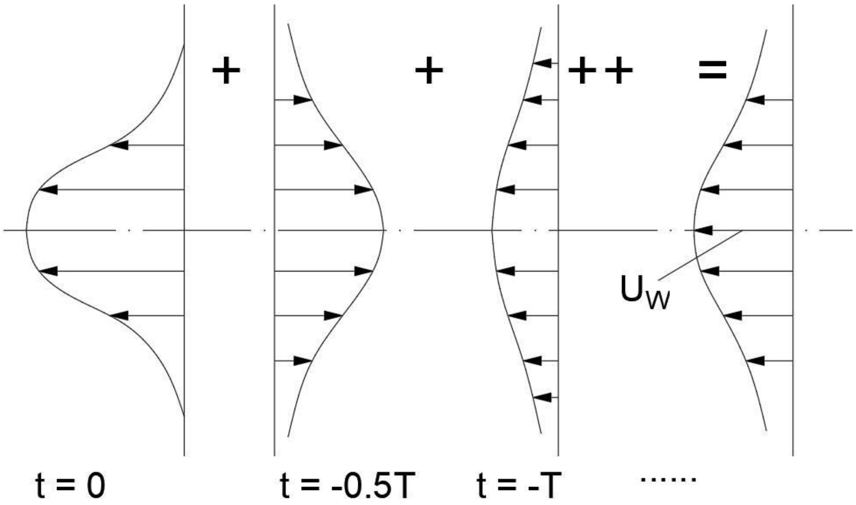

Fig. 2.2. Summation of the wake velocity profiles (adapted with permission from Huse and Muren, 1987).

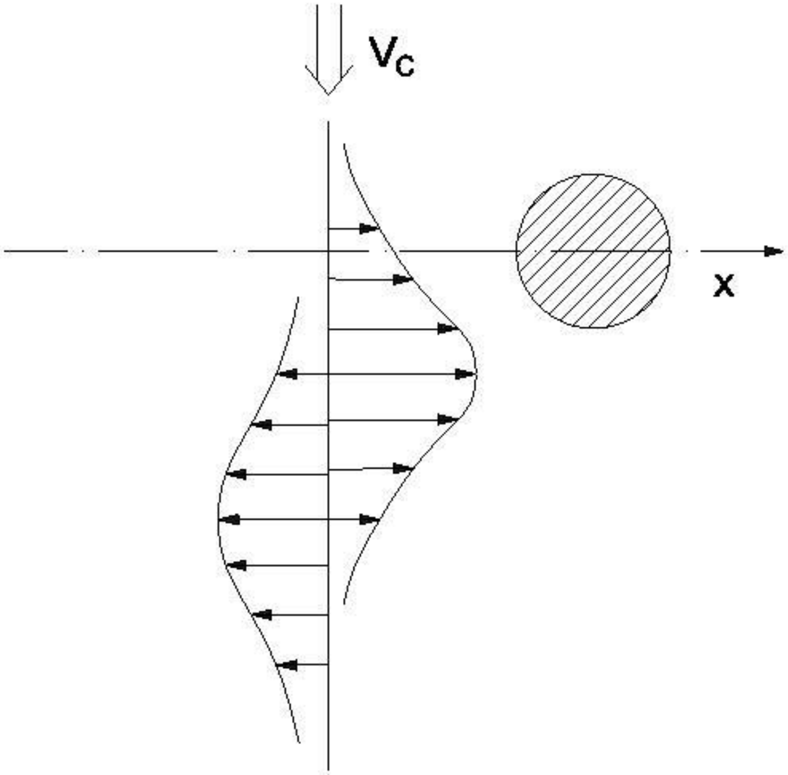

Fig. 2.3. Wake velocity profiles washed away by a cross current (adapted with permission from Huse and Muren, 1987).

2.3 Comparison of Wake Flow Models

The various wake flow models and their mathematical formulations of the wake velocity u_1 are presented in Table 2.1. Interestingly, each of the models was developed based upon Prandtl's mixing theories. In their formulation Huse and Muren (1987) simplified the value of the constant coefficient in the classical solution of the maximum wake velocity u_m to unity, while Huse's new model (1993) made additional modifications to the expression of x, i.e. the in-line distance between the cylinder and the downstream wake velocity profile. The wake velocity predicted by Huse and Muren's model and

Huse's modified model is compared to the two classical solutions in Fig. 2.4 and Fig. 2.5, respectively. In Fig. 2.4 one can observe that Huse and Muren's original model and the two classical solutions are quite similar. The ratio that compares their predicted magnitudes of u_1 is found to be less than 1.12 when the transverse coordinate to half wake width ratio $y/b_{1/2}$ is within -1.7 and 1.7, which corresponds to the main wake region. However, in Fig. 2.5 the difference between Huse's modified model and the classical solutions is seen to vary with the value of x, and that the differences can become quite large when x is small. If for example for a value of $C_{ds} = 0.9$, in the same wake region of $-1.7 < y/b_{1/2} < 1.7$, the ratio that compares their predicted magnitudes of u_1 is found to be less than 0.85 and 0.65 when $x = 7.5D$ and $x = 2.5D$, respectively. This suggests that for some marine applications the magnitude of the wake velocity behind a slender cylindrical structure, that Huse and Muren's wake flow model will provide predictions consistent with the classical solutions and that the deviance in using Huse's modified model could be quite large.

Huse and Muren (1987) took the summation of the maximum velocity of each individual wake profile as the velocity correction term U_W that affected the cylinder, and they addressed two flow conditions. First, when the stationary cylinder is only subjected to an in-line oscillatory flow (or when the cylinder is oscillating in calm water), as shown in Table 2.2, the approximation of $-\sum_{i=1}^{\infty}(-1)^i \frac{1}{\sqrt{i}} \approx \frac{1}{\sqrt{e}}$ is reasonably accurate when there are sufficiently large number of wake velocity profiles in the flow regime and this corresponds to a fully developed wake flow. However, one also observes that this approximation could cause significant overestimation in U_W when the flow regime is dominated by a few couples of wake velocity profiles, which might occur at the initial stage when the oscillatory flow just starts to encounter the cylinder or when the cylinder begins to oscillate in calm water. Thus, this approximation is considered valid only when the wake flow has fully developed. The wake velocity correction U_W leads to a modification in the "true" relative velocity V_r between the cylinder and the flow, which results in a correction to the stationary drag coefficient C_{ds} when substituted into the Morison wave force equation. The drag coefficient correction ratios presented in Fig. 2.6 are obtained by selecting values of $C_{ds} = 0.3$ and $C_{ds} = 1.2$ as the lower and upper bound estimate according to DNV-RP (2014). Since the correction ratio expressed in Eq. (2.20) would unrealistically increase to infinity as the ratio A_0/D approaches 0, the lower end of the curves is truncated at $N_{KC} = 5$, or $A_0/D = 1.59$. Meanwhile, the upper end of the curves is truncated at $N_{KC} = 50$, or $A_0/D = 15.9$. These curves decrease in magnitude and flatten in shape as the value of the ratio A_0/D increases. The variation of the drag coefficient correction ratio based upon Huse and Muren's original model is between 1.6 and 2.35 at $A_0/D = 1.59$, and between 1.17 and 1.36 at $A_0/D = 15.9$. This figure also illustrates that Huse's modified model produces flattened curves and predicts smaller correction ratios. In order to assess the applicability to use in offshore design problems it is important to investigate their performance when compared to experimental data and to see if they can provide a means to serve as an upper or lower bound to the experimental data.

When the cylinder in the in-line oscillatory flow is also subjected to a steady cross current, Huse and Muren (1987) made another approximation in the formulation of the wake velocity correction U_W as shown in Table 2.3. Fig. 2.7 and Fig. 2.8 illustrate that when the ratio of the oscillation amplitude to cylinder diameter A_0/D is greater than 1.5, the ratio that compares the magnitudes of the approximated and the exact solutions is between 0.95 and 1.0. Thus, the error caused by this approximation is considered small and could be neglected. However, in practical applications it should be noted that the "true" relative velocity they defined for this crossflow condition is not necessarily in the in-line direction, which might be a source of error. Then, the drag coefficient correction ratio predicted by Eq. (2.31) and Eq. (2.32) is plotted against the ratio N_{CF}/N_{KC} in Fig. 2.9 with an assumed fixed value of 0.9 for the stationary drag coefficient C_{ds}. In Fig. 2.9 one observes that when the ratio N_{CF}/N_{KC} approaches zero, the influence of the cross current diminishes and the drag coefficient correction ratio simply recovers its value in the in-line oscillatory flow formulation as expressed in Eq. (2.20) and Eq. (2.21). Further, when the ratio N_{CF}/N_{KC} becomes large, the values of the coefficients k_n and k'_n as shown in Eq. (2.25) and Eq. (2.33) decrease fast to zero, in which case the drag coefficient correction ratio is dominated by the influence of the cross current as represented by the ratio N_{CF}/N_{KC}. As a result, the drag coefficient correction ratios predicted by both the original model and the modified model at different values of N_{KC} are found to converge. However, verification of these model predictions using experimental data is needed.

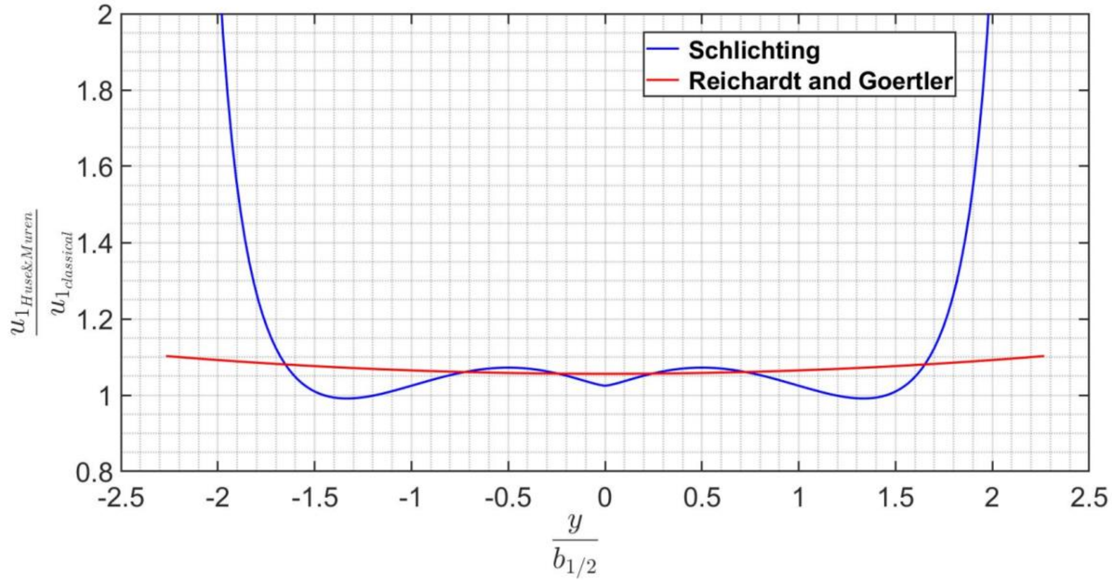

Fig. 2.4. Comparison of Huse and Muren's original solution (1987) of the wake velocity to the classical solutions.

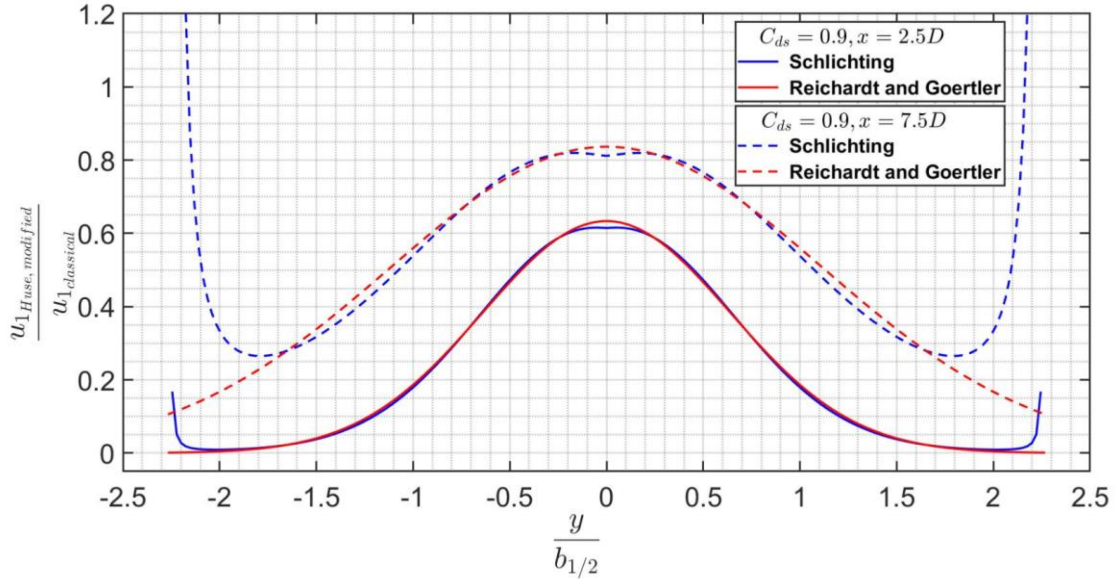

Fig. 2.5. Comparison of Huse's modified solution (1993) of the wake velocity to the classical solutions at $\boldsymbol{x = 2.5D}$ and $\boldsymbol{x = 7.5D}$ with $\boldsymbol{C_{ds} = 0.9}$.

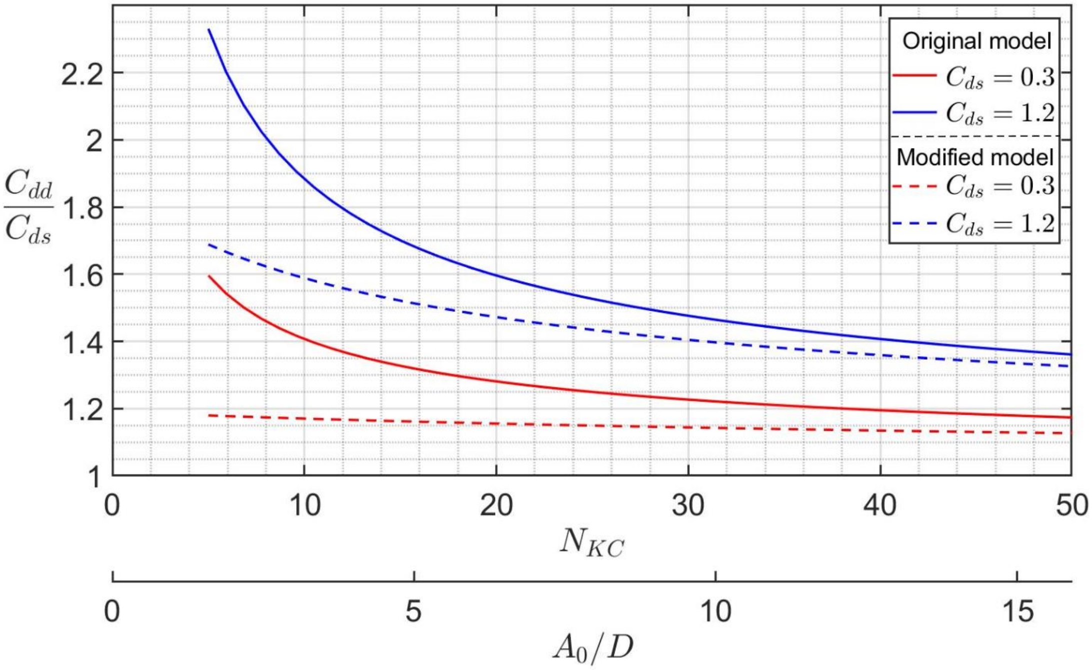

Fig. 2.6. The drag coefficient correction ratio for in-line oscillatory flow.

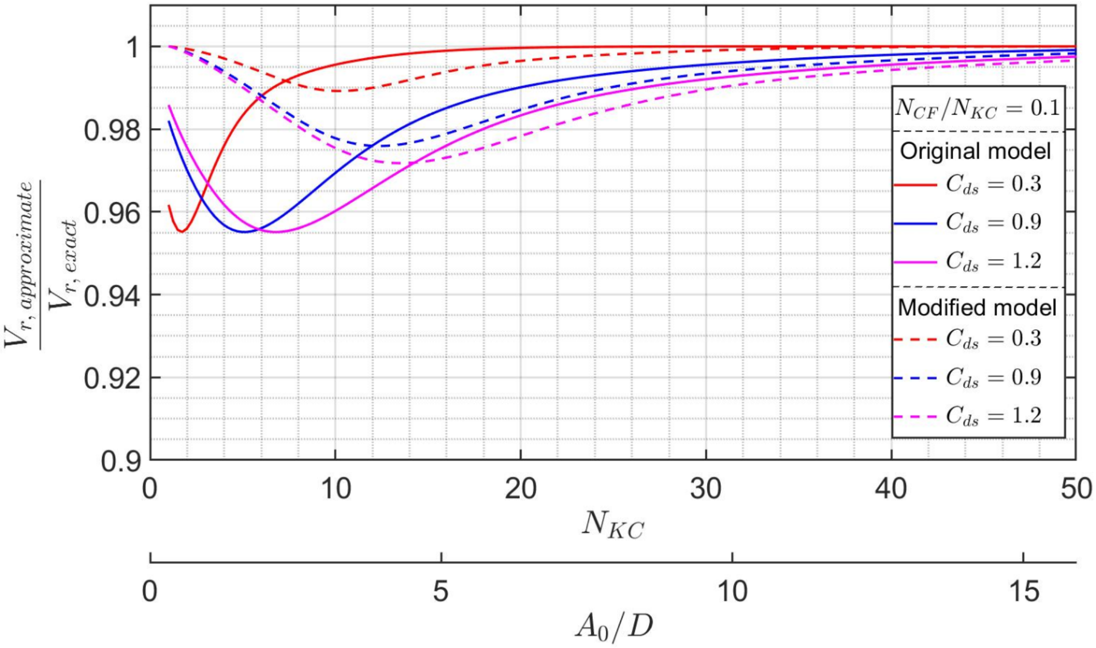

Fig. 2.7. Ratio of the approximate “true” relative velocity to the theoretical value in crossflow.

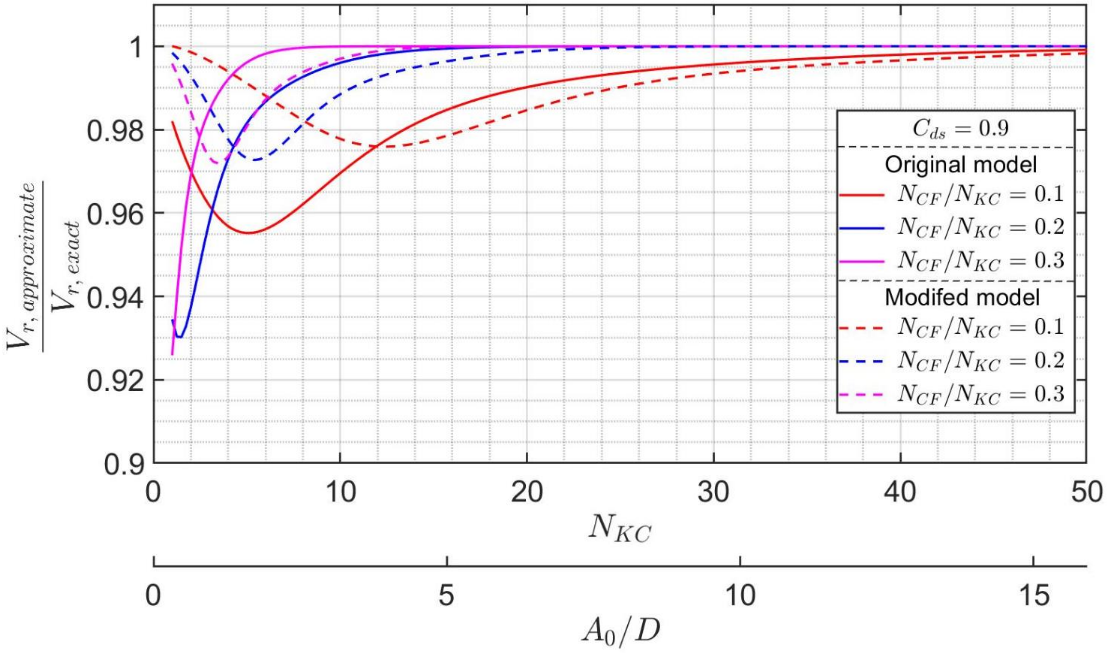

Fig. 2.8. Ratio of the approximate "true" relative velocity to the theoretical value in the crossflow for different values $\boldsymbol{N_{CF}/N_{KC}}$.

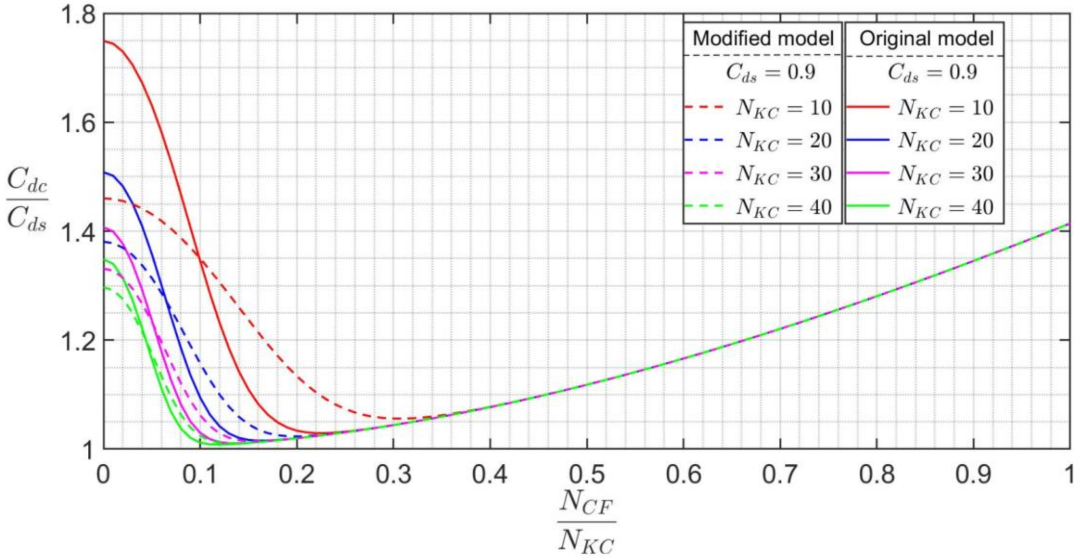

Fig. 2.9. The drag coefficient correction ratio as a function of $\boldsymbol{N_{CF}/N_{KC}}$.

Table 2.1. Comparison of the various theoretical wake flow models.

Item	Schlichting's Model	Reichardt and Goerter's solution to Schlichting's Model	Huse and Muren's Model	Huse's modified model
Assumption	$\tau_t = \rho\, l^2 \left\lvert\frac{\partial u}{\partial y}\right\rvert \frac{\partial u}{\partial y}$	$\tau_t = \rho\, \kappa_1\, \mathcal{B}\, (u_{max} - u_{min}) \frac{\partial u}{\partial y}$	Utilize Prandtl's Assumptions & Schlichting's Model	Utilize Prandtl's Assumptions & Schlichting's Model
$b_{1/2}$	$b_{1/2} = \frac{1}{4}\sqrt{C_{ds}\, D\, x}$	$b_{1/2} = \frac{1}{4}\sqrt{C_{ds}\, D\, x}$	$b_{1/2} = \frac{1}{4}\sqrt{C_{ds}\, D\, x}$	$b_{1/2} = \frac{1}{4}\sqrt{C_{ds}\, D\, \left(x + \frac{4D}{C_{ds}}\right)}$
u_m	$u_m = 0.976\, V \sqrt{\frac{C_{ds}\, D}{x}}$	$u_m = 0.947\, V \sqrt{\frac{C_{ds}\, D}{x}}$	$u_m = V \sqrt{\frac{C_{ds}\, D}{x}}$	$u_m = V \sqrt{\frac{C_{ds}\, D}{x + \frac{4D}{C_{ds}}}}$
u_1	$u_1 = u_m \left\{1 - \left(\frac{0.441y}{b_{1/2}}\right)^{\frac{3}{2}}\right\}^2$	$u_1 = u_m\, e^{-0.7014\left(\frac{y}{b_{1/2}}\right)^2}$	$u_1 = u_m\, e^{-0.693\left(\frac{y}{b_{1/2}}\right)^2}$	$u_1 = u_m\, e^{-0.693\left(\frac{y}{b_{1/2}}\right)^2}$

Table 2.2. Comparison of the summation expression with Huse and Muren's (1987) Approximation.

Number of terms, i	2	6	10	100	1000	10,000	100,000	1000,000	$1/\sqrt{e}$
$\sum_{i=1}^{\infty}(-1)^i \frac{1}{\sqrt{i}}$	0.2929	0.4092	0.4507	0.5550	0.5891	0.5999	0.6033	0.6044	0.6065

Table 2.3. Comparison of the theoretical and the approximate wake velocities for the crossflow formulation.

Item	Exact wake velocity correction directly derived from Huse and Muren's model (1987)	Approximated wake velocity correction (Huse and Muren, 1987)
Velocity sum	$U_w = V \sqrt{\frac{C_{ds}\,\pi}{N_{KC}}} \sum_{i=1}^{\infty} -(-1)^i \frac{1}{\sqrt{i}}\, e^{-\frac{8.7085\ N_{KC}}{C_{ds}}\left(\frac{N_{CF}}{N_{KC}}\right)^2 i^2}$	$U_w = V \sqrt{\frac{C_{ds}\,\pi}{N_{KC}\,e}} \left(\frac{2\,e^{-\frac{8.7\,N_{KC}}{C_{ds}}\left(\frac{N_{CF}}{N_{KC}}\right)^2}}{1+e^{-\frac{8.7\,N_{KC}}{C_{ds}}\left(\frac{N_{CF}}{N_{KC}}\right)^2}} \right)^{1.2}$

2.4 Verification Against Experimental Data

A vertical cylinder subject to longitudinal oscillatory flow

Sarpkaya (1976) measured the drag coefficients of smooth horizontal cylinders of different diameters in a U-tube water tunnel as illustrated in Fig. 2.10. The water tunnel used in Sarpkaya's experimental studies was 9.14m long and 0.91m wide. The two vertical legs were designed with a height of 4.88m and a length of 1.83m. The cross section of the two legs was 1.83m by 0.91m while the cross section of the test section in the middle of the tunnel was 0.91m by 0.91m. The cylinders tested were 91.28cm long and with diameters that varied from 5.057cm to 16.447cm. The test cylinders were fixed on both ends and were subjected to a harmonically oscillatory flow, and the wake effects were implicit in the measured data. Sarpkaya also defined a parameter as a ratio to relate the Reynolds number to the Keulegan-Carpenter number as follows:

$$\beta = \frac{Re}{N_{KC}} = \frac{D^2}{\upsilon T} \tag{2.35}$$

where, Re is the Reynolds number and υ is the fluid kinematic viscosity. The definition of β provided a dimensionless parameter that eliminated the measured data's dependence on velocity.

Huse and Muren's original comparison of their wake-corrected drag coefficient C_{dd} to Sarpkaya's data is reproduced in Fig. 2.11. The values of the data points plotted in this figure are also summarized in Table 2.4 and are compared to DNV (2014) recommended values of the stationary drag coefficient C_{ds} in Fig. 2.12. As shown in Fig. 2.11, Huse and Muren (1987) reported good agreements with the data when the Keulegan-Carpenter number N_{KC} was larger than 20. However, in Fig. 2.12 one observes that the values of the stationary drag coefficient C_{ds} used by Huse and Muren are extremely close to DNV recommended values for cylinders with a roughness value of $k/D = 1 \times 10^{-4}$, and the curves are significantly different from the suggested values for a smooth cylinder. Thus, Huse and Muren might have assumed a roughness of $k/D = 1 \times 10^{-4}$ for Sarpkaya's smooth test cylinders. To address these discrepancies and to investigate the bounding of the experimental data, a new verification is performed for both a smooth cylinder and an assumed rough cylinder with $k/D = 1 \times 10^{-4}$ using Sarpkaya's measured data, DNV-RP (2014) and Sumer and Fredsøe's (1997) recommended values of the stationary drag coefficient. The lower and upper bound estimates of C_{ds} are taken as 0.3 and 1.2 based on DNV-RP as shown in Fig. 2.12.

First, Sarpkaya's test cylinders are treated as perfectly smooth and the bounding predicted by Huse and Muren's model is compared to the U-tube data in Fig. 2.13. One observes in this figure that the predicted curves successfully capture the data of $\beta = 497$ and $\beta = 1107$ in some ranges of the Keulegan-Carpenter number N_{KC} or the ratio A_0/D. However, these predictions no longer agree with the data of larger β values. One also observes that the bounding predicted by Huse's modified model does not show a better agreement with the data.

Then, Sarpkaya's test cylinders are assumed to have a roughness of $k/D = 1 \times 10^{-4}$ and the bounding of the data is investigated in Fig. 2.14. In this figure, it can be seen that the values of the data points of $\beta = 497$ are identical to the previous figure. This is also observed for the data set of $\beta = 1107$ when $N_{KC} < 23.6$ or $A_0/D < 7.5$. This phenomenon could be explained by examining DNV recommended values of C_{ds}, which remain unchanged for this rough cylinder when $Re < 3 \times 10^4$. The correction ratios calculated from the data of $\beta = 1985$ are still found to fall out of the predicted range, although the deviations are reduced. One also observes a distinct trend in the calculated results of the data sets of $\beta = 3123$ and $\beta = 5260$, which go into the lower bound and rise above the upper bound. This might be attributed to the rapid decrease in the values of C_{ds} in the critical flow regime. These observations indicate that assuming a roughness of $k/D = 1 \times 10^{-4}$ does not improve the bounding's ability to capture the data. Thus, for all practical purposes Sarpkaya's smooth test cylinders can be assumed to be perfectly smooth.

Table 2.5 provides a summary of the Reynolds number Re and the flow regimes that are identified in the range of $5 < N_{KC} < 50$ (or $1.59 < A_0/D < 15.9$). The bounding of the data of $\beta = 497$ and $\beta = 1107$ are investigated in Fig. 2.15 and Fig. 2.16, respectively, while the original values of C_{ds} are maintained for both Huse and Muren's model and Huse's modified model. In Fig. 2.15, one observes that when $\beta = 497$, for $C_{ds} = 1.2$ Huse and Muren's model provides a good upper-bound estimate of the data when $N_{KC} > 20$ while Huse's modified model does not give a quite satisfactory estimation. For $C_{ds} = 0.3$, the lower-bound estimates given by both two models successfully capture the data. However, Huse and Muren's original model illustrates a significantly better performance in capturing the trend of the data points, especially when $N_{KC} > 20$. In Fig. 2.16, one observes that for the higher value of $\beta = 1107$, when $C_{ds} = 1.2$ the upper-bound estimate given by Huse and Muren's model could even capture the data when the value of N_{KC} is reduced to 5, although the maximum overestimation of the data could reach approximately 40%. Huse's modified model, however, does not improve the performance and it deviates from the data in the range of $10 < N_{KC} < 18$. For $C_{ds} = 0.3$ the lower-bound estimate given by Huse and Muren's model only agrees with the data when $5 < N_{KC} < 22$ while Huse's modified model is slightly better in the upper side as it is able to capture the data when N_{KC} rises to 28. However, Huse's modified model shows much higher underestimation of the data at small values of N_{KC}. Thus, in applications the drag coefficient correction ratio predicted by Huse and Muren's model at $C_{ds} = 1.2$ could provide a reasonably good upper-bound estimate on the amplification of C_{ds} when $497 < \beta < 1107$ and $N_{KC} > 20$, although this prediction might overestimate the measured data by as much as 40%. For $C_{ds} = 0.3$, the lower-bound estimate produced by Huse and Muren's model has a more limited range of applications. Their model is observed to agree with the measurements only when $497 < \beta < 1107$ and $5 < N_{KC} < 22$. However, Huse's modified model is not expected to predict a better bounding of the data.

When the value of β becomes large and the flow approaches the critical flow regime, Fig. 2.13 illustrates that the predicted upper bound deviates from the data. It could overestimate the data of $\beta = 3123$ and $\beta = 5260$ by more than 200% at large N_{KC} values. The lower-bound estimate predicted at $C_{ds} = 0.3$ is also observed to deviate significantly from the data. These deviances might be attributed to the simplifications Huse and Muren made in their analytical derivation of the wake-corrected drag coefficient, which could not capture enough the complicated fluid-cylinder interactive response behavior in the highly turbulent flow regime that is characterized by large values of β and Re. Thus, the predicted bounding on the drag coefficient correction ratio based on these analytical wake flow models might have a very limited range of applicability.

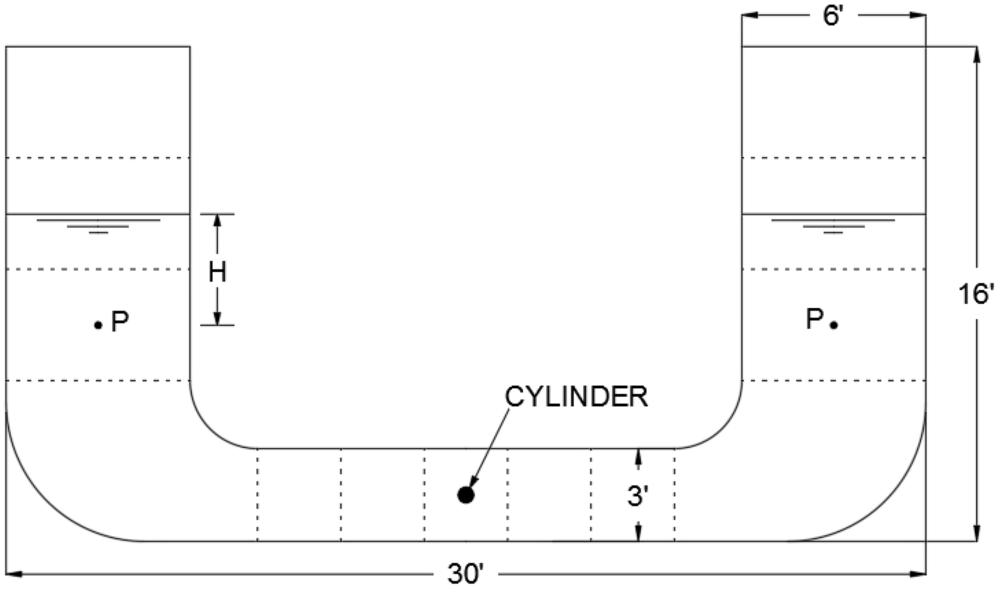

Fig. 2.10. Schematic of the U-shaped water tunnel (reprinted from Sarpkaya, 1976)

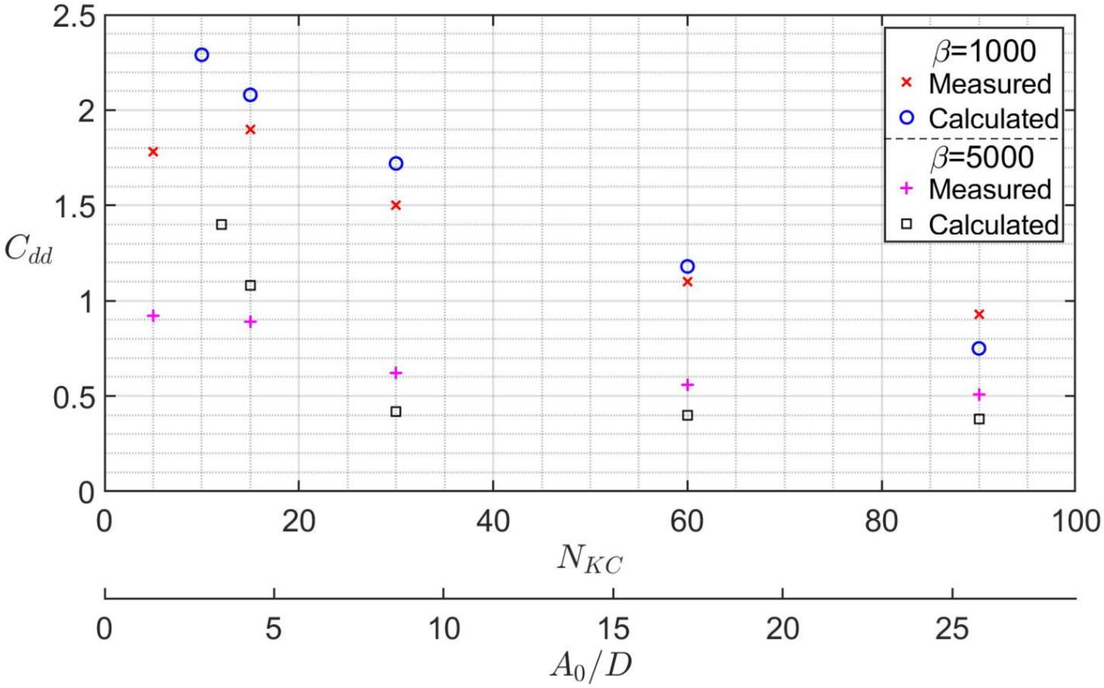

Fig. 2.11. Reproduction of Huse and Muren's original comparison (1987) of their wake-corrected drag coefficients with Sarpkaya's in-line oscillatory flow measurements (adapted with permission from Huse and Muren, 1987).

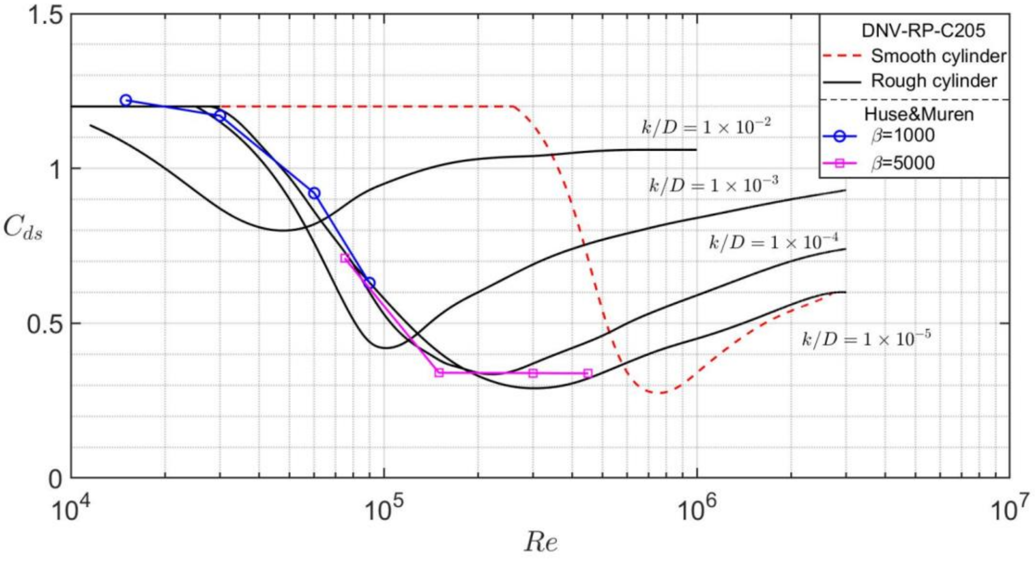

Fig. 2.12. Comparison of DNV (2014) recommended stationary drag coefficients with Huse and Muren's (1987) selected values (adapted from DNV-RP-C205, 2014).

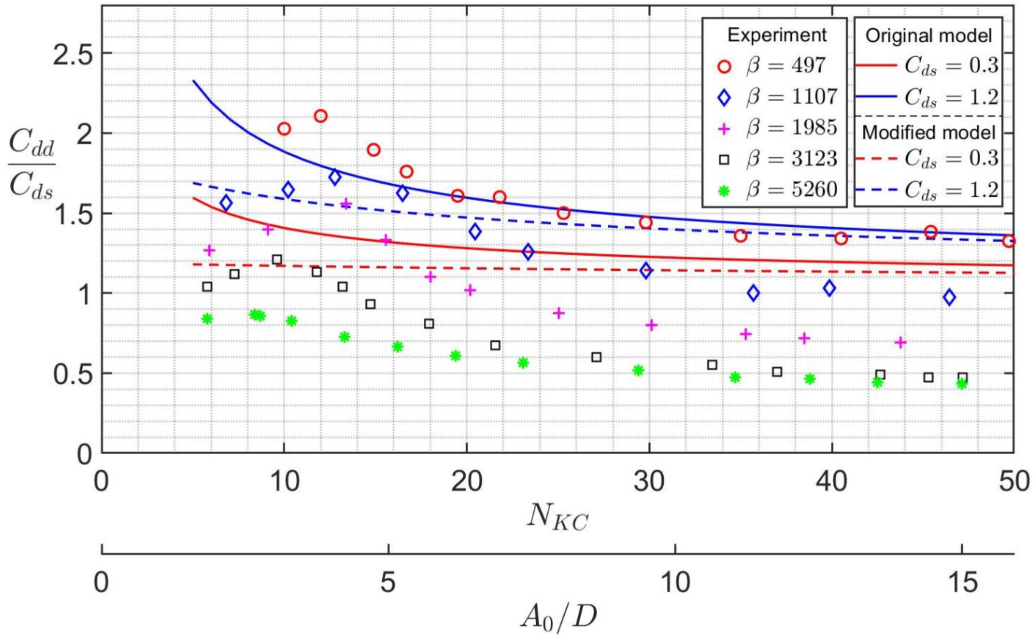

Fig. 2.13. Predicted bounding of the drag coefficient correction ratio with Sarpkaya's data for a smooth cylinder.

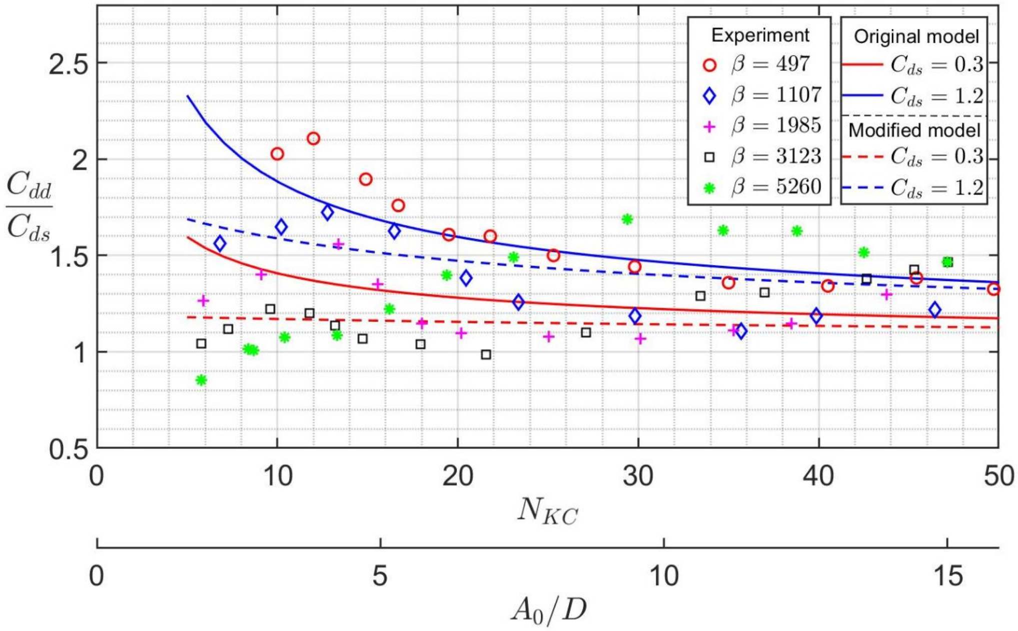

Fig. 2.14. Predicted bounding of the drag coefficient correction ratio with Sarpkaya's data for $\boldsymbol{k/D = 1 \times 10^{-4}}$.

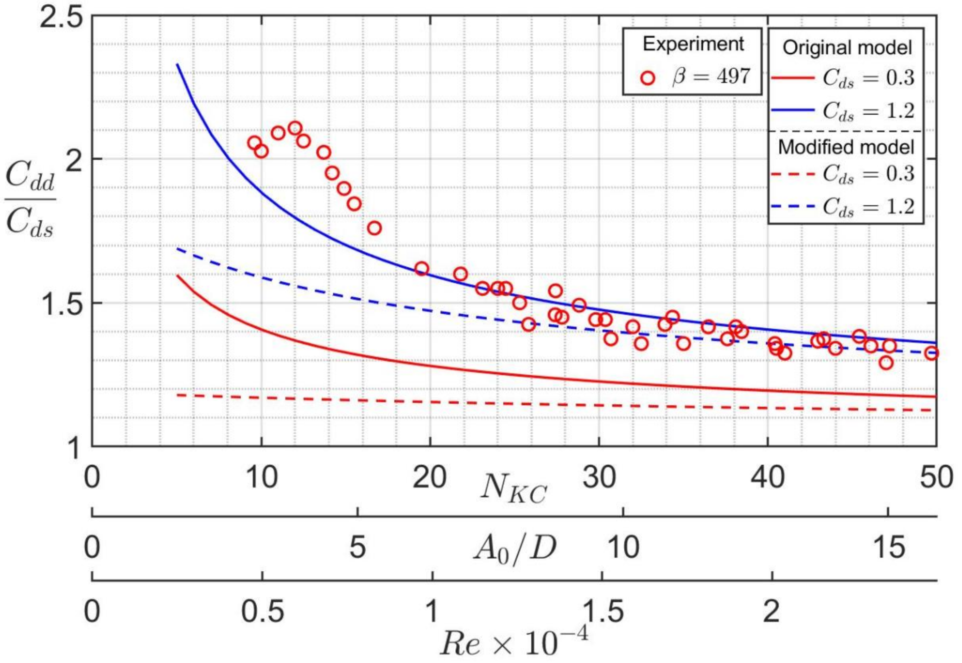

Fig. 2.15. Predicted bounding of the drag coefficient correction ratio with Sarpkaya's data of $\boldsymbol{\beta = 497}$ for a smooth cylinder.

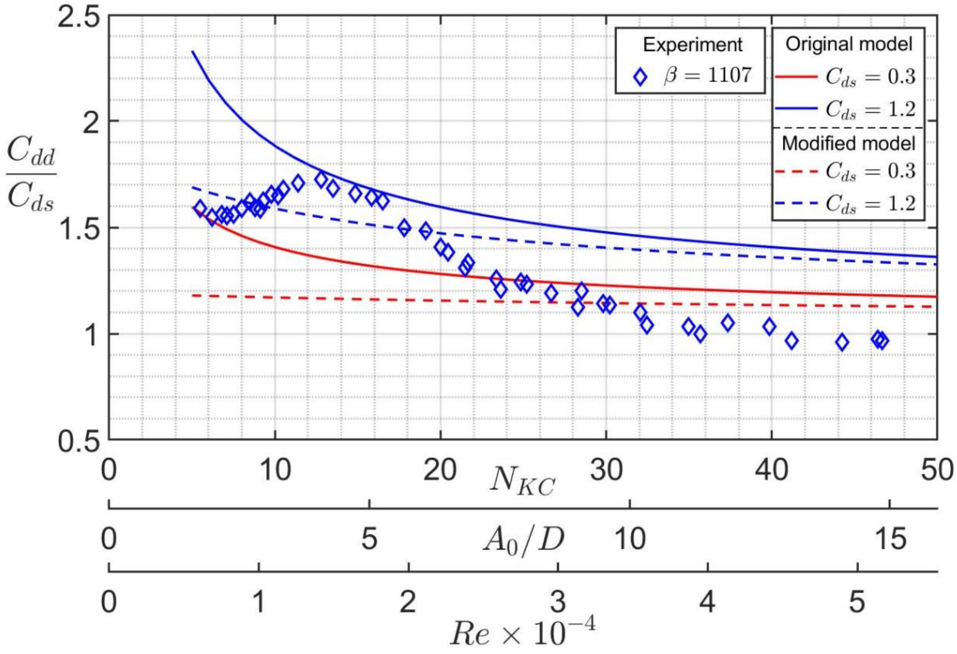

Fig. 2.16. Predicted bounding of the drag coefficient correction ratio with Sarpkaya's data of $\boldsymbol{\beta = 1107}$ for a smooth cylinder.

Table 2.4. Parameters used by Huse and Muren's comparison (1987) to Sarpkaya's measurements (1976).

$\beta = 1000$				
N_{KC}	15	30	60	90
C_{dd}	2.08	1.72	1.18	0.75
C_{ds}	1.22	1.17	0.92	0.63
Re	1.5×10^4	3×10^4	6×10^4	9×10^4
$\beta = 5000$				
N_{KC}	15	30	60	90
C_{dd}	1.08	0.42	0.4	0.38
C_{ds}	0.71	0.34	0.339	0.338
Re	7.5×10^4	1.5×10^5	3×10^5	4.5×10^5

Table 2.5. Reynolds number and flow regimes corresponding to Sarpkaya's $\boldsymbol{\beta}$ parameters.

β	The Reynolds number corresponding to the range of $5 < N_{KC} < 50$ ($1.59 < A_0/D < 15.9$) in the verification	Flow regimes around a cylinder in uniform steady current	
		Smooth cylinder	Rough cylinder with $k/D = 1 \times 10^{-4}$
497	$2.485 \times 10^3 < Re < 2.485 \times 10^4$	Subcritical	Subcritical
1107	$5.535 \times 10^3 < Re < 5.535 \times 10^4$	Subcritical	Subcritical to critical
1985	$9.925 \times 10^3 < Re < 9.925 \times 10^4$	Subcritical	Subcritical to critical
3123	$1.562 \times 10^4 < Re < 1.562 \times 10^5$	Subcritical	Subcritical to critical
5260	$2.63 \times 10^4 < Re < 2.63 \times 10^5$	Subcritical	Subcritical to supercritical

2.5 Numerical Simulation

A vertical cylinder subject to both longitudinal oscillatory flow and steady cross current

In offshore applications vertical cylindrical structures might experience wind waves and currents coming from different directions. For example, in areas such as the Gulf of Mexico or the outlet of major rivers strong currents may occur without a storm (API, 1998). Huse and Muren (1987) addressed a representative case when the incoming current was at right angles with the oscillatory flow and they investigated the influence of the cross current on the drag coefficient in the in-line oscillatory flow direction. Since no experimental data were available for this flow condition, a numerical simulation is performed as the only alternative to investigate the predictive behavior of their wake flow model.

According to ABS (2017) and API (1993) guidelines, the top end of the riser can either be modeled as fixed when it is connected on a collapsed telescopic joint or as pinned when it is connected on a gimbal, a ball joint. The bottom end of the riser, on the other hand, can either be fixed on the seafloor or connected to flex and ball joints under normal operations, or can be hung as a free end during riser deployment, retrieve, or storm hang off. To address these different boundary conditions in the investigation, a rigid, a pinned-end, and a slender cylinder subjected to this crossflow formulation are studied. As shown in Table 2.6, their lengths are taken as 15.24m, 152.4m, and 304.8m, respectively. The three cylinders are treated as steel pipes with an outer diameter of 0.6096m and a wall thickness of 5.08 cm. The stationary drag coefficient C_{ds} is taken as 0.9. The magnitude of the in-line oscillatory flow velocity is assumed to range between 0.44 m/s and 2.5m/s, and the velocity of the steady cross current is taken as 0.44 m/s, with reference to the speed range of the Gulf Current.

Blevins (1977) studied cylinders' vibrations in an oscillatory flow and his analytical formulas are utilized to estimate the three cylinders' fundamental periods of oscillation. The rigid cylinder is treated as a beam rigidly fixed at both ends. A lower-bound estimate on its stiffness is first made based on the case that a point load acts at the center of the beam. Accordingly, an upper-bound estimate on its fundamental period of oscillation could be obtained. This study then simplifies the pinned-end cylinder as a simply supported uniform beam and the slender cylinder with a free end as a cantilevered uniform beam. Based upon Blevins' formulas, the fundamental periods of oscillation of the rigid, the pinned-end, and the slender cylinder are estimated to be 0.13s, 18s, and 198s, respectively. With these estimations the values of the Keulegan-Carpenter number N_{KC} of the three cylinders are calculated. It is found that the maximum value of N_{KC} of the rigid cylinder is below 1.0 while the value of N_{KC} of the slender cylinder is unrealistically high. Only the value of N_{KC} of the pinned-end cylinder is within a reasonable range. Thus, only the pinned-end cylinder will be studied in the following investigation.

To investigate the behavior of the predicted wake effects on the pinned-end cylinders subjected to this crossflow formulation, four additional pinned-end cylinders are introduced, and they are assumed to have a fundamental period of oscillation of 9s, 14s, 23s, and 27s. The correction ratios for the stationary drag coefficient C_{ds} are calculated and plotted in Fig. 2.17. One observes that the curves predicted by both Huse and Muren's original wake model and Huse's modified model converge completely since the value of the ratio N_{CF}/N_{KC} in this case is relatively large. The maximum drag coefficient correction ratios of each cylinder are observed to be 1.42 at the minimum value of N_{KC}. As the value of N_{KC} increases, all the correction ratios are observed to approach one. It is also noted that all the curves share a similar shape and show a tendency to move to the right as the period of oscillation increases. Thus, when the ratio N_{CF}/N_{KC} is relatively large, a family of curves of the drag coefficient correction ratios could be obtained. These curves might be potentially developed to design curves to estimate the range of amplification in the value of the stationary drag coefficient C_{ds} for slender cylindrical offshore structures subjected to this crossflow formulation, provided that the structure could be properly simplified as a pinned-end cylinder. However, future experimental data is required for verification.

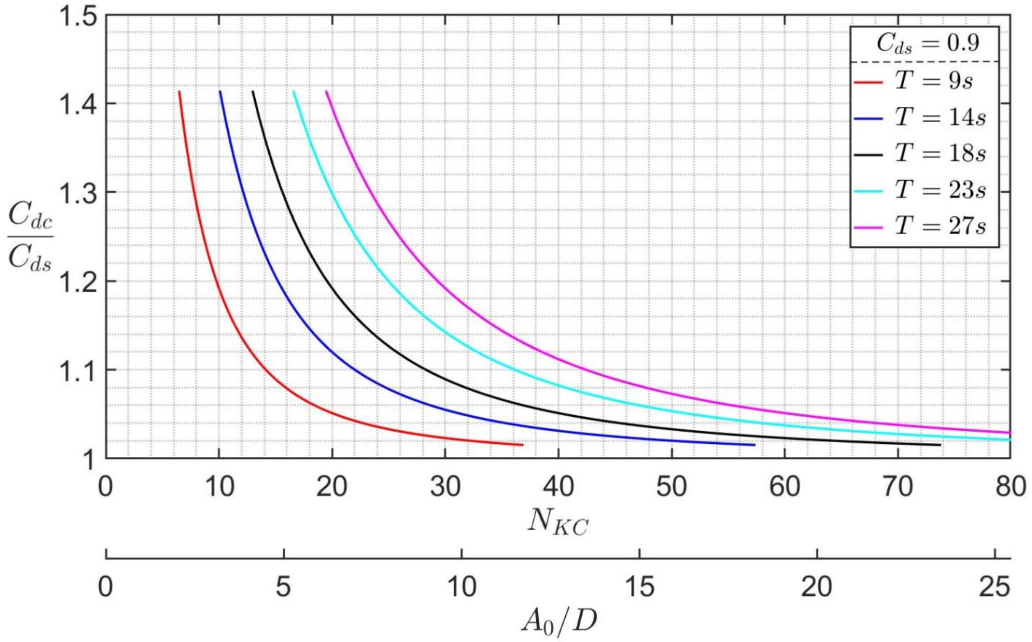

Fig. 2.17. Predicted drag coefficient correction ratios for Blevins' pinned-end cylinders subjected to the crossflow formulation.

Table 2.6. Cylinder properties and flow conditions in the numerical simulation.

Cylinder type	Rigid	Pinned end	Slender
Length	15.24 m	152.4 m	304.8 m
Outer diameter	0.6096 m	0.6096 m	0.6096 m
Wall thickness	5.08 cm	5.08 cm	5.08 cm
Boundary conditions	Fixed	Pinned	Top end: fixed Bottom end: free
Estimated fundamental period of oscillation	0.13 sec	18 sec	198 sec
Stationary drag coefficient, C_{ds}	0.9	0.9	0.9
Magnitude of in-line oscillatory flow velocity	0.44 m/s to 2.5 m/s	0.44 m/s to 2.5 m/s	0.44 m/s to 2.5 m/s
Cross current velocity	0.44 m/s	0.44 m/s	0.44 m/s

2.6 Summary

This chapter investigates Huse and Muren's wake flow model and Huse's modified model predictions regarding the influence of wake effects on fluid drag force coefficients for a slender vertical cylinder. Initially it focuses on examining the assumptions and approximations used in the development of their analytical formulations that addressed the amplification of the stationary flow drag coefficient to account for oscillatory flows and oscillatory flows with a cross current. It is shown that the wake velocity profile approximated by Huse and Muren only deviates slightly from Schlichting's classical solutions. However, for Huse's modified model the deviance could become quite large, especially when the wake profile is within two diameters downstream of the cylinder. This study also identifies and quantifies potential sources of errors in the formulations. Their estimation of the wake velocity correction for in-line oscillatory flow is found valid only for fully developed wake flows. In the crossflow formulation they utilized the concept of a "true" relative velocity to estimate the drag coefficient in the in-line direction even though it does not necessarily lie in this direction and consequently could be a source of error.

Further analysis of these models leads to the development of dimensionless expressions for the drag coefficient correction ratio and Keulegan-Carpenter parameter useful for the cross-flow cases. Both the DNV-RP recommended drag force coefficients and some of Sarpkaya's U-tube measurements are used to investigate whether these analytical models could be used to bound the experimental data. The Keulegan-Carpenter number, A_0/D ratios, Sarpkaya's Beta parameter and Reynold's number are also introduced to interpret their range of applicability. Based upon a comparison with Sarpkaya's U-tube experimental data the bounding of the experimental data predicted by Huse and Muren's original model is observed to agree with the measurements for a limited range of the dimensionless parameters. Unfortunately, there is no improvement observed using Huse's modified model in the range of data considered attesting to the complexity of the flow. In the crossflow formulation, a new dimensionless ratio is identified from the variables in their original formulations and is helpful to better understand the impact of the steady cross current with respect to the inline oscillatory flow. The drag coefficient correction ratios predicted as a function of the cross-flow parameter N_{CF} and the standard Keulegan-Carpenter number N_{KC} are found to converge as their ratio increases. This convergence is also observed in the numerical simulation in which the value of the ratio is relatively large. The simulated curves of the correction ratios for the pinned-end cylinders are found to bear a similar shape. Potentially, this could lead to the development of a family of design curves for offshore applications, but future experimental data will be required for verification.

Thus, the estimated bounding on the drag coefficient correction ratio formulated from the Huse-Muren analytical wake flow models appears to have limited range of applications even for a simplified flow condition of a single slender vertical cylinder subjected to a harmonically oscillatory flow. When it comes to the more complicated random sea conditions, this analytical approach might not be able to capture the essential characteristics in the observed fluid-cylinder response behavior. These observations lead to the research study in the following chapters where a general statistical approach based on extremal statistical methodology is formulated to investigate the measured data obtained in two industrial scale model basin test programs (Rijiken and Niedzwecki, 1997, Chitwood and Niedzwecki, 1998) performed at the Offshore Technology Research Center (OTRC) located at Texas A&M University.

3 . STATISTICAL ANALYSIS OF RANDOM WAVE INTERACTIONS WITH VERTICAL CYLINDER ARRAYS*

Closely spaced vertical deep-water cylinder arrays are widely used in offshore platform designs. Their interactions with random waves are very complicated and it is extremely difficult to model their motions in a direct analytical approach. Accurate characterization of the observed extreme values in their response behavior is of vital importance for the safety of the designed structure. In this chapter a general statistical methodology based on generalized extreme value (GEV) family of distributions (Coles, 2001) is formulated for the characterization of both laboratory and field data associated with the wave-cylinder interactions in random waves. An iterative process is developed to determine the most appropriate block size and the corresponding statistical model for the block maxima constructed from the time series of the target variable. The model's capability to fit the data is assessed using the Anderson-Darling (AD) test criterion (Anderson and Darling, 1954), visually with quantile plots and histograms. Special attention is paid to the quality of fit in the upper tail of the distribution, which corresponds to the data points of the extreme statistical events. Case studies are also performed to investigate the performance of the statistical methodology in characterizing the measured data from an industrial scale model basin test program (Rijken and Niedzwecki, 1997).

---

* Reprinted from "Analysis of random wave interactions with cylinders using extremal statistical methods" by Jiangnan Lu and Niedzwecki (in-press), 2020, *Applied Ocean Research*. Copyright by Elsevier (the publisher).

The test program addresses the data on the in-line interactions of closely spaced deep-water cylinder arrays for two- and three-cylinder configurations. The random seaways were generated using JONSWAP wave amplitude spectrum. The effectiveness of this statistical methodology in characterizing the response behavior observed in the model basin experimental data is discussed in detail using both tabular and graphical interpretations.

3.1 Theoretical Background

The theoretical background of the extremal statistical methods and goodness of fit techniques used in this study are briefly introduced in the following sections.

3.1.1 Generalized extreme value (GEV) distribution

Suppose the series $X_1, X_2, \ldots, X_n$ is a sequence of independent random variables that share the same distribution function F, the extreme value theory is focused on the investigation of the statistical behavior of the maximum value M_n (Coles, 2001) that can be expressed as

$$M_n = \max\{X_1, X_2, \ldots, X_n\} \tag{3.1}$$

where, when in practice the sequence $X_1, X_2, \ldots, X_n$ is frequently used to represent the time series of a random process measured at a fixed interval of δt and M_n becomes the maximum observed value in a duration of $n\delta t$. The probability that M_n is less than or equal to z can be obtained

$$
\begin{aligned}
P(M_n \leq z) &= P\{X_1 \leq z,\, X_2 \leq z, \dots, X_n \leq z\} \\
&= P(X_1 \leq z) \dots\, P(X_n \leq z) \qquad (3.2) \\
&= [F(z)]^n
\end{aligned}
$$

One observes that the above equation could not be calculated without the explicit form of the distribution function F. Coles (2001) indicated that the common practice to estimate F from the sample data does not work, since a small deviance between F and the estimated distribution function F_n could cause significant errors between F^n and F_n^n. As an alternative, he suggested that one could simply accept that F is unknown and investigate the approximated form of F^n directly based on the data points of the extreme values only. In his formulation he found that for any $z < z_+$, where z_+ is the smallest value of z such that $F(z) = 1$, F^n would decrease to zero as n becomes large. Consequently, the distribution of M_n would degenerate to a point mass on z_+. To solve this problem, Coles (2001) performed a linear renormalization on M_n as follows

$$M_n^* = \frac{M_n - b_n}{a_n} \qquad (3.3)$$

where, a_n and b_n are a sequence of constants. For sequences where $a_n > 0$ and $b_n > 0$ the extremal types theorem (Coles, 2001) produces the following

$$P\left(\frac{M_n - b_n}{a_n} \leq z\right) \rightarrow G, \text{ as } n \rightarrow \infty \qquad (3.4)$$

where, G is a non-degenerated distribution function and it belongs to one of the three familiar extreme value distributions Gumbel, Fréchet, or Weibull (Coles, 2001). Coles

(2001) noted a remarkable feature that the distribution of M_n^* would only approach one of the above three families of extreme value distributions, disregarding the form of the unknown function F, and he also reported that each of the three distribution functions has distinct types of tail behavior. For convenience, the three possible forms of the distribution function of G could be combined as the generalized extreme value (GEV) distribution

$$G(z) = \exp\left\{-\left[1 + \xi\left(\frac{z-\mu}{\sigma}\right)\right]^{-\frac{1}{\xi}}\right\} \tag{3.5}$$

where, ξ is the shape parameter, μ is the location parameter, and σ is the scale parameter. $G(z)$ is defined on $\{z\colon 1 + \xi(z-\mu)/\sigma > 0)\}$ for $-\infty < \mu < +\infty$, $\sigma > 0$ and $-\infty < \xi < \infty$. Note that when $\xi = 0$, the GEV simply recovers the form of the Gumbel distribution, while the Fréchet and Weibull families of distributions correspond to the cases when $\xi > 0$ and $\xi < 0$, respectively. Statistical applications become much more convenient with the introduction of GEV distribution, which enables one to determine the most appropriate types of tail behavior based on the data directly by changing the value of ξ, and no presumptions on the distribution function are required (Coles, 2001).

Thus, suppose the data $\{X_1, X_2, \ldots\}$ is a series of independent observed values of a random process, where each element X_i is recorded at a time interval of δt. If one subdivides the sequence $\{X_1, X_2, \ldots\}$ into m blocks of equal length n (both m and n must be large), a series of block maxima can be generated as $\{M_{n,1}, M_{n,2}, \ldots, M_{n,m}\}$, where each $M_{n,i}$ represents the maximum value observed in each block with a block length of $n\delta t$. By examining the GEV distribution fitted to the series of the block maxima

$\{M_{n,1}, M_{n,2}, \dots, M_{n,m}\}$, one is able to characterize the statistical behavior of the extreme values in the series $\{X_1, X_2, \dots\}$. Coles (2001) reported the highlight of this approach is that even when the series of the target variable $\{X_1, X_2, \dots\}$ shows a temporal dependence and the extreme events occur in clusters, one can still appropriately approximate the block maxima $\{M_{n,1}, M_{n,2}, \dots, M_{n,m}\}$ as independent random variables and fit it with the GEV distribution. This approximation is found valid as long as the long-range dependence at the extreme levels is weak (Coles, 2001), and it significantly expands the applicability of the GEV family of distributions.

3.1.2 Anderson-Darling (AD) test criterion and goodness of fit assessment

In applications the observed values from a population are usually described as the realizations of independent random variables from a specific distribution. In practice, the observed data might not follow the specified distribution exactly and goodness of fit techniques are required to assess how well the proposed distribution function fits the data. In this study, the Anderson-Darling (AD) test criterion (Anderson and Darling, 1954), quantile plots and histograms are utilized to examine the quality of fit of the model.

Suppose $\{Y_1, Y_2, \dots, Y_n\}$ is a sequence of independent and identically distributed random variables that have the same continuous cumulative distribution function F. If one denotes F_0 as the proposed form of the distribution function and F_n as the empirical cumulative distribution function based on the data, the quantitative goodness of fit criterion proposed by Cramér and von Mises (1928) is frequently utilized to evaluate the degree to which F_0 agrees with the observed data as follows

$$Q_n = n\int_{-\infty}^{\infty}[F_n(y) - F_0(y)]^2\ \mathrm{w}(y)\ dF_0(y) \tag{3.6}$$

where, $\mathrm{w}(y)$ is the weight function and the empirical cumulative distribution function $F_n(y)$ is expressed as

$$F_n(y) = \frac{1}{n}\sum_{i=1}^{n} I(Y_i \le y) \tag{3.7}$$

where, with a proper selected form for $\mathrm{w}(y)$ the above criterion would be able to detect the deviance between $F_n(y)$ and F_0 in the tails of the distribution (Cramér and von Mises, 1928). When the weighting function $\mathrm{w}(y)$ is defined as unity, one recovers the original Cramér–von Mises criterion denoted as W_n^2 of the form

$$W_n^2 = \int_{-\infty}^{\infty}[F_n(y) - F_0(y)]^2\ dF_0(y) \tag{3.8}$$

denote $u = F_0(y)$ and thus $x = F_0^{-1}(u)$, following the derivation of Anderson (1962) one obtains

$$\begin{aligned} W_n^2 &= n\int_0^1 \left[F_n\left(F_0^{-1}(u)\right) - F_0\left(F_0^{-1}(u)\right)\right]^2 du \\ &= n\int_0^1 \left[F_n\left(F_0^{-1}(u)\right) - u\right]^2 du \\ &= n\sum_{i=1}^{n+1}\int_{U_{(i-1)}}^{U_{(i)}} \left[F_n\left(F_0^{-1}(u)\right) - u\right]^2 du \\ &= n\sum_{i=1}^{n+1}\int_{U_{(i-1)}}^{U_{(i)}} \left[\frac{i-1}{n} - u\right]^2 du \end{aligned} \tag{3.9}$$

$$= \frac{n}{3}\sum_{i=1}^{n+1}\left[\left(\frac{i-1}{n} - U_{(i-1)}\right)^3 - \left(\frac{i-1}{n} - U_{(i)}\right)^3\right]$$

$$= \frac{n}{3}\sum_{i=1}^{n}\left[\left(\frac{i}{n} - U_{(i)}\right)^3 - \left(\frac{i-1}{n} - U_{(i)}\right)^3\right]$$

$$= \sum_{i=1}^{n}\left[U_{(i)} - \frac{2i-1}{2n}\right]^2 + \frac{1}{12n}$$

where, $U_{(i)} = F_0(Y_{(i)})$, $U_{(0)} = 0$, $U_{(n+1)} = 1$, and $U_{(1)}$, $U_{(2)}$, …, $U_{(n)}$ are the order statistics of a random sample following a uniform (0, 1) distribution. One observes in the above equation that the Cramér–von Mises criterion shows no dependence on the distribution function F_0. However, D'Agostino and Stephens (1986) indicated that this criterion is not sensitive enough to detect the difference between F_0 and $F_n(y)$ in the tails of the distribution while the tail fit is most crucial in many statistical applications. This inadequacy could be corrected by introducing a modified weight function that was proposed by Anderson and Darling (1954) as follows

$$\mathrm{w}(y) = \left[F_0(y)\left(1 - F_0(y)\right)\right]^{-1} \tag{3.10}$$

The Anderson-Darling (AD) test criterion is more sensitive to the deviances in the tails of the distribution (D'Agostino and Stephens, 1986), of which the upper tail is typically the focus of extreme value analysis. The expression of AD test criterion can be obtained as follows (Anderson and Darling, 1954):

$$\begin{aligned} A_n^2 &= n \int_{-\infty}^{\infty} \frac{[F_n(x) - F_0(x)]^2}{\left[F_0(x)\left(1 - F_0(x)\right)\right]}\, dF_0(x) \\ &= -n - \frac{1}{n}\sum_{i=1}^{n}(2i-1)\left\{log\left[F_0\left(X_{(i)}\right)\right] + log\left[1 - F_0\left(X_{(n+1-i)}\right)\right]\right\} \\ &= -n - \frac{1}{n}\sum_{i=1}^{n}(2i-1)\, log\left[F_0\left(X_{(i)}\right)\right] - \frac{1}{n}\sum_{i=1}^{n}(2n+1-2i)\, log\left[1 - F_0\left(X_{(i)}\right)\right] \\ &= -n - \frac{1}{n}\sum_{i=1}^{n}(2i-1)\, log\left[U_{(i)}\right] - \frac{1}{n}\sum_{i=1}^{n}(2n+1-2i)\, log\left[1 - U_{(i)}\right] \end{aligned} \tag{3.11}$$

where, in practice, the goodness of fit can be evaluated with the calculated p-value of the Anderson-Darling test by the generally accepted guidelines as presented in Table 3.1.

For the same set of random variables $\{Y_1, Y_2, \ldots, Y_n\}$ that have a specified cumulative distribution function F_0 and an empirical distribution function F_n, if one denotes Q_0 as the quantile function of F_0 and lets $\hat{Q}$ represent the sample quantile based on the data, a quantile plot would place Q_0 on the horizontal axis and $\hat{Q}$ on the vertical axis. The horizontal and vertical coordinate of the n data points in the quantile plot can be expressed as $(Q_0(u_i), \hat{Q}\,(u_i))$, where, $u_i = \frac{i-0.5}{n}\ ,\ i = 1, 2, \ldots, n$.

The quantile plot provides a graphical technique to virtually examine the degree to which a proposed distribution model agrees with the measured data. It enables one to easily identify the outliers in the upper tail of the distribution, which is typically the focus of extreme value analysis. Thus, the quantile plot could serve as a supplement to the AD test criterion to better illustrate what does the fit in the upper tail of the distribution look like.

In addition to the quantile plot, histograms are frequently used in statistical applications to approximately display the density of the underlying distribution of the observed data. A histogram is constructed by first dividing the range of the values of the data into a sequence of intervals and then counting the number of the data points within each interval. By overlaying the histogram over the probability density function of the fitted model, one is able to visually check the agreement between the model and the data.

Table 3.1. General guidelines for goodness-of-fit assessment based on the p-value

p-value	$p < 0.01$	$0.01 < p < 0.05$	$0.05 < p < 0.15$	$0.15 < p < 0.25$	$p > 0.25$
Goodness of fit	Unacceptable	Poor	Moderately good	Good	Excellent

3.2 Statistical Methodology Formulation

The proposed statistical methodology is developed with the intent to characterize both laboratory and field data for wave-cylinder interactive response behaviors in random waves. As shown in Fig. 3.1, the flowchart of this methodology is started by the construction of the block maxima $\{Z_{n,i}\}$ from the measured time series of the target variable $X(t)$. As indicated by Coles (2001), the selection of the block size n could be critical, which is a trade-off between bias and variance. If the block size n is too small, the approximation in the extremal types theorem for the GEV distribution might no longer be valid and the bias in the estimation could become quite large. Conversely, if the block size n is taken too large, only a few block maxima would be generated while many data points of the extreme values in $X(t)$ are wasted, which could cause large variance in the estimation. Thus, the block size n needs to be appropriately determined to make sure that there are enough number of data points in the constructed block maxima $\{Z_{n,i}\}$ and the data of the peak values in the measured time series $X(t)$ are well captured. To determine the most appropriate block size and the corresponding statistical model for each set of the measured data, an iterative process is formulated as follows:

(1) Plot the partial autocorrelation function (PACF) of the measured time series $X(t)$ and choose an initial block size n where the dependence between X_i and X_{i+n} are within or very close to the 95% confidence interval (C.I.) bounds of a strict white noise.

(2) Construct the sequence of the block maxima $\{Z_{n,i}\}$ from the time series $X(t)$ with the selected block size n.

(3) Plot and examined the PACF of $\{Z_{n,i}\}$ to make sure that there is no or only weak long-range dependence.

(4) Fit the GEV distribution to the sequence of the block maxima $\{Z_{n,i}\}$.

(5) Examine the estimated values of the GEV model parameters $\hat{\xi}$, $\hat{\sigma}$, and $\hat{\mu}$. Where, $\hat{\xi}$, $\hat{\sigma}$, and $\hat{\mu}$ are the maximum likelihood estimates (MLE) of ξ, σ, and μ based on the sequence $\{Z_{n,i}\}$. Note one needs to fit Gumbel distribution to $\{Z_{n,i}\}$ for further comparison against the GEV distribution if the value 0 is within the 95% confidence interval of $\hat{\xi}$.

(6) Evaluate the goodness of fit of the model by interpretation of the Anderson-Darling test p-value and examination of the degree to which the model quantiles agrees with the empirical quantiles. Additionally, a histogram of the block maxima $\{Z_{n,i}\}$ is used to visually check the agreement between the fitted model and the observed data. Note one needs to pay special attention to the quality of fit in the upper tail of the distribution in the quantile plot.

(7) Change the value of the block size n when the goodness of fit of the model is found unsatisfactory.

(8) Repeat step (2) - (7) until both the main body and the upper tail of the distribution are satisfactorily captured by the fitted model.

The statistical computing language R (R Core Team, 2019) is utilized in the above iterative process. Coles (2001) observed that it was usually unrealistic to satisfy the temporal independence assumption for the data where extreme value statistical models were used. Instead, he noted that when the series has only weak long-range dependence at extreme levels, the block maxima still converges to the GEV family of distributions. Thus, the partial autocorrelation function (PACF) is first utilized to make sure that the constructed block maxima sequence $\{Z_{n,i}\}$ has no or only weak long-range dependence. The sensitivity of the model's performance to the selection of the block size is also examined by the Anderson-Darling test criterion and the quantile plots. In this study, maximum likelihood estimates (MLE) are used to fit the GEV distribution to the data. However, one should also note that there are many other fitting approaches such as minimizing the Anderson-Darling statistics that might produce better results for GEV distributions under certain circumstances as reported by Vanem (2015). In marine applications the risk analysis of offshore and coastal cylindrical structures is often focused on investigating the behavior of the maximum response amplitudes observed in laboratory and field measurements. The statistical characteristics of these data points of the maximum values are highly sensitive to the upper tail of the distribution. Thus, the quality of fit in this region needs special attention. To obtain a satisfactory fit in the upper tail of the distribution, multiple values of the block size are examined to find the optimal block size where the constructed sequence $\{Z_{n,i}\}$ converges best to the GEV family of distributions. The selected models could then be used to estimate the threshold-crosssing probabilities of the block maxima $\{Z_{n,i}\}$, and the predicted results could provide a quantitative basis in the process of assessing the safety of offshore cylindrical structures subjected to random seaways.

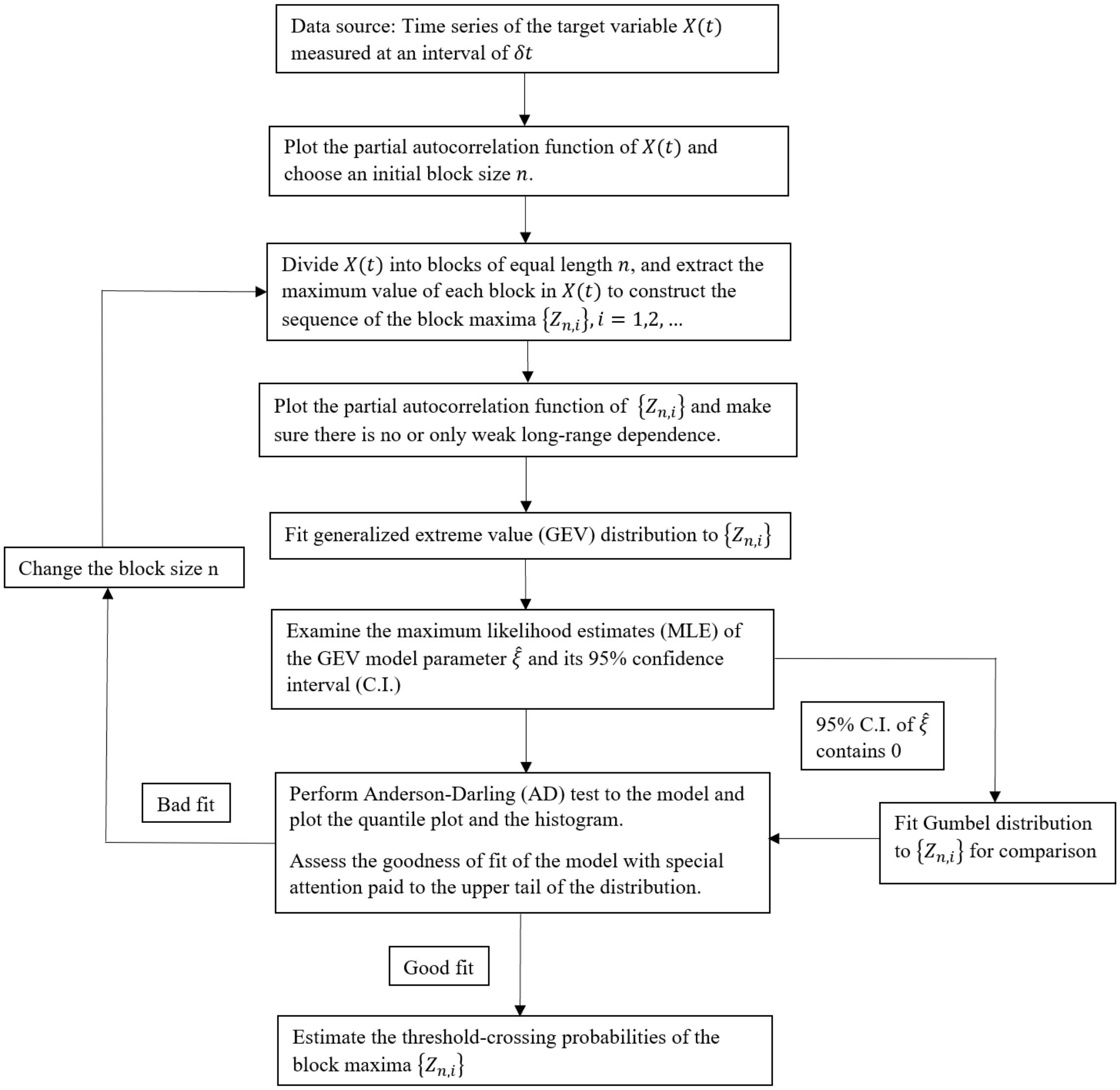

Fig. 3.1. Flowchart of the proposed statistical methodology

3.3 Case Study: Interactions of Densely Spaced Deep-Water Cylinder Arrays

The experimental data of the in-line interactions of densely spaced deep-water cylinder arrays in random waves were obtained in an industrial scale model basin test program conducted by Rijken and Niedzwecki (1997, 1998) at Offshore Technology

Research Center (OTRC). The schematic of the experimental setup is presented in Fig. 3.2, where P represents the center-to-center spacing and D is the cylinder's diameter. The OTRC tank is 45m long, 30m wide, and 5.79m deep. In the center of the tank there is a pit that is 17.76m deep from the free surface. Rijken and Niedzwecki utilized several tendons from a previous industry TLP model test program and aligned them in both paired and triple configurations in-line with the incoming waves. The prototype tendons were originally designed for an offshore TLP platform to operate at a water depth of approximately 914m (3000ft). The model test cylinders were constructed based on the Froude scaling law and the model scale was determined to be 1:55. Each cylinder had a length of 15.4m and an outer diameter of 11.9mm, and the slenderness ratio was thus approximately 1300. The outer shell of the test cylinder was made of light blue ABS tubing. In the middle of the cylinder there was an inner steel wire core of a diameter of 2.8mm that could be pretensioned. The diameter ratio between the outside diameter of the ABS tubing and the steel wire core was 4.25. The random wave conditions in the test were generated by a JONSWAP spectrum to represent an one hour realization of a 100-year storm in the North Atlantic with a significant wave height $H_S = 13.9m$, a peak period $T_p = 16.3s$, and a peak enhancement factor $\gamma = 2.0$. A white target tape with a width of 12.7mm was fixed to each test cylinder at a depth of 5.39m below the free surface and an optical tracking system was utilized to measure the target tape's displacements. Both in-line and transverse displacement time series of the target tape were recorded in their studies (Rijken and Niedzwecki, 1997, 1998). The schematic of paired and triple cylinder array configurations in-line with the incoming waves is presented in Fig. 3.3. They were tested at three pitch to diameter ratios of 3.0, 4.4, and 8.75 respectively. Two prototype top tensions of 7.023MN and 12.023MN were selected for the experimental study, and the corresponding model scale top tensions were thus approximately 42N and 72N in accordance with the Froude scaling law. In Fig. 3.4, a photo taken for the paired cylinder during the model test program was also presented for illustration.

To investigate the statistical characteristics of the response behavior of these cylinder arrays, the relative displacement $R(t)$ between adjacent cylinders is calculated as the target variable and the corresponding normalized time series are plotted in Fig. 3.5 to Fig. 3.8. Where in the test of triple cylinder arrays R_{12} and R_{23} represent the relative displacement between the two upstream elements and the two downstream elements, respectively. Each time series contains 16640 recorded data points and it lasts for a duration of 3085.2 sec. To determine an initial block size n for the block maxima $\{Z_{n,i}\}$, both the complete and zoomed-in plots of the partial autocorrelation function (PACF) of $R(t)$ are examined in Fig. 3.9 through Fig. 3.12, where the time lag represents the number of data points recorded in $R(t)$. In these figures one observes that the value of PACF remains small and stable after approximately a time lag of 150 data points. Although some exceedance over the 95% confidence interval (C.I.) boundary of a strict white noise is observed, the level of exceedance remains small. Thus, it is reasonable to initially start the iterative process with a block size of 160, and two additional block sizes of 240 and 320 are also selected for further analysis.

Then, the GEV families of distributions are fitted to the constructed block maxima $\{Z_{n,i}\}$ and the estimated parameters of the selected models at the three block sizes are summarized in Table 3.2 along with the calculated Anderson-Darling (AD) test p-values. To study the sensitivity of the model's performance to the block size, the PACF of the block maxima sequence $\{Z_{n,i}\}$, the quantile plots of the model and $\{Z_{n,i}\}$, and the histograms of $\{Z_{n,i}\}$ are presented in Fig. 3.13 through Fig. 3.21 for each of the three block sizes of 160, 240, and 320.

For the paired cylinders spaced at a pitch to diameter ratio P/D of 3.0, one observes in Fig. 3.13 that when the block size n = 160, the PACF of $\{Z_{n,i}\}$ shows significant short-range dependence while no strong long-range dependence is detected. With the block size increased to 320, the PACF falls within the 95% confidence interval (C.I.) of a strict white noise. However, one also observes that the model agrees pretty well with the data in both the quantile plots and the histograms at the three block sizes, and the corresponding AD test p-values shown in Table 3.2 are all above 0.25. These observations indicate that model's good performance is relatively insensitive to the varying block size for this case, which confirms Coles' (2001) conclusion that the block maxima still converges to the GEV family of distributions provided the long-range dependence at extreme levels is weak. When the ratio P/D of the paired cylinders was increased to 4.4, the quantile plots shown in Fig. 3.14 clearly demonstrate that the data agrees best with the model when the block size n is 240, although the corresponding PACF of $\{Z_{n,i}\}$ shows significant short-range dependence at a time lag of 1 block. This observation is also supported by the highest AD test p-value of 0.880 presented in Table 3.2. When the block size is further increased to 320, both the quantile plots and the decreasing AD test p-value indicate a higher divergence between the model and the data, although the PACF shows smaller temporal dependence. Thus, an optimal block size of 240 is determined for this cylinder pair. Finally, for the cylinder pair with a ratio P/D of 8.75, one observes in Fig. 3.15 that the PACF only shows small short-range dependence at the three difference block sizes. In general, the models agree well with the trend of the data in both the quantile plots and the histograms. Although a block size of 240 yields the highest AD test p-value of 0.721 as shown in Table 3.2, the quantile plots illustrate that a better fit in the upper tail of the distribution could be achieved when the block size is raised to 320, where the AD test p-value of 0.279 is still above 0.25. Thus, the final block size is chosen to be 320 for this cylinder pair with the largest P/D ratio.

In the investigation of the PACF of $\{Z_{n,i}\}$ for the two upstream cylinders in the triple cylinder array, one observes in Fig. 3.16 through Fig. 3.18 that given a block size of 160, the PACF shows significant short-range dependence when spaced at a ratio P/D of 3.0 and 4.4, and minor short-range dependence when the ratio P/D = 8.75. No long-range dependence is detected in these plots. When the block size n is increased to 320, the PACF shows only minor temporal dependence for the cylinder array with P/D = 3.0. With the ratio P/D increased to 4.4 and 8.75, the PACF stays within the 95% C.I. of a strict white noise. When it comes to the relative displacement between the two downstream cylinders, one observes in Fig. 3.19 through Fig. 3.21 that provided a block size of 160, the PACF shows significant short-range dependence and no long-range dependence when the cylinders were spaced at a ratio P/D of 3.0. When the ratio P/D was increased to 4.4 and 8.75, the PACF falls within the 95% C.I. of the white noise. When provided with a larger block size of 320, the PACF shows minor temporal dependence for P/D = 3.0 and 4.4 but stays within the 95% C.I. for P/D = 8.75. An interesting observation in Fig. 3.16 through Fig. 3.21 is that the data of $\{Z_{n,i}\}$ agrees pretty well with the model in both the quantile plots and the histograms for each of the three block sizes considered, and only small variations in the fit of the upper tail are found. In Table 3.2, the AD test p-values for most of the triple cylinder array cases considered are far above 0.25, and even the minimum p-value of 0.128 still indicates a moderately good fit. These observations again confirm Coles' (2001) approximation that when the long-range dependence at extreme levels is weak, the block maxima $\{Z_{n,i}\}$ still follows the GEV family of distributions.

In the following investigations of the optimal block size for the triple cylinder arrays, special attention is paid to the quality of fit in the upper tail of the distribution, which could be examined in the quantile plots. For the models fitted for the two upstream cylinders as shown in Fig. 3.16 through Fig. 3.18, one observes in Fig. 3.16 that the tail fit is almost identical at the three different block sizes when the cylinders were spaced at a ratio P/D of 3.0, and the increase in the AD test p-value could be attributed to the removal of the outlier in the lower tail of the distribution, which ceases being a block maxima given a larger block size. When the ratio P/D was increased to 4.4, the quantile plots shown in Fig. 3.17 clearly illustrate that the model provides a better fit in the upper tail when the block size is 320, under which the outlier in the lower tail no longer existed. When a ratio P/D of 8.75 was applied in the experiment, one observes in Fig. 3.18 that the models show slightly better performance in fitting the upper tail when the block size is increased to 240 and 320. In the examination of the models selected for the two downstream cylinders shown in Fig. 3.19 through Fig. 3.21, one observes in Fig. 3.19 that the models only have minor difference in the tail fit at the three block sizes given a ratio P/D of 3.0, although the AD test p-value presented in Table 3.2 favors a block size of 240. For the cylinders spaced at a ratio P/D of 4.4, the models at three block sizes are almost identical in fitting the upper tails as shown in the quantile plots of Fig. 3.20. When the ratio P/D was further increased to 8.75, one observes in Fig. 3.21 that the models with a block size of 160 and 320 fit the upper tail equally well, while the model with a block size of 240 is slightly unconservative in the upper tail. In general, the models for the triple cylinder array show significantly less variations in fitting the upper tails compared to the models selected for the paired cylinders. Thus, a uniform block size of 320 is preferred for the triple cylinder array considering the convenience in the following analysis of cylinder array's risk of collisions.

These selected models based on the most appropriate block sizes provide a way to assess the risk of cylinder collisions. Based on these models the threshold-crossing probabilities of the paired cylinder's maximum relative displacement in a duration of 44.5 sec (block size n = 240) and 59.3 sec (block size n = 320) are predicted in Table 3.3. In Table 3.3, one observes that when the top tension is 42N, although the crossing probabilities over 1.0D to 2.0D are predicted for a shorter duration of 44.5 sec for the paired cylinders at a ratio P/D of 4.4, they are still 1.84 to 4.34 times higher than corresponding predictions for the cylinder pair spaced at a ratio P/D of 8.75. This observation is found to be consistent with practical experience that collisions are more likely to occur in cylinder arrays that are more densely spaced. When the paired cylinders were spaced at a smaller P/D ratio of 3.0 and applied a higher top tension of 72N, they are predicted to encounter approximately 25% to 65% less crossing probabilities in a duration of 44.5 sec over all the three threshold values from 1.0D to 2.0D, compared to the cylinder pair with a ratio P/D of 4.4 and a top tension of 42N. When a larger block size of 320 is chosen for the cylinder pair spaced at $P/D = 3.0$, they are still predicted to have 18% to 31% smaller crossing probabilities over 1.5D to 2.0D, although in a longer duration of 59.3 sec, than the predicted probabilities corresponding to a shorter duration of 44.5 sec for the paired cylinders with $P/D = 4.4$. These observed results are also consistent with the experience that increasing the top tension could effectively reduce the amplitude of relative displacement of deep-water cylinder arrays and thus make them less susceptible to collisions.

Since a uniform block size of 320 is selected for the triple cylinder arrays, the predicted probabilities presented in Table 3.4 represent the threshold-crossing probabilities of adjacent cylinders' maximum relative displacement in a duration of 59.3 sec. In Table 3.4, it is observed that when the triple cylinder array was spaced at a ratio P/D of 4.4, cylinder 2 and 3 are predicted to have higher threshold-crossing probabilities than cylinder 1 and 2 at relatively low threshold values of 1.0D and 1.5D. When the threshold value was increased to 2.0D, cylinder 2 and 3 are predicted to have approximately 47% less crossing probabilities than the first two cylinders, and this difference in the crossing probabilities could reach an order of 10 when the threshold value was increased to 3.0D. Similar observations could also be found for the cylinder array spaced at a ratio P/D of 8.75. Although cylinder 2 and 3 are predicted to have 30% higher crossing probabilities over a low threshold of 1.0D than the two upstream elements, the calculated probabilities again show a reverse trend as the threshold becomes large. Given a larger threshold value of 1.5D, cylinder 1 and 2 are predicted to have 4 times higher crossing probabilities than cylinder 2 and 3, and this difference in the crossing probabilities again rose above an order of 10 when the threshold value was further increased to 2.0D and 3.0D. These observations are found to be consistent with the calculation experience reported by Huse (1993) that in a deep-water riser array the two most upstream elements are usually the first to encounter collisions. When the cylinders were placed at a ratio P/D of 3.0, cylinder 2 and 3 are unexpectedly predicted to have a significantly higher collision probability for $Z > 2.0D$ than the two upstream elements. This unexpected result is also found in agreement with the measured time series in Fig. 3.6. One could easily notice that $R_{23}(t)$ has two peaks larger than 1.5D and another four peaks ranging from 1.2D to 1.5D while the maximum value of $R_{12}(t)$ does not exceed 1.2D. These observations not only demonstrate the complexity of the interactive response behavior of densely spaced deep-water cylinder arrays in random waves, but also illustrate the capacity of this statistical methodology to characterize industrial scale model basin data, capture unexpected response phenomena and suggest targets for further investigative studies.

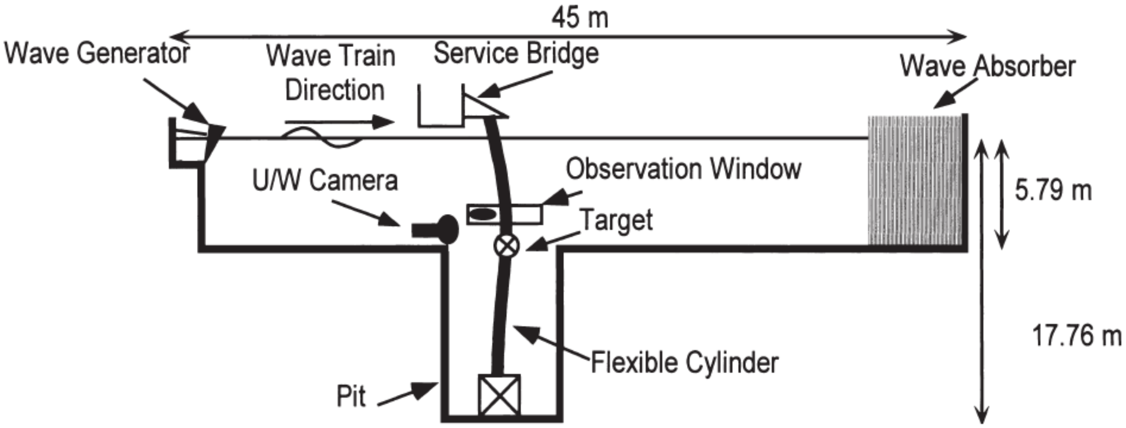

Fig. 3.2. Schematic of the experimental set up of cylinder arrays in the model basin (reprinted from Rijken and Niedzwecki, 1998)

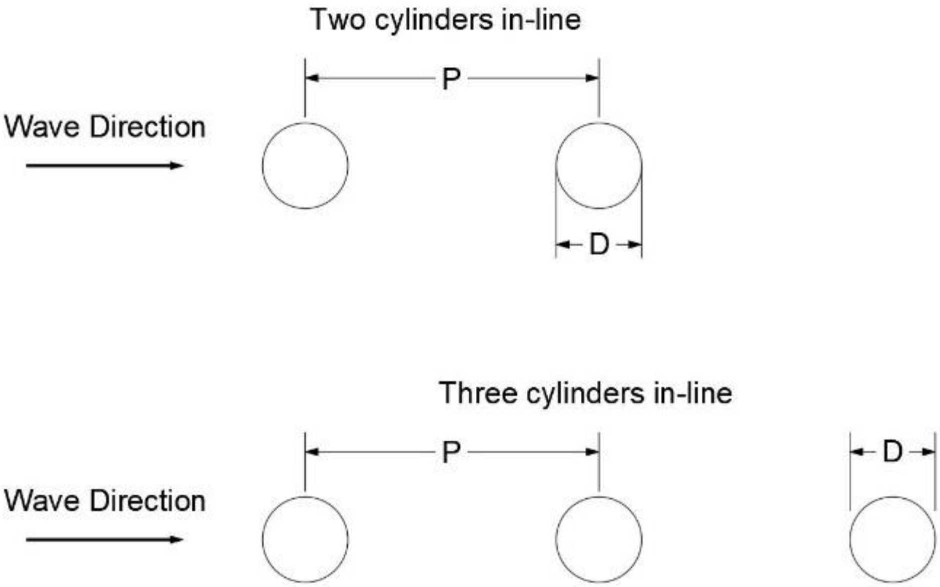

Fig. 3.3. Top view of cylinder array configurations (reprinted from Lu and Niedzwecki, 2020)

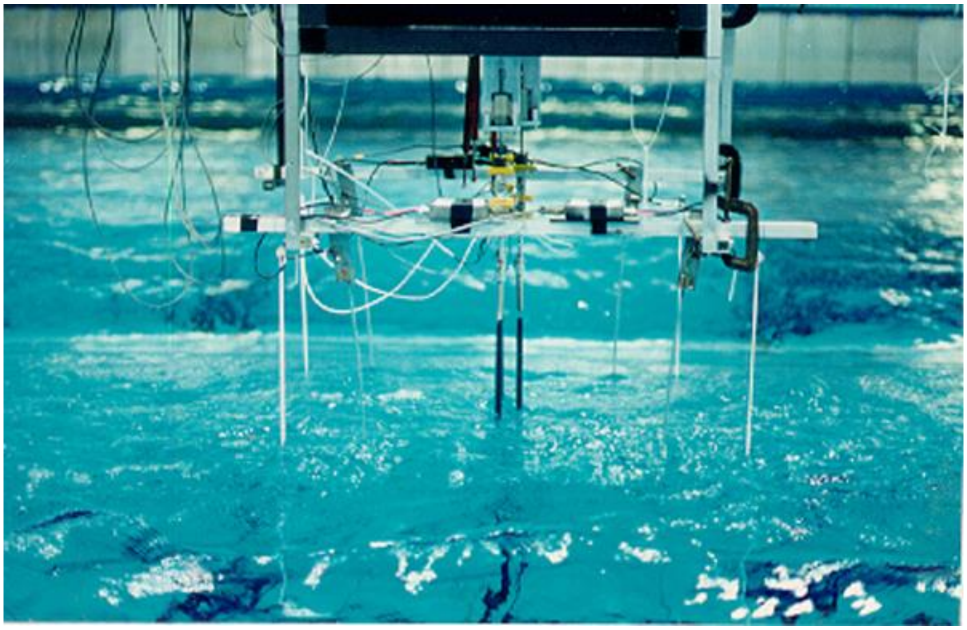

Fig. 3.4. Paired cylinder array in the test (Rijken and Niedzwecki, 1998)

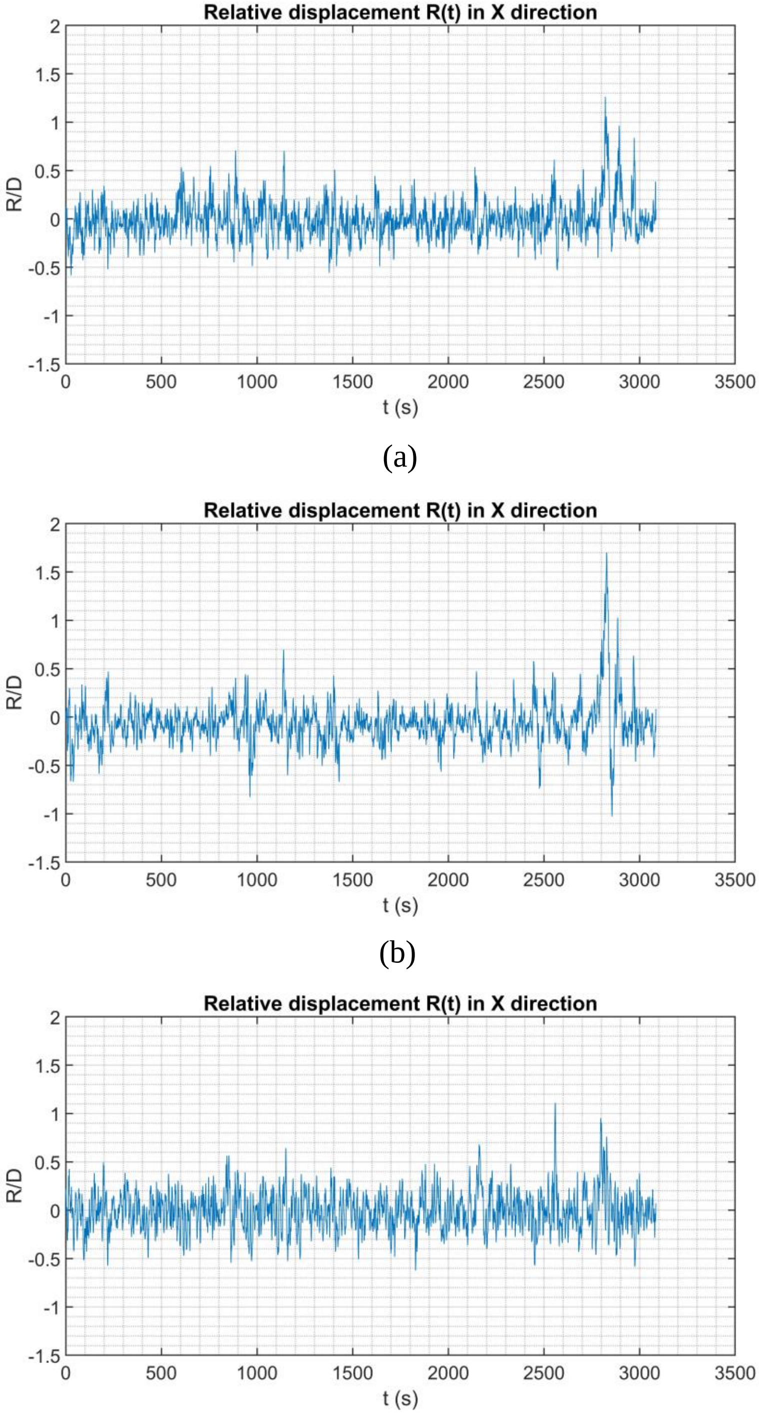

(a)

(b)

(c)

Fig. 3.5. Normalized in-line relative displacement between the paired cylinders at a ratio $\boldsymbol{P/D}$ of (a) 3.0, (b) 4.4, (c) 8.75.

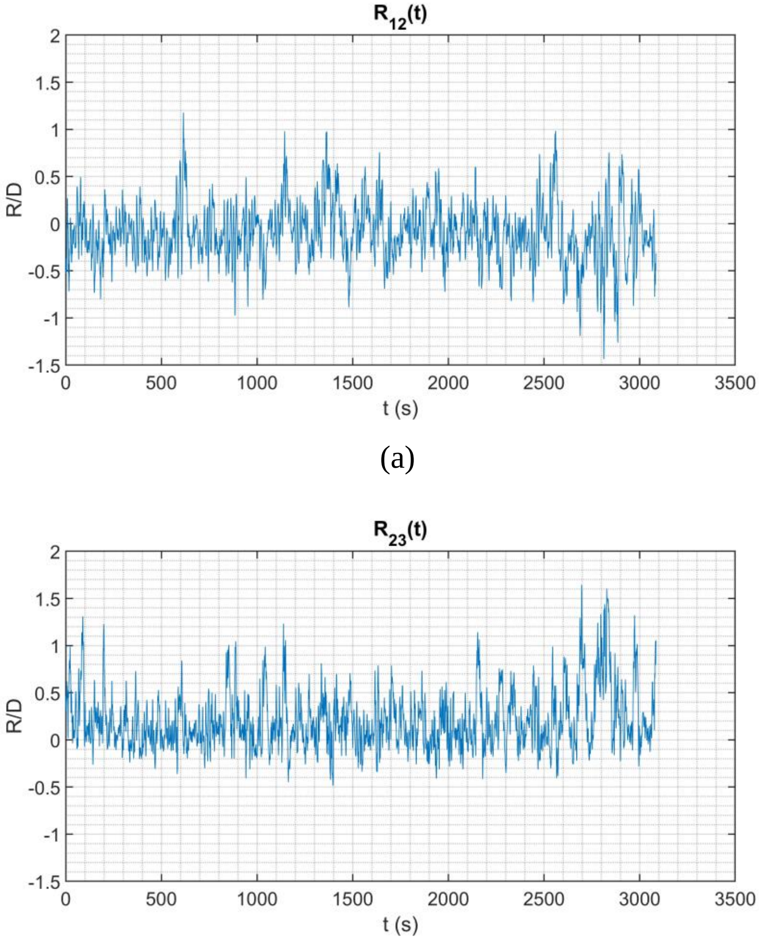

(a)

(b)

Fig. 3.6. Normalized in-line relative displacement of the triple cylinder array at a ratio $\boldsymbol{P/D}$ of 3.0 between (a) cylinder 1 and cylinder 2, (b) cylinder 2 and cylinder 3.

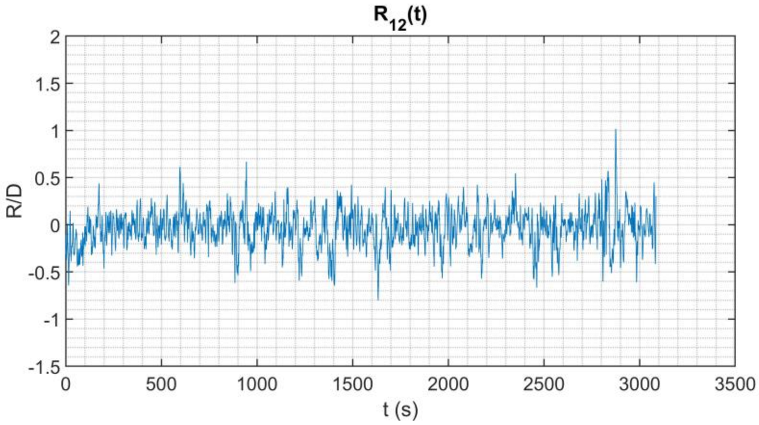

(a)

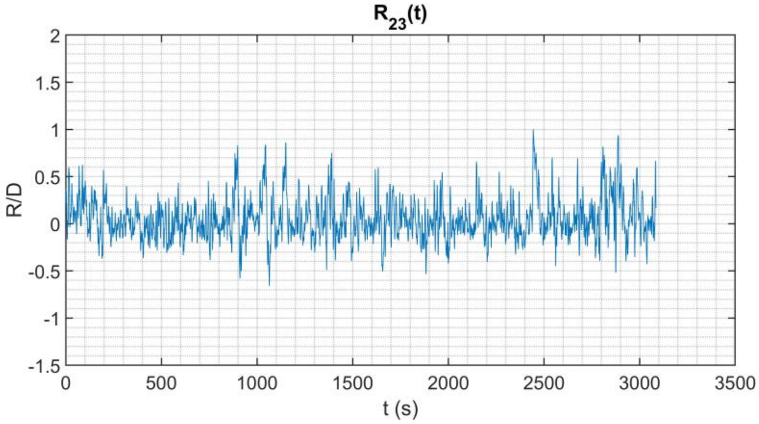

(b)

Fig. 3.7. Normalized in-line relative displacement of the triple cylinder array at a ratio $\boldsymbol{P/D}$ of 4.4 between (a) cylinder 1 and cylinder 2, (b) cylinder 2 and cylinder 3.

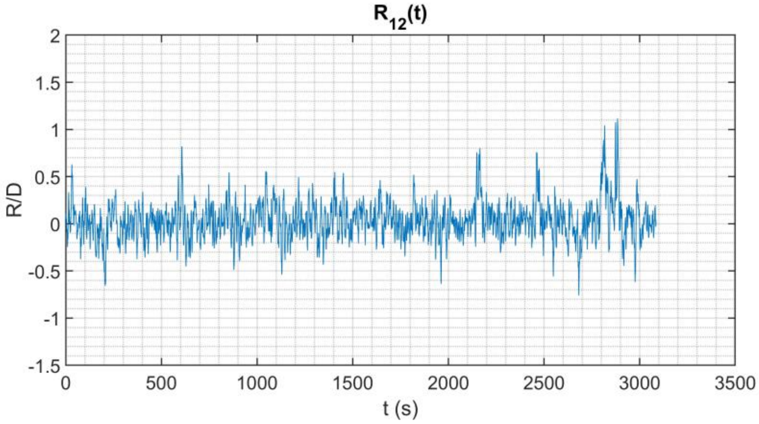

(a)

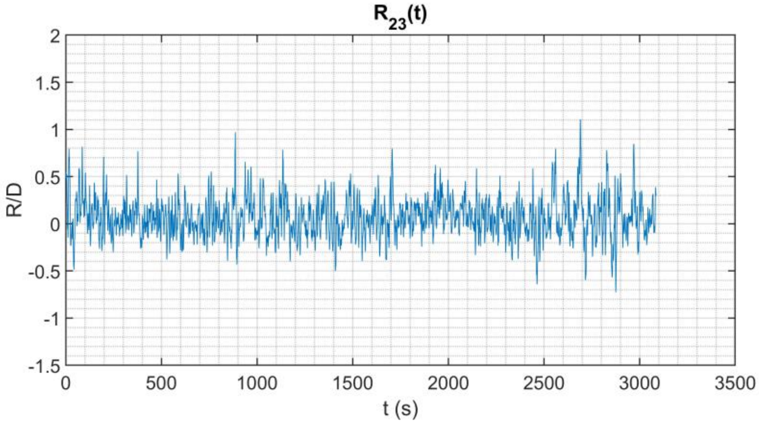

(b)

Fig. 3.8. Normalized in-line relative displacement of the triple cylinder array at a ratio P/D of 8.75 between (a) cylinder 1 and cylinder 2, (b) cylinder 2 and cylinder 3.

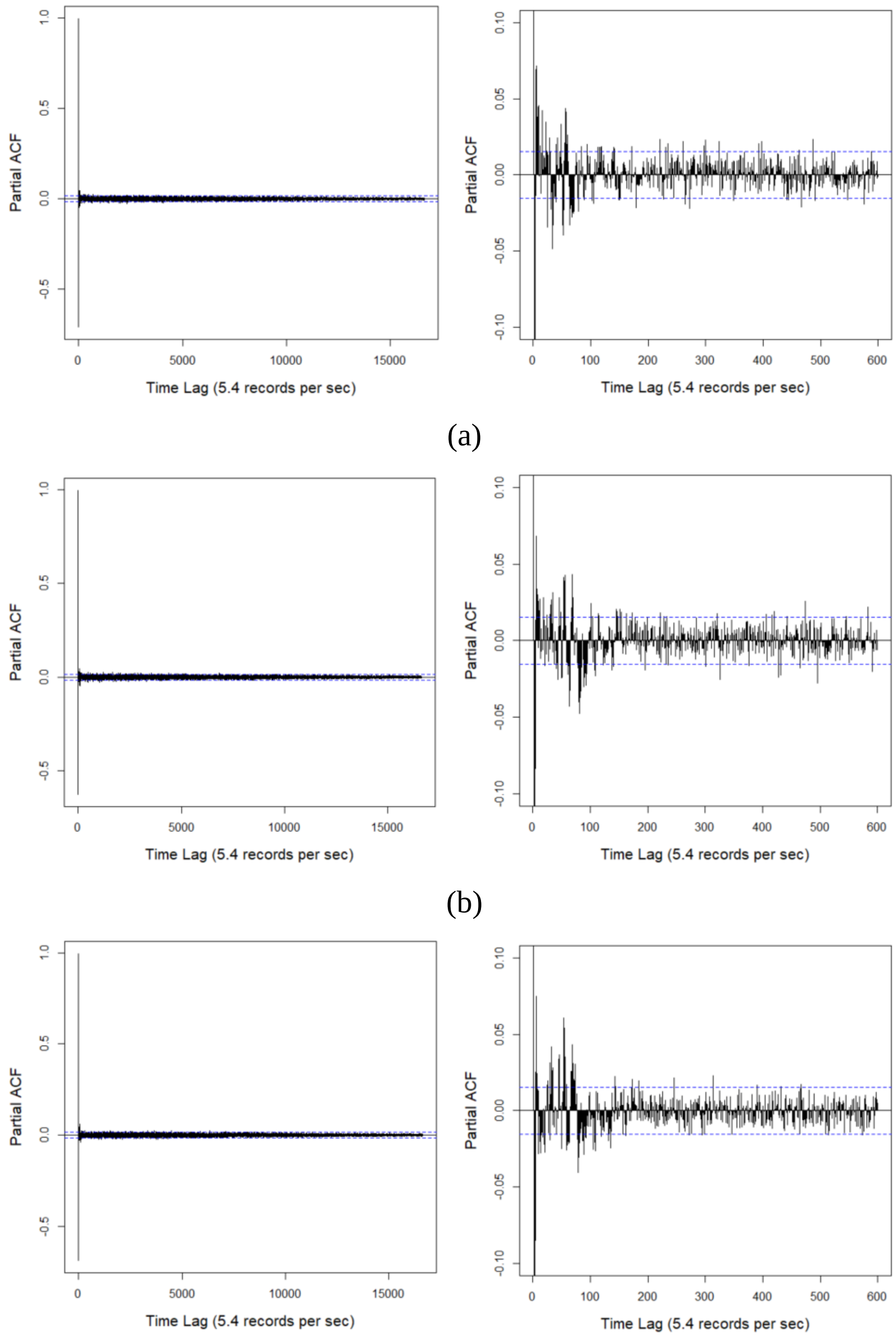

(a)

(b)

(c)

Fig. 3.9. PACF of the in-line relative displacement $R(t)$, complete plot of the 16640 data points (left) and zoomed-in plot for the first 600 data points (right), between the paired cylinders at a ratio P/D of (a) 3.0, (b) 4.4, (c) 8.75.

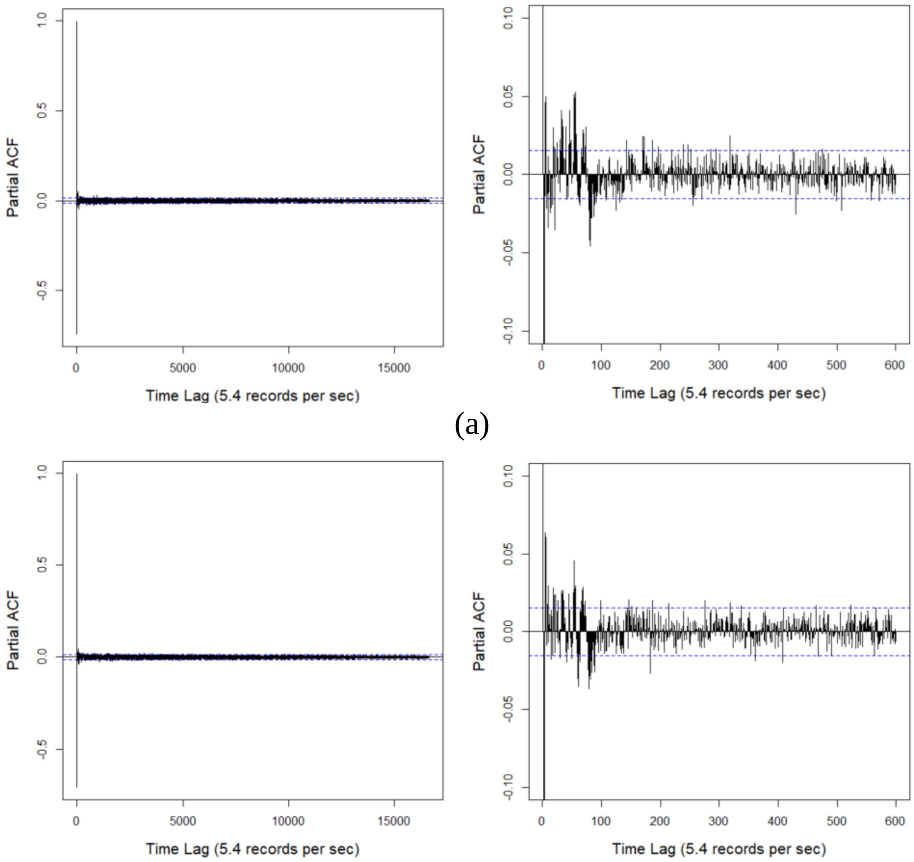

(a)

(b)

Fig. 3.10. PACF of the in-line relative displacement $R(t)$, complete plot of the 16640 data points (left) and zoomed-in plot for the first 600 data points (right), of the triple cylinder array at a ratio P/D of 3.0 between (a) cylinder 1 and cylinder 2, (b) cylinder 2 and cylinder 3.

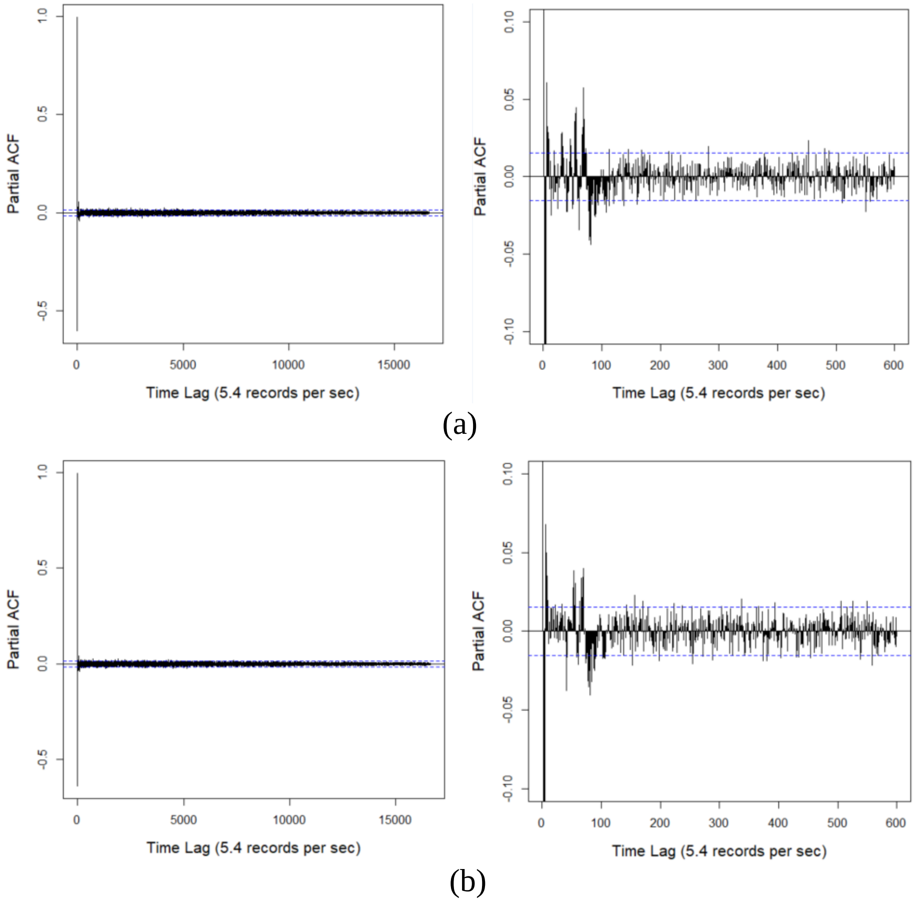

Fig. 3.11. PACF of the in-line relative displacement $\boldsymbol{R(t)}$, complete plot of the 16640 data points (left) and zoomed-in plot for the first 600 data points (right), of the triple cylinder array at a ratio $\boldsymbol{P/D}$ of 4.4 between (a) cylinder 1 and cylinder 2, (b) cylinder 2 and cylinder 3.

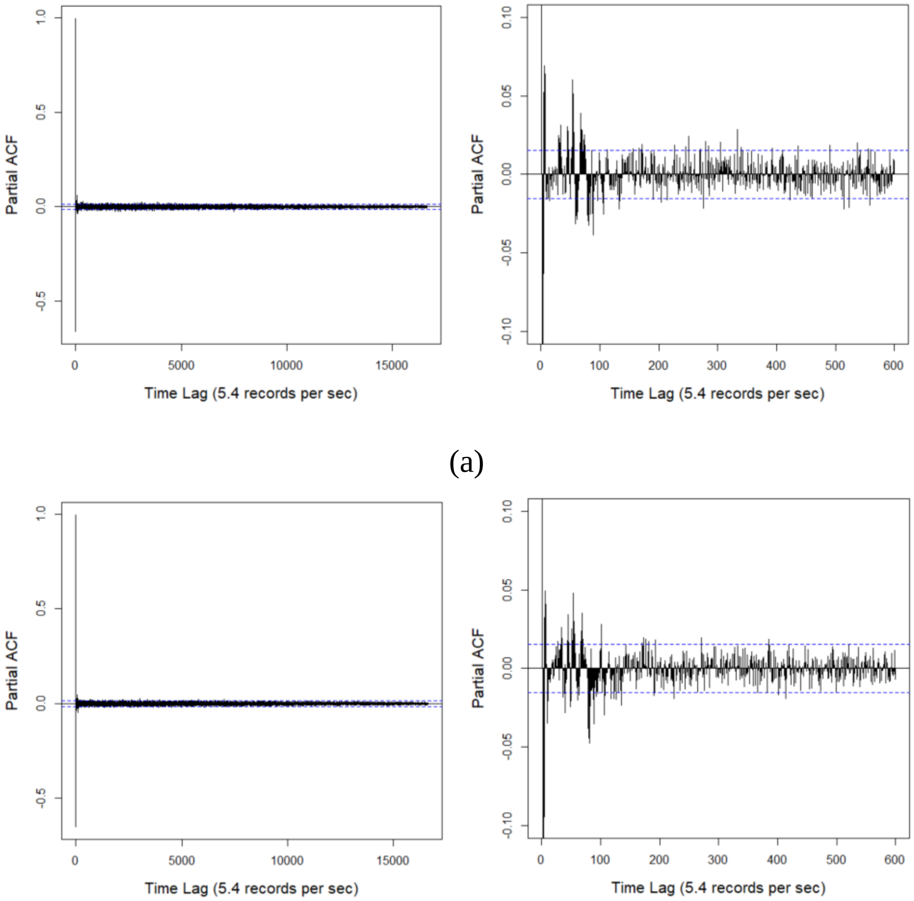

(a)

(b)

Fig. 3.12. PACF of the in-line relative displacement $\boldsymbol{R(t)}$, complete plot of the 16640 data points (left) and zoomed-in plot for the first 600 data points (right), of the triple cylinder array at a ratio $\boldsymbol{P/D}$ of 8.75 between (a) cylinder 1 and cylinder 2, (b) cylinder 2 and cylinder 3.

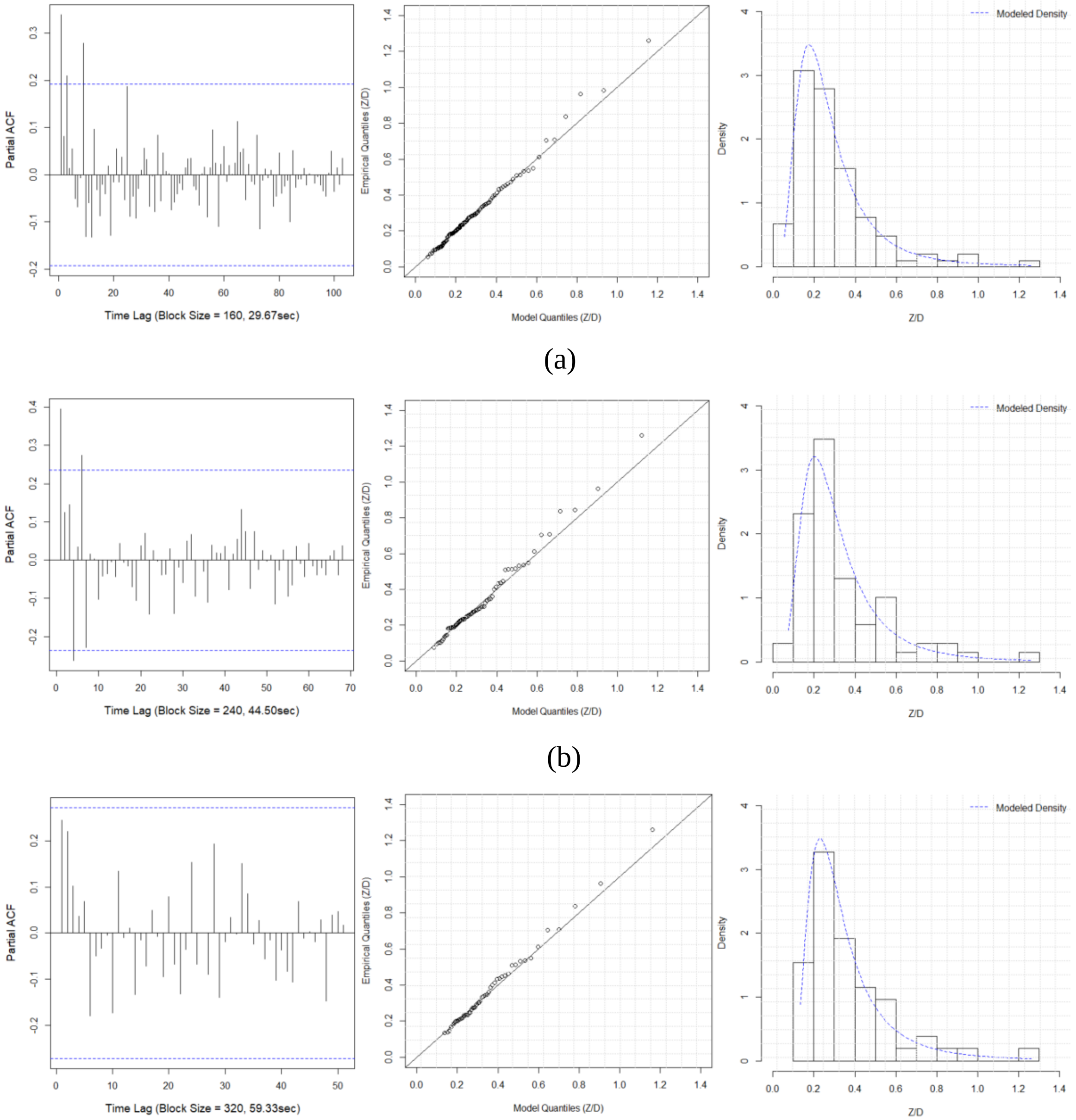

(a)

(b)

(c)

Fig. 3.13. PACF of the block maxima $\{\boldsymbol{Z_{n,i}}\}$ (left), quantile plots of the GEV model fitted to $\{\boldsymbol{Z_{n,i}}\}$ (middle), and density plot of the fitted GEV model compared with the histograms of $\{\boldsymbol{Z_{n,i}}\}$ (right) for the relative displacement between the paired cylinders at a ratio $\boldsymbol{P/D}$ of 3.0, with a block size of (a) n = 160; (b) n = 240; (c) n = 320.

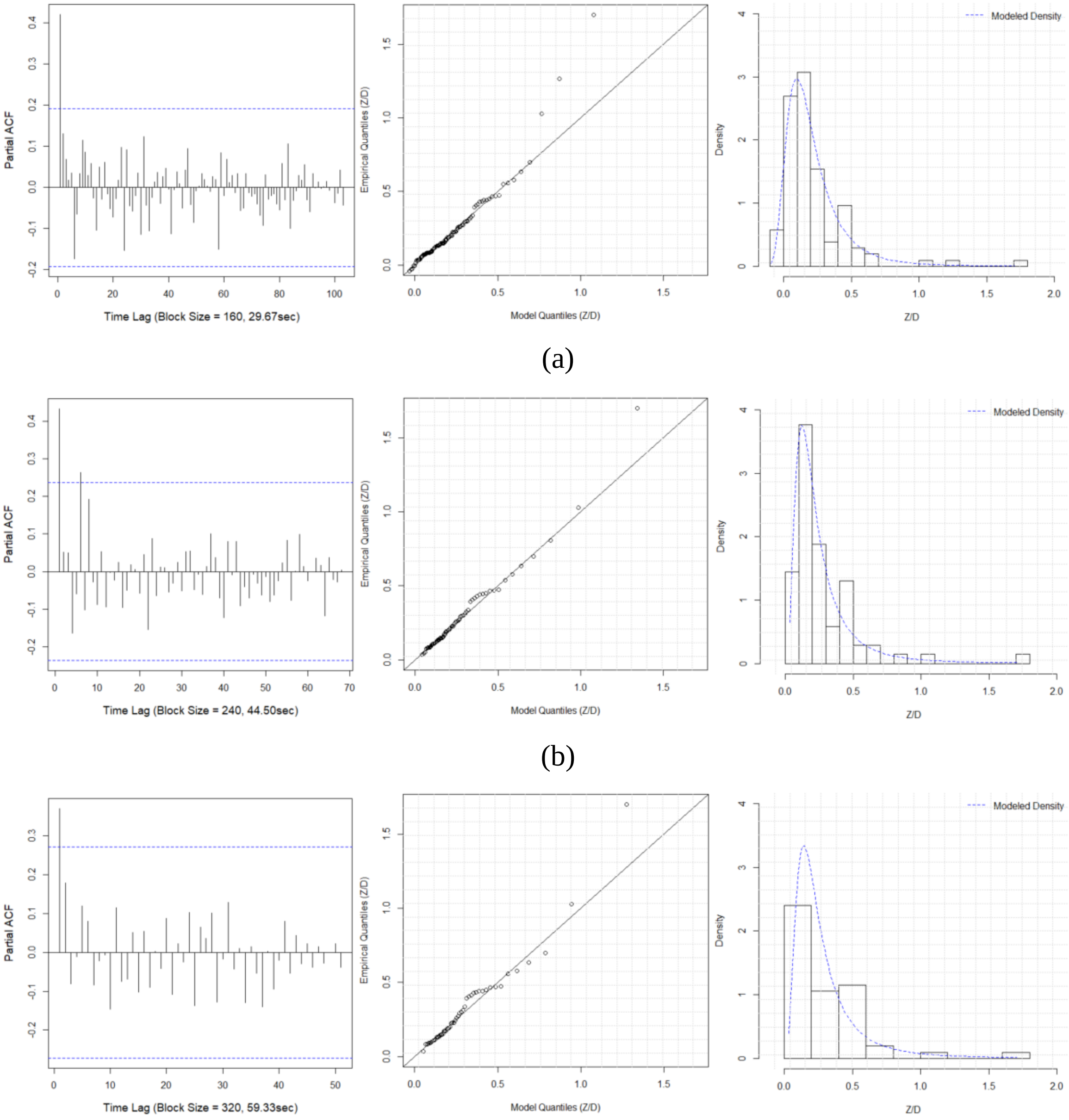

(a)

(b)

(c)

Fig. 3.14. PACF of the block maxima $\{\boldsymbol{Z_{n,i}}\}$ (left), quantile plots of the GEV model fitted to $\{\boldsymbol{Z_{n,i}}\}$ (middle), and density plot of the fitted GEV model compared with the histograms of $\{\boldsymbol{Z_{n,i}}\}$ (right) for the relative displacement between the paired cylinders at a ratio $\boldsymbol{P/D}$ of 4.4, with a block size of (a) n = 160; (b) n = 240; (c) n = 320.

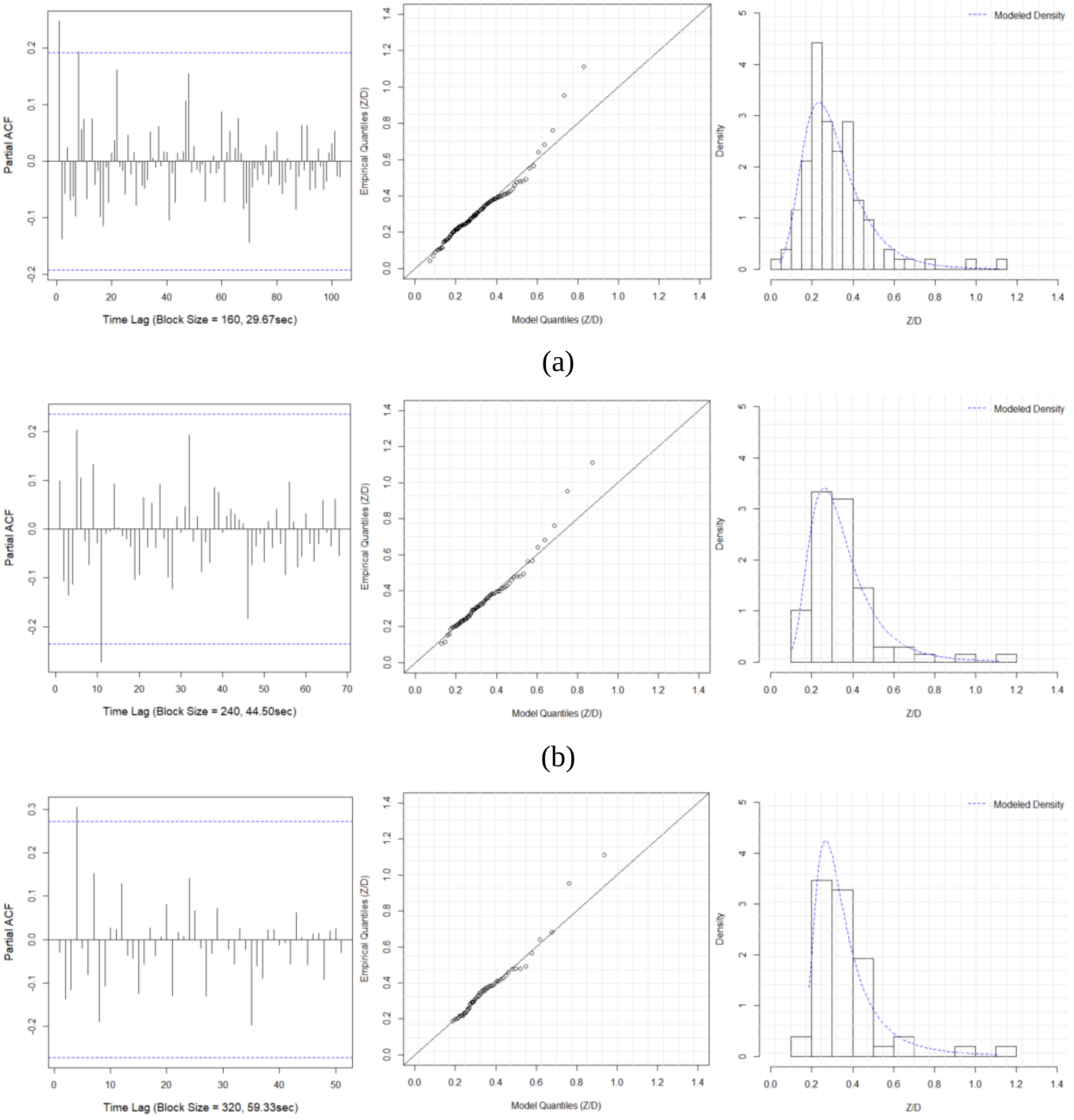

(a)

(b)

(c)

Fig. 3.15. PACF of the block maxima $\{\boldsymbol{Z_{n,i}}\}$ (left), quantile plots of the GEV model fitted to $\{\boldsymbol{Z_{n,i}}\}$ (middle), and density plot of the fitted GEV model compared with the histograms of $\{\boldsymbol{Z_{n,i}}\}$ (right) for the relative displacement between the paired cylinders at a ratio $\boldsymbol{P/D}$ of 8.75, with a block size of (a) n = 160; (b) n = 240; (c) n = 320.

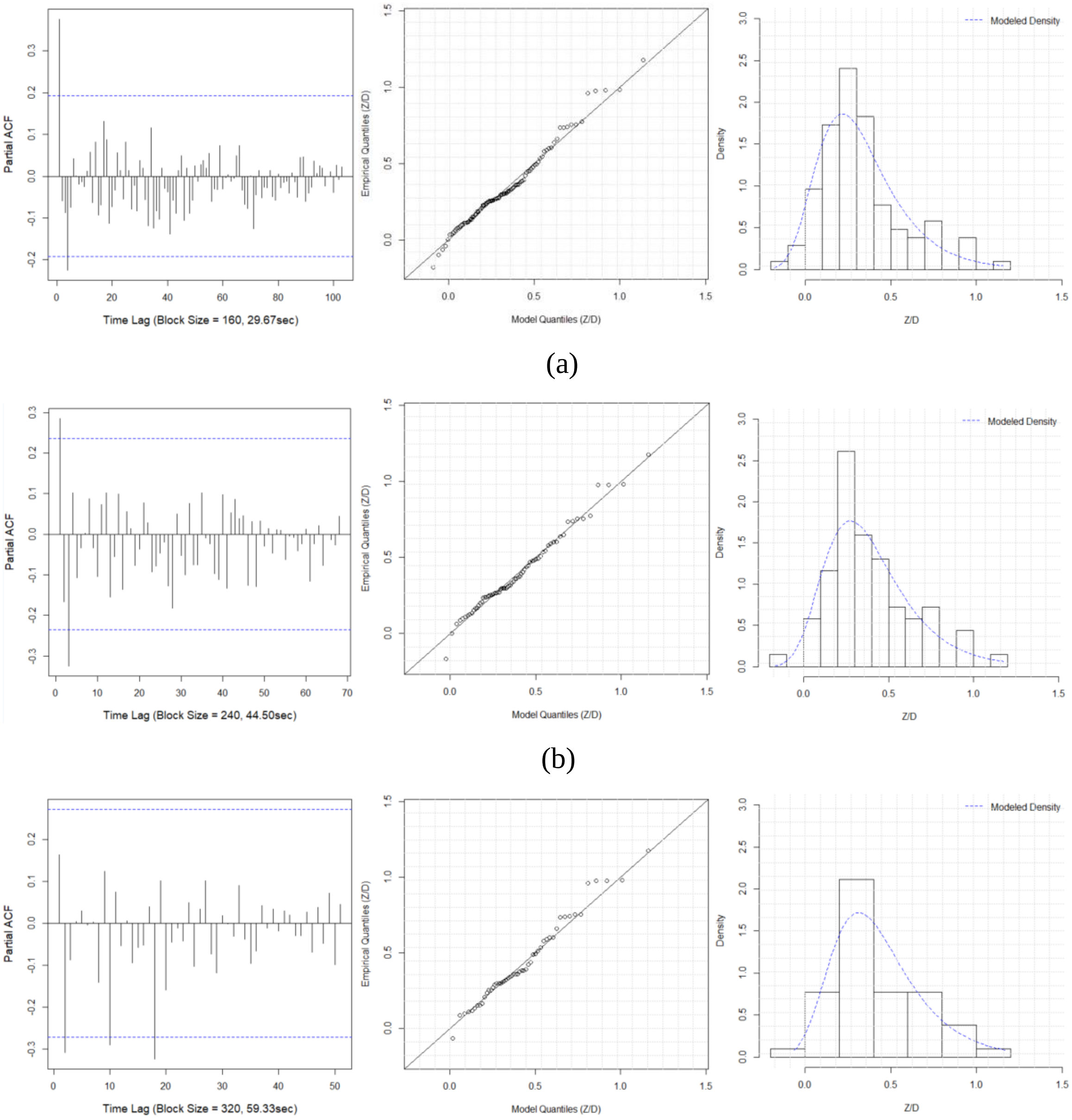

(a)

(b)

(c)

Fig. 3.16. PACF of the block maxima $\{\boldsymbol{Z}_{\boldsymbol{n},\boldsymbol{i}}\}$ (left), quantile plots of the Gumbel model fitted to $\{\boldsymbol{Z}_{\boldsymbol{n},\boldsymbol{i}}\}$ (middle), and density plot of the fitted Gumbel model compared with the histograms of $\{\boldsymbol{Z}_{\boldsymbol{n},\boldsymbol{i}}\}$ (right) for the relative displacement between cylinder 1 and cylinder 2 of the triple cylinder array at a ratio $\boldsymbol{P}/\boldsymbol{D}$ of 3.0, with a block size of (a) n = 160; (b) n = 240; (c) n = 320.

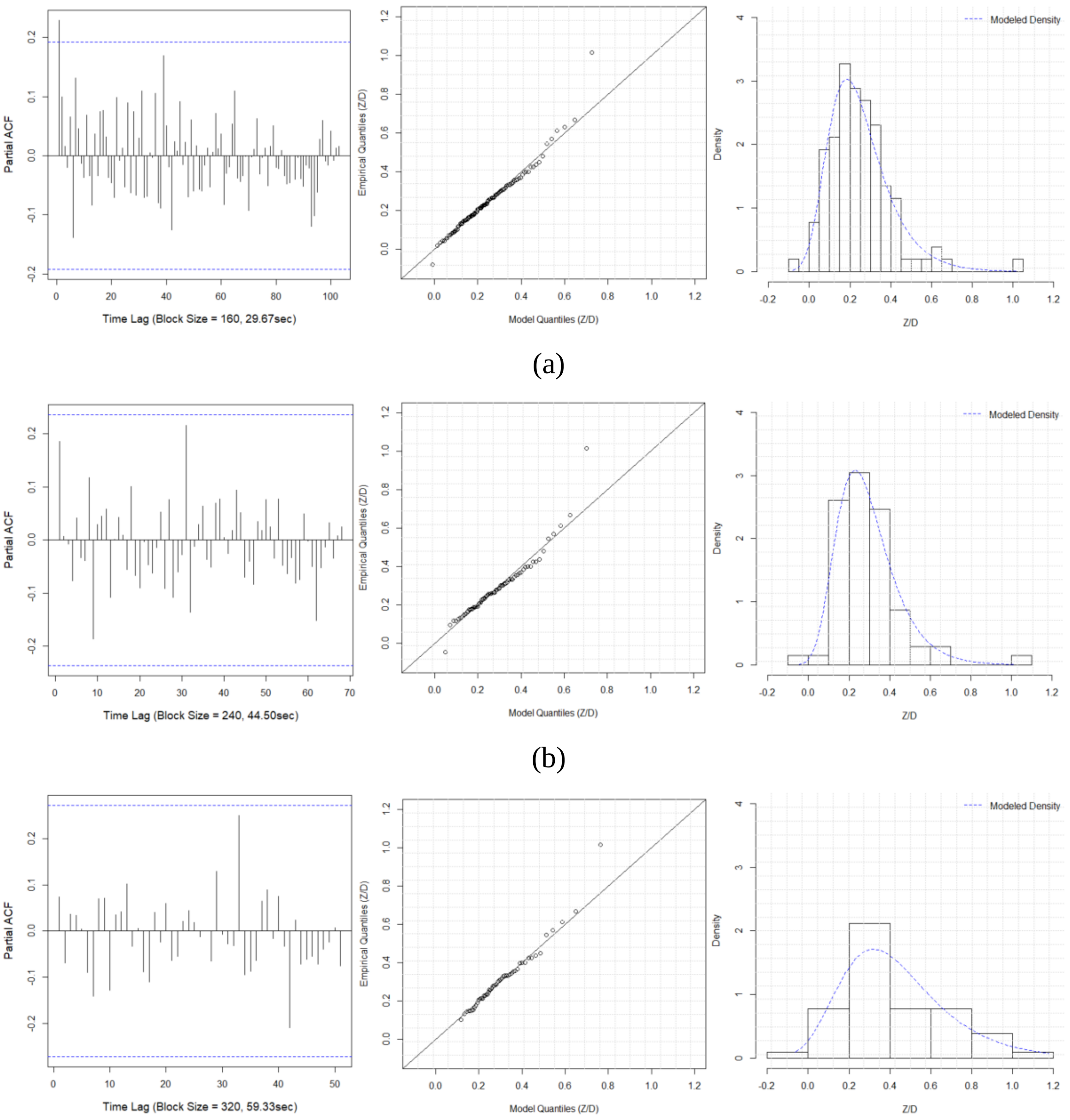

(a)

(b)

(c)

Fig. 3.17. PACF of the block maxima $\{\boldsymbol{Z_{n,i}}\}$ (left), quantile plots of the GEV model fitted to $\{\boldsymbol{Z_{n,i}}\}$ (middle), and density plot of the fitted GEV model compared with the histograms of $\{\boldsymbol{Z_{n,i}}\}$ (right) for the relative displacement between cylinder 1 and cylinder 2 of the triple cylinder array at a ratio $\boldsymbol{P/D}$ of 4.4, with a block size of (a) n = 160; (b) n = 240; (c) n = 320.

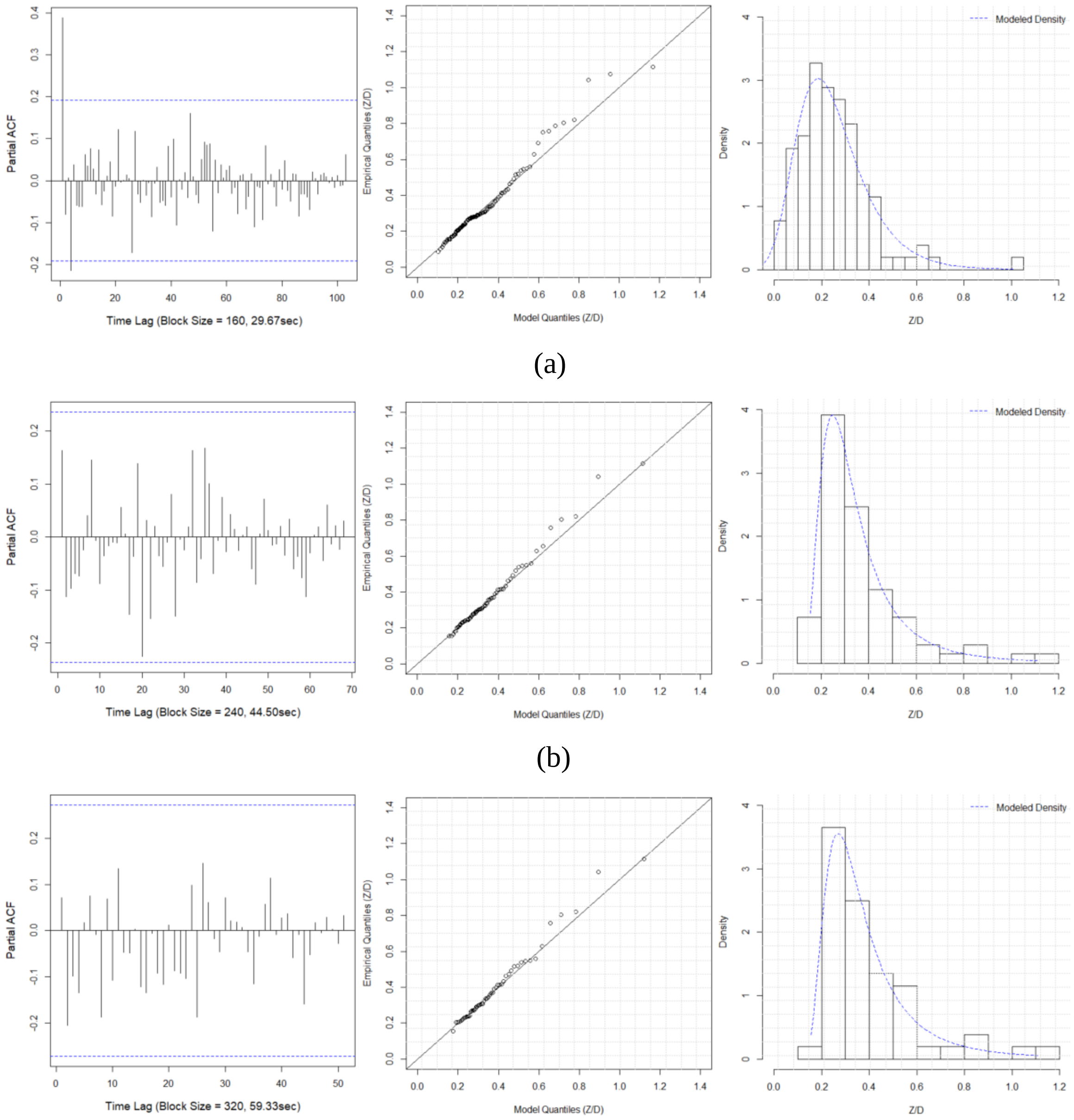

(a)

(b)

(c)

Fig. 3.18. PACF of the block maxima $\{Z_{n,i}\}$ (left), quantile plots of the GEV model fitted to $\{Z_{n,i}\}$ (middle), and density plot of the fitted GEV model compared with the histograms of $\{Z_{n,i}\}$ (right) for the relative displacement between cylinder 1 and cylinder 2 of the triple cylinder array at a ratio P/D of 8.75, with a block size of (a) n = 160; (b) n = 240; (c) n = 320.

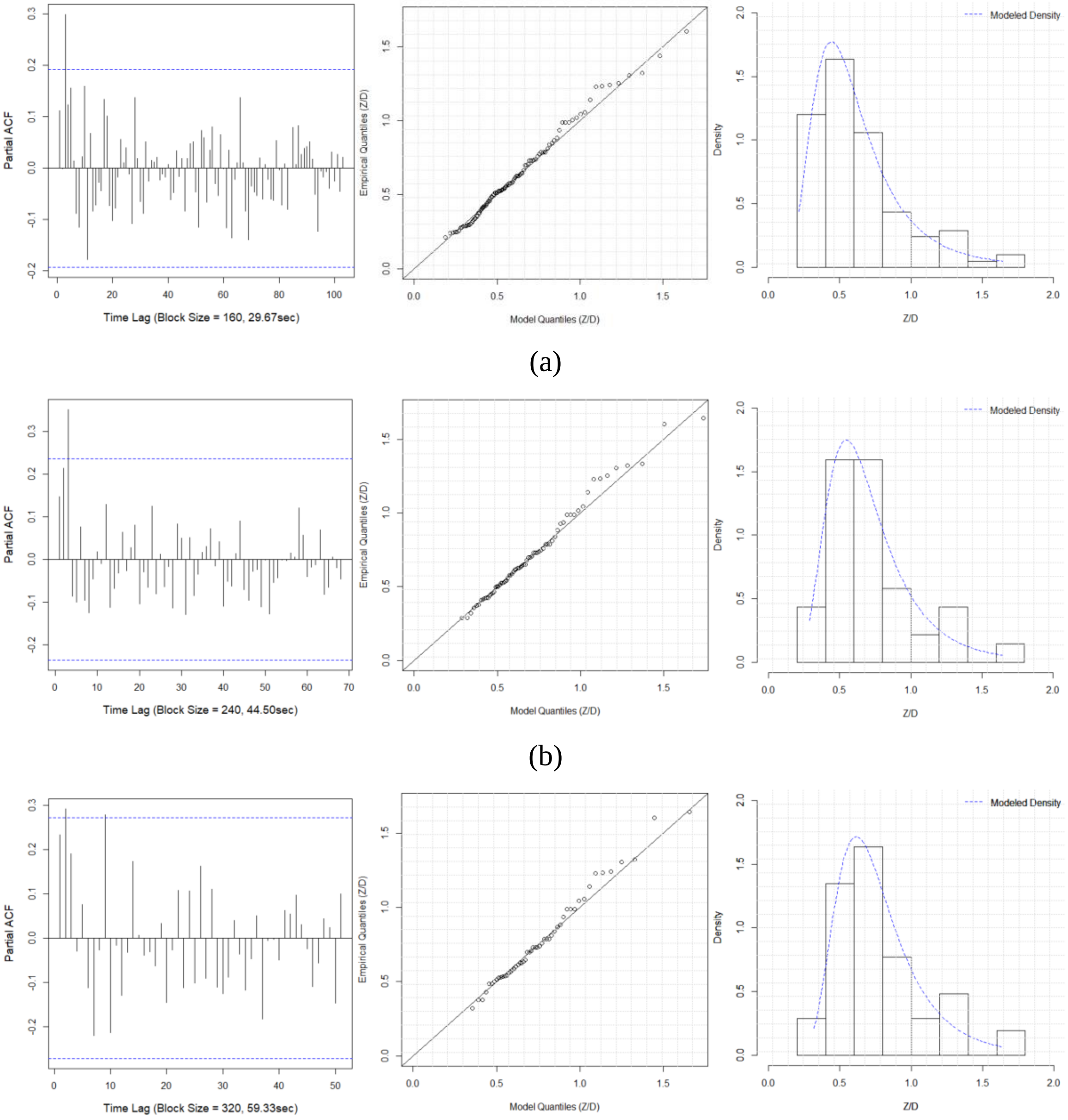

(c)

Fig. 3.19. PACF of the block maxima $\{\boldsymbol{Z_{n,i}}\}$ (left), quantile plots of the GEV model fitted to $\{\boldsymbol{Z_{n,i}}\}$ (middle), and density plot of the fitted GEV model compared with the histograms of $\{\boldsymbol{Z_{n,i}}\}$ (right) for the relative displacement between cylinder 2 and cylinder 3 of the triple cylinder array at a ratio $\boldsymbol{P/D}$ of 3.0, with a block size of (a) n = 160; (b) n = 240; (c) n = 320.

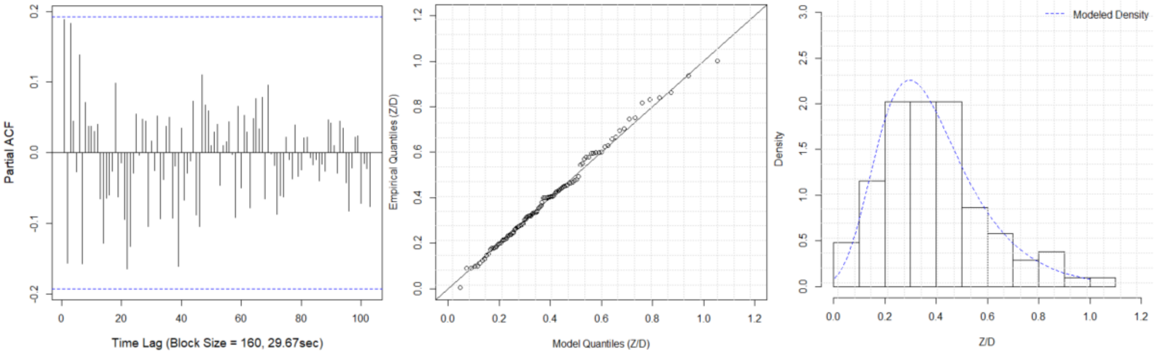

(a)

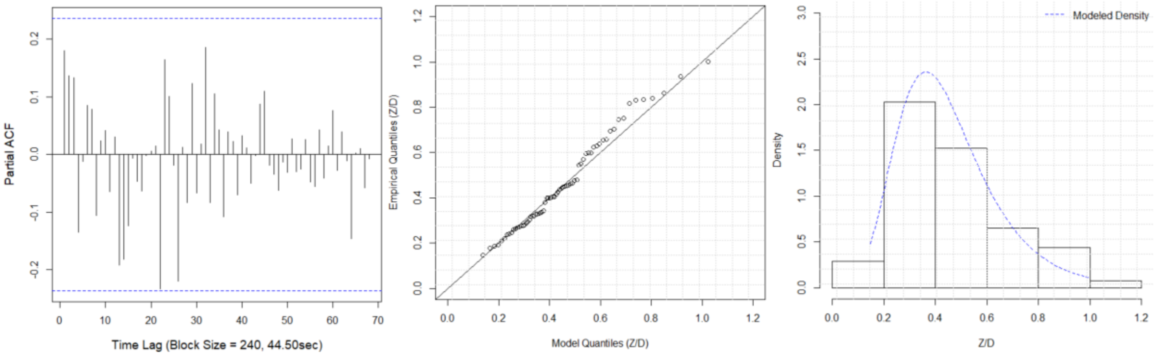

(b)

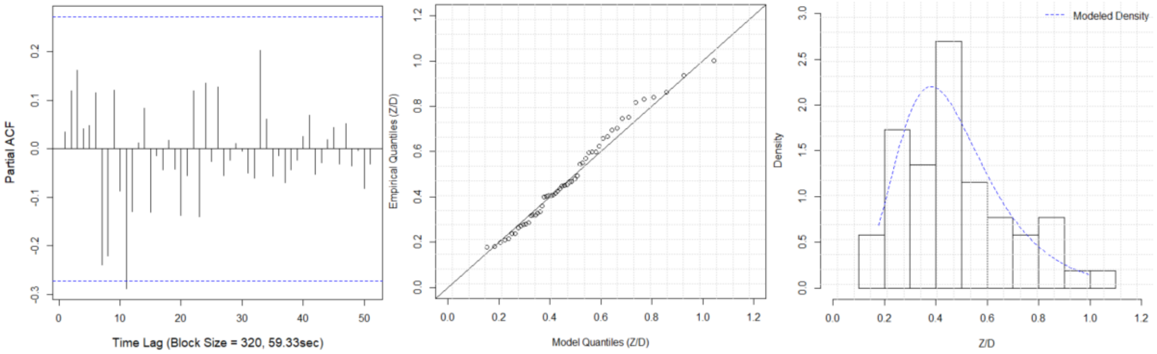

(c)

Fig. 3.20. PACF of the block maxima $\{\boldsymbol{Z}_{n,i}\}$ (left), quantile plots of the Gumbel model fitted to $\{\boldsymbol{Z}_{n,i}\}$ (middle), and density plot of the fitted Gumbel model compared with the histograms of $\{\boldsymbol{Z}_{n,i}\}$ (right) for the relative displacement between cylinder 2 and cylinder 3 of the triple cylinder array at a ratio $\boldsymbol{P/D}$ of 4.4, with a block size of (a) n = 160; (b) n = 240; (c) n = 320.

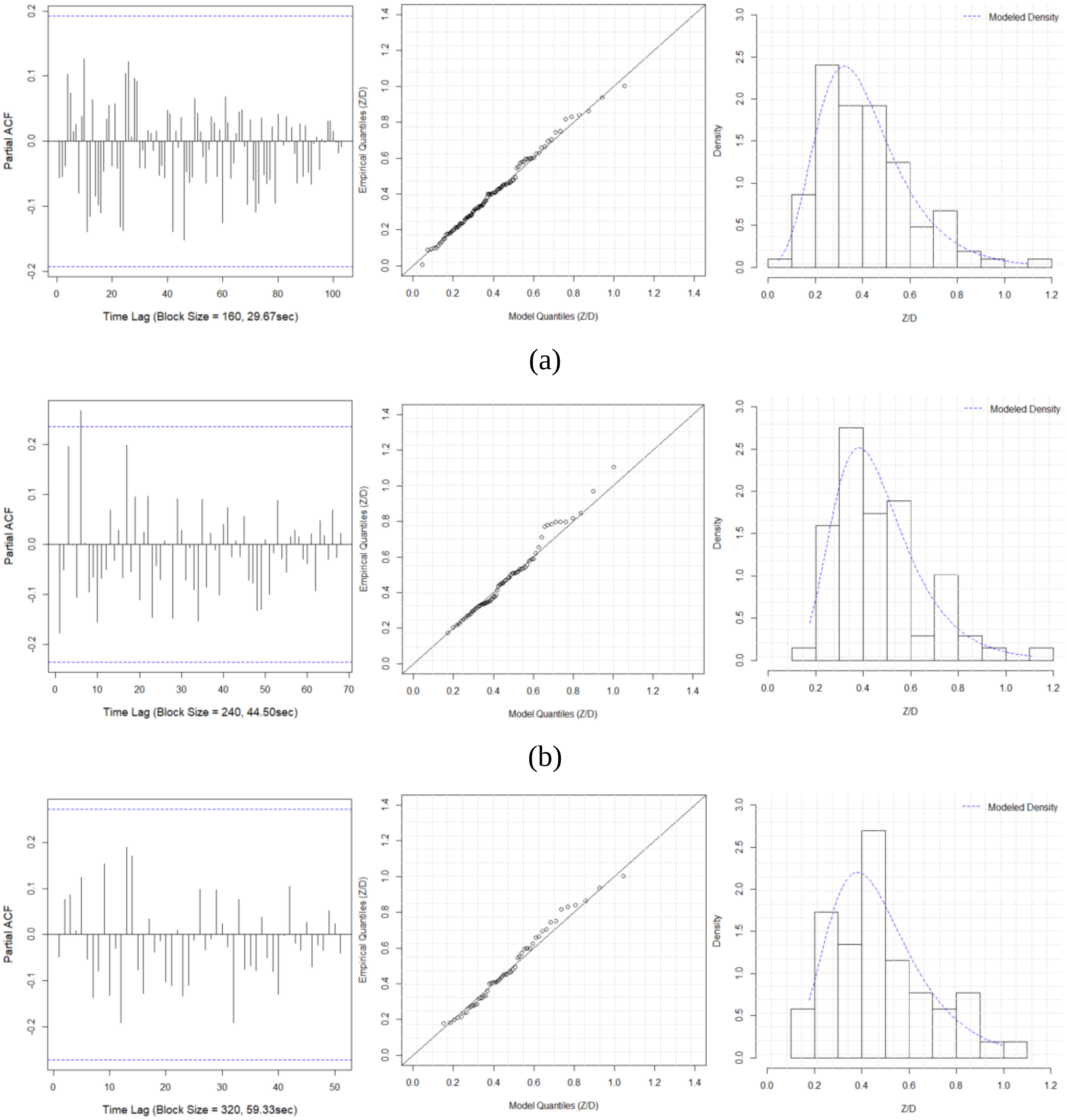

(a)

(b)

(c)

Fig. 3.21. PACF of the block maxima $\{\boldsymbol{Z_{n,i}}\}$ (left), quantile plots of the Gumbel model fitted to $\{\boldsymbol{Z_{n,i}}\}$ (middle), and density plot of the fitted Gumbel model compared with the histograms of $\{\boldsymbol{Z_{n,i}}\}$ (right) for the relative displacement between cylinder 2 and cylinder 3 of the triple cylinder array at a ratio $\boldsymbol{P/D}$ of 8.75, with a block size of (a) n = 160; (b) n = 240; (c) n = 320.

Table 3.2. Comparison of statistical models for paired and triple cylinder arrays at three different block sizes

	Block size **n=160**				Block size **n=240**				Block size **n=320**			
	$\hat{\mu}$	$\hat{\sigma}$	$\hat{\xi}$	AD test p-value	$\hat{\mu}$	$\hat{\sigma}$	$\hat{\xi}$	AD test p-value	$\hat{\mu}$	$\hat{\sigma}$	$\hat{\xi}$	AD test p-value
Relative displacement between the paired cylinders, top tension = 72N for P/D = 3, and 42N for P/D = 4.4 and 8.75												
p/d = 3, GEV	0.1982	0.1088	0.2507	0.879	0.2292	0.1179	0.2514	0.402	0.2606	0.1107	0.3286	0.930
p/d = 4.4, GEV	0.1189	0.1259	0.1980	0.167	0.1565	0.1051	0.4049	0.880	0.1789	0.1173	0.3856	0.354
p/d = 8.75, GEV	0.2394	0.1130	0.0490	0.224	0.2728	0.1087	0.1198	0.721	0.2885	0.0895	0.2774	0.279
Relative displacement between cylinder 1 and 2 of the triple cylinder array, top tension = 42N												
p/d = 3, Gumbel	0.2170	0.1979	-	0.160	0.2760	0.2084	-	0.394	0.3133	0.2140	-	0.449
p/d = 4.4, GEV	0.1825	0.1214	-0.017	0.701	0.2260	0.1193	-0.0287	0.128	0.2418	0.0996	0.1339	0.795
p/d = 8.75, GEV	0.2423	0.1091	0.2375	0.291	0.2732	0.0980	0.3019	0.943	0.2969	0.1079	0.3019	0.924
Relative displacement between cylinder 2 and 3 of the triple cylinder array, top tension = 42N												
p/d = 3, GEV	0.4733	0.2100	0.1650	0.397	0.5699	0.2119	0.1190	0.950	0.6338	0.2151	0.0896	0.841
p/d = 4.4, Gumbel	0.2968	0.1629	-	0.936	0.3628	0.1560	-	0.238	0.3821	0.1670	-	0.573
p/d = 8.75, Gumbel	0.3227	0.1538	-	0.577	0.3829	0.1462	-	0.290	0.4338	0.1697	-	0.639

Table 3.3. Selected statistical models and predicted threshold-crossing probabilities for paired cylinder arrays

P/D	Top Tension	Model	Block size	Duration of block length	$\hat{\mu}$	$\hat{\sigma}$	$\hat{\xi}$	AD test p-value	$P(Z > 1.0D)$	$P(Z > 1.5D)$	$P(Z > 2.0D)$
3.0	72N	GEV	320	59.3 sec	0.2606	0.1107	0.3286	0.930	2.874×10^{-2}	9.091×10^{-3}	3.941×10^{-3}
3.0	72N	GEV	240	44.5 sec	0.2292	0.1179	0.2514	0.402	2.071×10^{-2}	5.422×10^{-3}	1.988×10^{-3}
4.4	42N	GEV	240	44.5 sec	0.1565	0.1051	0.4049	0.880	2.767×10^{-2}	1.109×10^{-2}	5.685×10^{-3}
8.75	42N	GEV	320	59.3 sec	0.2885	0.0895	0.2774	0.279	1.500×10^{-2}	3.615×10^{-3}	1.309×10^{-3}

Table 3.4. Selected statistical models and predicted threshold-crossing probabilities for triple cylinder arrays with a block size of 320

P/D	Top Tension	Relative displacement	Model	Block size	Duration of block length	AD-test p-value	$\hat{\mu}$	$\hat{\sigma}$	$\hat{\xi}$	$P(Z > 1.0D)$	$P(Z > 1.5D)$	$P(Z > 2.0D)$	$P(Z > 3.0D)$
3.0	42N	Cylinder 1 and 2	Gumbel	320	59.3 sec	0.449	0.3133	0.2140	-	3.960×10^{-2}	3.898×10^{-3}	3.775×10^{-4}	-
		Cylinder 2 and 3	GEV	320	59.3 sec	0.841	0.6338	0.2151	0.0896	1.854×10^{-1}	3.160×10^{-2}	6.531×10^{-3}	-
4.4	42N	Cylinder 1 and 2	GEV	320	59.3 sec	0.795	0.2418	0.0996	0.1339	5.242×10^{-3}	6.146×10^{-4}	1.163×10^{-4}	9.441×10^{-6}
		Cylinder 2 and 3	Gumbel	320	59.3 sec	0.576	0.3821	0.1670	-	2.442×10^{-2}	1.238×10^{-3}	6.202×10^{-5}	1.556×10^{-7}
8.75	42N	Cylinder 1 and 2	GEV	320	59.3 sec	0.924	0.2969	0.1079	0.3019	2.688×10^{-2}	7.553×10^{-3}	3.015×10^{-3}	8.140×10^{-4}
		Cylinder 2 and 3	Gumbel	320	59.3 sec	0.639	0.4338	0.1697	-	3.494×10^{-2}	1.866×10^{-3}	9.812×10^{-5}	2.708×10^{-7}

3.4 Summary

This chapter presents a general statistical methodology that was shown to accurately capture the extreme interactive response behavior that was observed in the response of densely spaced vertical deep-water cylinder arrays subject to random seaways. The methodology presented is based on the extremal types theorem, which lays the foundation for the generalized extreme value (GEV) family of distributions. Initially, the sequence of block maxima $\{Z_{n,i}\}$ is constructed from the time series $X(t)$ of the target variable measured at an interval of δt. The block size n that is selected needs to be carefully determined to well capture the peak values in $X(t)$. An iterative process is applied to select the most appropriate block size and the corresponding GEV family of distributions fitted to the block maxima $\{Z_{n,i}\}$. The degree to which the fitted models agree with the data is assessed using the Anderson-Darling (AD) test criterion together with quantile plots and histograms, where the quality of fit in the upper tail of the distribution is paid special attention. If the goodness of fit is found unsatisfactory, the value of the block size is changed and the reconstructed block maxima sequence $\{Z_{n,i}\}$ is then used in the next iteration. This iterative process is repeated until the fitted model can most accurately capture the data in both the main body and the upper tail of the distribution. The result of this process is the identification of the most appropriate block size and the corresponding extremal statistical model for each data set. The sensitivity of the models' performance to the block size is also investigated. The selected statistical models are then used to predict the threshold-crossing probabilities of $\{Z_{n,i}\}$, where each element $Z_{n,i}$ represents the maximum observed value in $X(t)$ in a duration of the block length $n\delta t$.

The statistical methodology is relatively straightforward to implement and can be used to capture and lead to a better understanding of the extremal behavior of measured time series data. In this chapter a random wave-cylindrical structure response case from earlier model basin studies (Rijken and Niedzwecki, 1997, 1998) was selected for investigation. The GEV family of distribution models produced by the methodology were found to provide an excellent representation of the extremal data. It is noted in the paired cylinder tests that closely spaced cylinder arrays were more likely to experience larger relative displacements than the cylinders that were more sparsely spaced. In addition, the predicted probabilities confirm that increasing the top tension could effectively reduce the magnitudes of the relative displacement between adjacent cylinders. For the in-line interaction of triple cylinder array, the selected model captures the unexpected phenomenon that downstream cylinders experienced a higher risk of collision than the two most upstream elements in the equally spaced cylinder array. These research findings based on the OTRC model basin data indicate that the extremal statistical methodology presented could be useful to capture the essential characteristics of the stochastic random wave-cylinder interactive response behavior. In the next chapter the applicability of this general statistical methodology is further investigated with the model basin data for an entirely different scenario of fluid-cylinder interactions, the flow-induced vibrations of a slender horizontal cylinder subjected to both random seaways and a steady current.

4 . STATISTICAL ANALYSIS OF FLOW-INDUCED VIBRATIONS ON A SLENDER HORIZONTAL CYLINDER*

The flow-induced vibrations of slender horizontal cylinders are also of significant interest in offshore applications such as pipeline design. When the horizontal cylinder is simultaneously subjected to random waves and current loadings, its response behavior is very complicated and it could be extremely difficult to satisfactorily characterize the fluid-cylinder interactions by a set of traditional deterministic parameters. In this section, the general extremal statistical methodology addressed in chapter 3 was utilized with traditional spectral analysis methods to investigate the time series of flow-induced response behavior of a flexible horizontal cylinder subject to both random waves and constant current conditions. The cylinder model was 29m long and had a slenderness ratio of approximately 760. The random waves were generated using a JONSWAP wave amplitude spectrum. In addition, for some tests the cylinder was towed at two different speeds to simulate the combined loading of random waves and constant current conditions. The data was initially analyzed using standard spectral analyses to interpret the cylinder's flow-induced response behavior and relate the findings to traditional deterministic parameters. Further analyses were again performed using the generalized extreme value (GEV) distribution procedure that involved dividing the time series into blocks and fitting

---

* Part of this chapter is reprinted from "Analysis of random wave interactions with cylinders using extremal statistical methods" by Jiangnan Lu and Niedzwecki (in-press), 2020, *Applied Ocean Research*. Copyright by Elsevier (the publisher).

the block maxima of the extreme values in the measured response times series data. The Anderson-Darling (AD) test criterion and quantile plots were then used to select the most appropriate block sizes and assess whether the GEV family of distributions provide a satisfactory fit to the data capturing the statistical characteristics in the flexible cylinder's flow-induced response behavior, which was stochastic in nature. For the data set analyzed, the extremal statistical methodology was observed to provide good to excellent results for the random wave cases and moderately good to good results for the combined random wave and constant current cases.

4.1 Background

Long flexible horizontal cylindrical structures such as offshore pipelines are widely used in the oil and gas industry. Their flow-induced vibrations when exposed to combined random wave and current loadings are very complicated and have been the focus of numerous experimental investigations reported in the open literature. Vandiver (1993) investigated the vortex-induced vibration of long flexible cylinders from numerous field experiments that he conducted and, in the process, identified important dimensionless parameters associated with predicting the observed response behavior. These parameters included the shear fraction $\Delta V/V_{max}$, the number of potentially excited modes N_s, the mass ratio $m/\rho_f D^2$, and the mass-damping parameter $S_G = r\omega/(\rho_f V^2)$. The expression of the mass-damping parameter S_G was first formulated by Griffin et al. (1975) to predict the maximum response amplitude of flexible structures and cables in water. However, Sarpkaya (1979, 2004) reported that this parameter S_G has many shortcomings while

Zdravkovich (1990) suggested that S_G was only valid for cylinders with a very high value of mass ratio. To address the limitations of this traditional mass-damping parameter, Vandiver (2012) introduced a revised damping parameter $c^* = 2c\omega/\rho U^2$ and it was found valid at all frequencies where synchronization occurs between the wake and cylinder motion, disregarding the value of the mass ratio.

A more recently studied parameter that is closely related to flexible cylinder's VIV response amplitude is the Reynolds number Re. Klamo et al. (2005) were the first to report that the peak value of VIV response amplitude will increase as Re becomes large while Swithenbank et al. (2008) later provided the datasets of the dimensionless VIV amplitude A/D vs. Re based on both laboratory and field test programs. Sometimes later, Resvanis and Vandiver et al. (2012) investigated the trends between Re and flexible marine riser's VIV response amplitude based on the experimental data obtained by Klamo (2005), Govardhan and Williamson (2006), and Shell's model basin test program (2011). They observed that for Re between 5×10^3 and 2.2×10^5, the riser exhibited a trend to experience larger amplitudes in both in-line and cross-flow directions but there also existed significant scatter between the predicted trends and the measured data.

A very important characteristic of flexible cylinder's VIV response behavior is its stochastic nature, but few relevant research studies could be found in the literature while most of the current popular VIV prediction programs in the industry are deterministic as reported by Resvanis and Vandiver (2017). By introducing a short-duration moving window and calculating the mean and standard deviation of RMS response amplitude A/D within each window, Resvanis and Vandiver (2017) were able to illustrate the statistical characteristics of the non-stationary VIV data obtained from Shell (2011). They concluded from their observations that future research effort is required to quantify the variability in flexible cylinder's VIV response behavior.

The purpose of this chapter is to investigate if the general extremal statistical methodology could also be used to capture the statistical characteristics of the extreme values in the flexible horizontal cylinder's flow-induced response amplitudes in-line with the flow direction. The experimental data were obtained in an industrial scale model basin test program (Chitwood, Niedzwecki and Vandiver, 1998). In this study a horizontal cylinder was pretensioned on both sides and tested under a combination of random waves and steady current speeds achieved by towing the model at a constant speed in the wave basin. The measured cylinder's mid-span displacement is selected for the analysis in each of the test run and is first examined using spectral analysis to characterize the response behavior and relate it to traditional deterministic parameters. Then, the general approach based on an extremal statistics methodology is utilized to investigate the statistical characteristics of the measured data. As part of this approach the performance of the statistical models for each data set is assessed by the goodness-of-fit test criterion that is widely used in statistical analyses.

4.2 Experimental Setup

An industrial scale model basin test program was performed at Offshore Technology Research Center (OTRC) located at Texas A&M University to investigate the flow-induced vibrations of a slender horizontal cylinder subjected to a combination of random waves and current loadings (Chitwood, Niedzwecki and Vandiver, 1998). A schematic of the test set up is illustrated in Fig. 4.1. The model scale was determined to be 1:16 in accordance with the Froude scaling law. The length of the test cylinder was approximately 29m and the outside and inside diameter were 38mm and 22mm, respectively. Thus, the slenderness ratio L/D was estimated to be 760. The unit weight of the composite test cylinder was 10.18N/m and the corresponding mass ratio was 0.91. The cylinder was submerged at a water depth of 0.61m and pretensions could be applied to both ends of the model through the two vertical I-beams, which were rigidly fixed on the OTRC bridge. Six biaxial accelerometers were placed inside the cylinder and they were kept dry by sealing the ends of the cylinder and maintaining a slight pressure inside the cylinder model. Three wave probes were fixed on the bridge to measure the water surface elevation at 7.62m west of the centerline, 1.58m east of the centerline, and 7.62m east of the centerline, respectively. The cylinder's mid-span displacement was measured at a time interval Δt of 0.025sec using a string-potentiometer that was mounted on the bridge.

In this study, the model random sea conditions were generated using a JONSWAP wave amplitude spectrum with a significant wave height of $H_S = 0.43\text{m}$ and a peak period of $T_p = 3\text{sec}$. For each unidirectional random wave test the instrumented test cylinder was tested for 300s. For the multi-directional random waves that were generated with a cosine square power model with a twenty-degree spreading angle, each test lasted for 600s. As part of the test program the cylinder model was towed at two different speeds during the random wave excitation. Due to the length of the model basin, the duration of each test was reduced. For the test where the towing speed was 0.244m/s the test lasted for only 60s and when the towing speed was increased to 0.366m/s, the duration was further reduced to 40s.

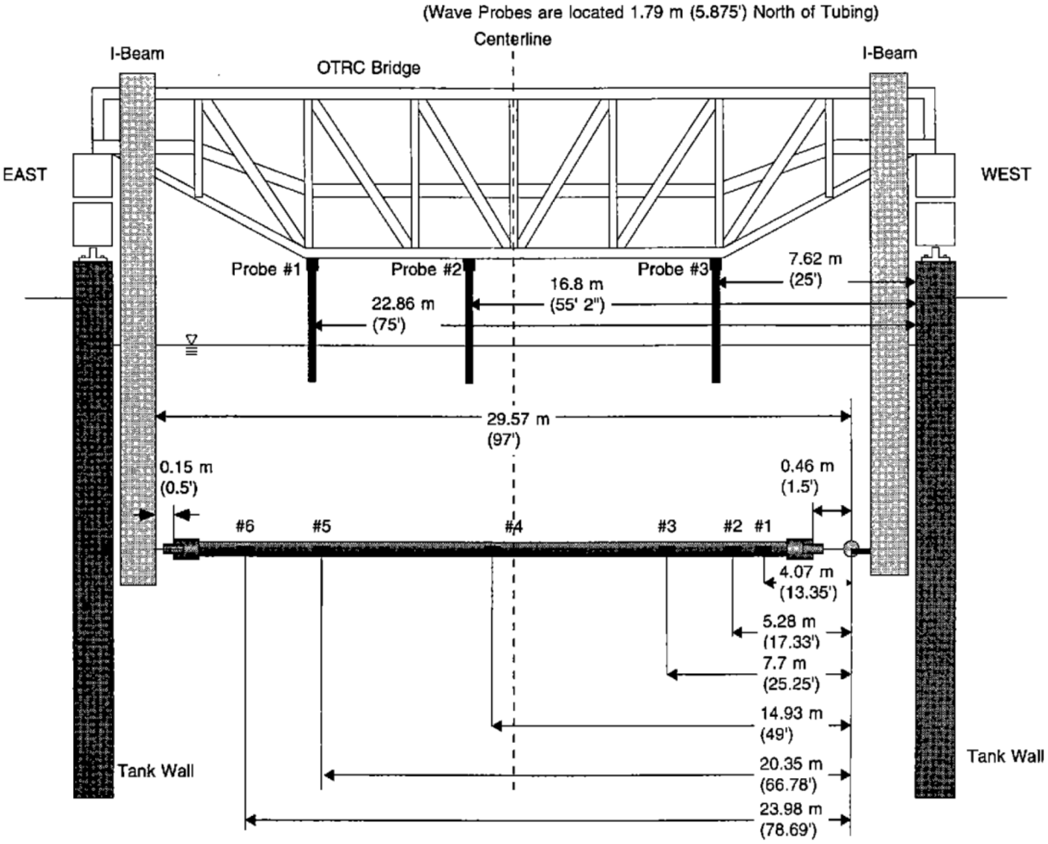

Fig. 4.1. Schematic of the horizontal cylinder in the model basin (reprinted from Chitwood, Niedzwecki and Vandiver, 1998)

4.3 Spectral Analysis Methodology

Spectral analysis is a widely used technique to study the measured time series $X(t)$ in the frequency domain. The power spectral density function, $S(f)$, which is the Fourier transform of the autocorrelation function of $X(t)$, presents the energy distributions of the time series $X(t)$ at each frequency. The expression of the i^{th} spectral moment was given by Nigam (1983) as follows

$$\lambda_i = \int_0^\infty f^i \, S(f) \, df \tag{4.1}$$

where, f is the frequency in Hz and the average frequency $\bar{f}$ could be obtained by the expression

$$\bar{f} = \lambda_1/\lambda_0 \tag{4.2}$$

To describe the dispersion of $S(f)$ with respect to its central frequency, Nigam (1983) defined a dimensionless spectral parameter in the following

$$q = \sqrt{1 - \frac{\lambda_1^2}{\lambda_0 \, \lambda_2}} \tag{4.3}$$

In addition, the bandwidth of the process $X(t)$ could be shown by a bandwidth parameter ε introduced by Cartwright and Longuet-Higgins (1956) as

$$\varepsilon = \sqrt{1 - \frac{\lambda_2^2}{\lambda_0 \, \lambda_4}} \tag{4.4}$$

The above spectral parameters can be useful for one to understand the characteristics of the process $X(t)$ measured in the time domain. However, when the process $X(t)$ is highly stochastic the values of these spectral parameters might vary significantly even under the same test conditions. In this case, it might no longer be feasible to characterize the process $X(t)$ by a set of deterministic parameters and one might need to seek alternatives to capture the global response behavior of $X(t)$.

4.4 Analysis of the Model Basin Data

For the analyses that follow the target variable is selected as the measured mid-span displacement $X(t)$. The power spectral densities are calculated based on Welch's method (Welch, 1967) and these results are used to initially interpret the cylinder's response behavior. Next the GEV statistical methodology is used to investigate the characterization of the cylinder's response behavior observed in the experimental data.

4.4.1 Spectral analysis of the cylinder mid-span displacement

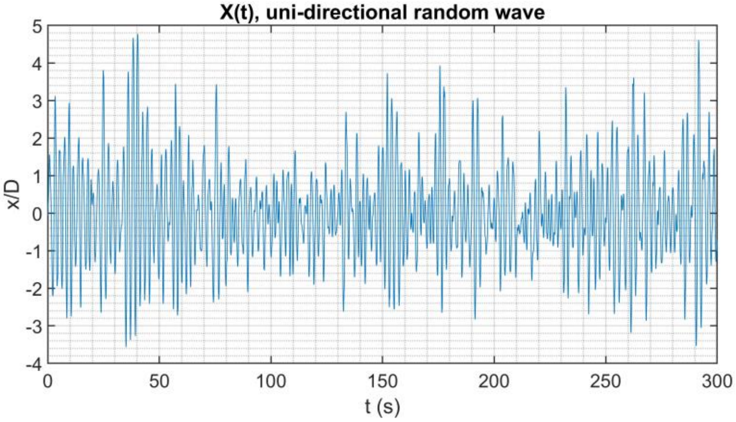

Fig. 4.2. Normalized time series $\boldsymbol{X(t)}$ under unidirectional random waves

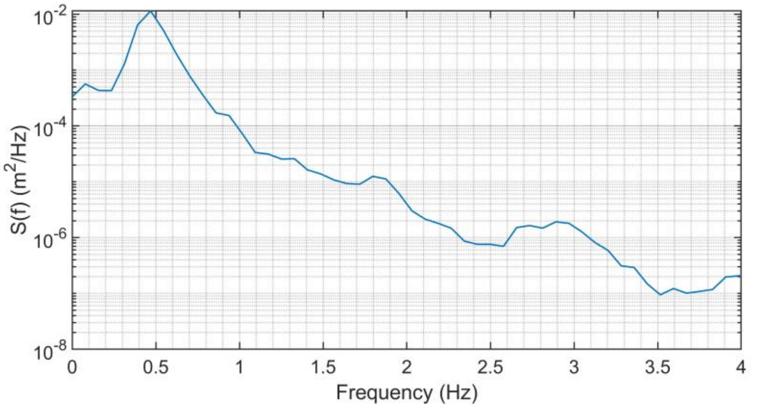

Fig. 4.3. Power spectral density of $\boldsymbol{X(t)}$ under unidirectional random waves

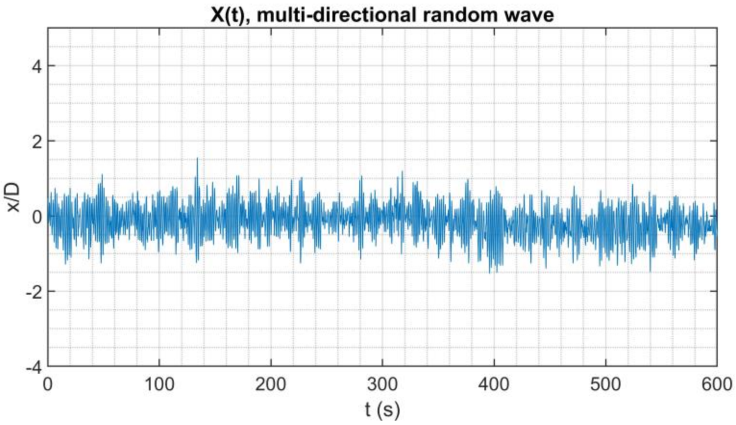

Fig. 4.4. Normalized time series $\boldsymbol{X(t)}$ under multi-directional random waves

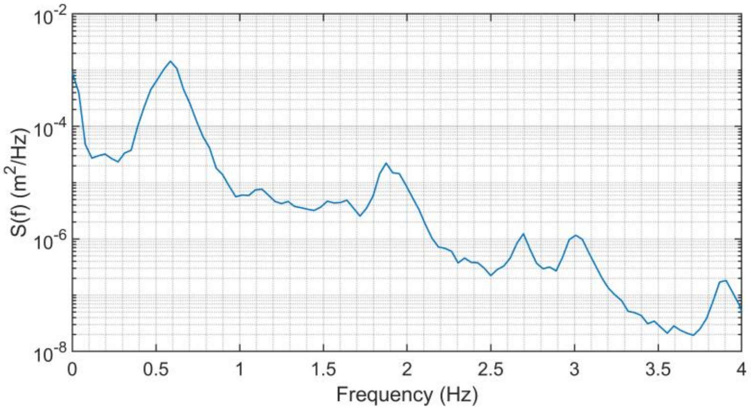

Fig. 4.5. Power spectral density of $\boldsymbol{X(t)}$ under multi-directional random waves

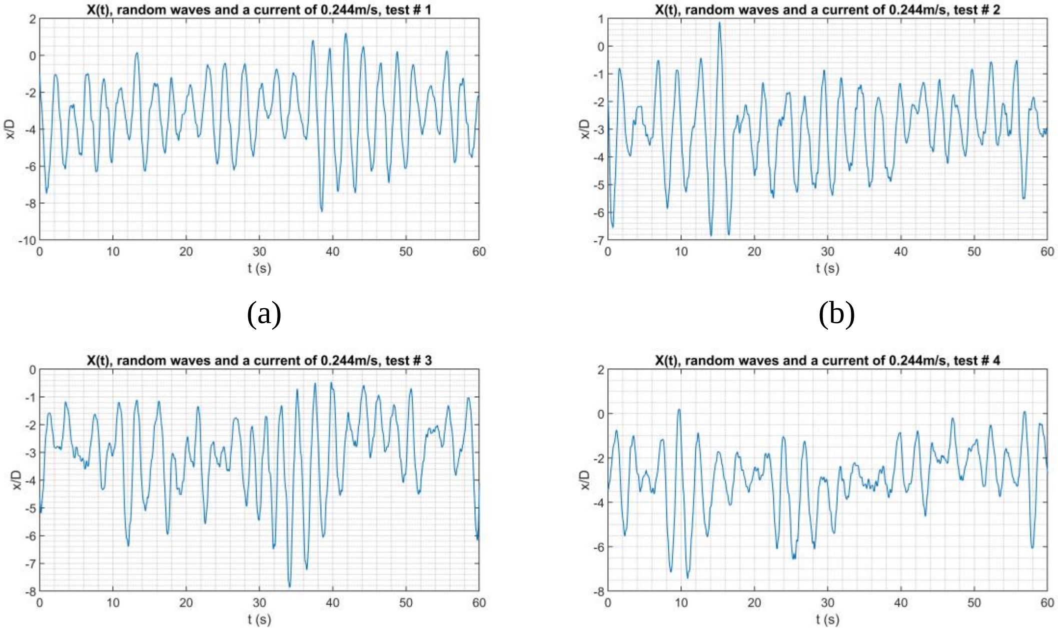

(a) (b)

(c) (d)

Fig. 4.6. Normalized time series of $\boldsymbol{X}(\boldsymbol{t})$ under random waves and a current of 0.244m/s, (a) test 1; (b) test 2; (c) test 3; (4) test 4.

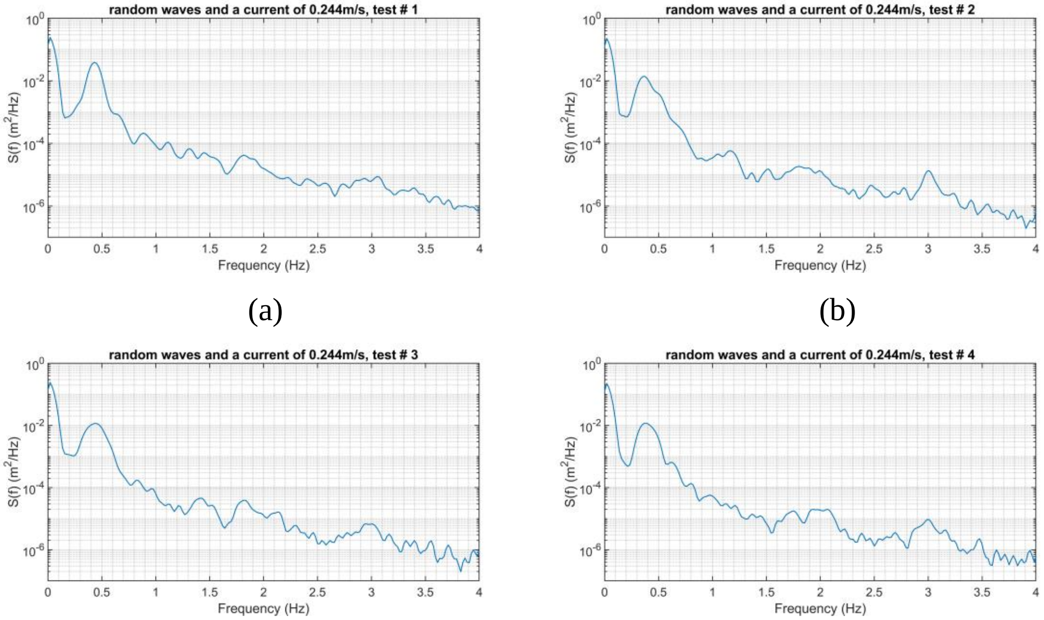

(a) (b)

(c) (d)

Fig. 4.7. Power spectral density of $\boldsymbol{X}(\boldsymbol{t})$ under random waves and a current of 0.244m/s, (a) test 1; (b) test 2; (c) test 3; (4) test 4.

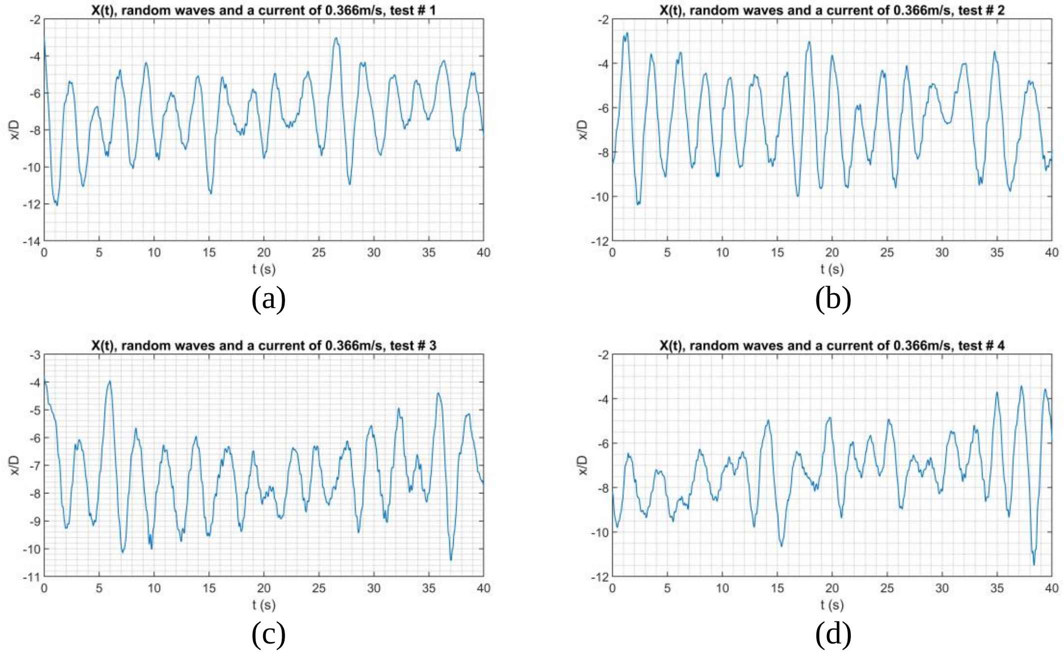

(a) (b)

(c) (d)

Fig. 4.8. Normalized time series of $\boldsymbol{X}(\boldsymbol{t})$ under random waves and a current of 0.366m/s, (a) test 1; (b) test 2; (c) test 3; (4) test 4.

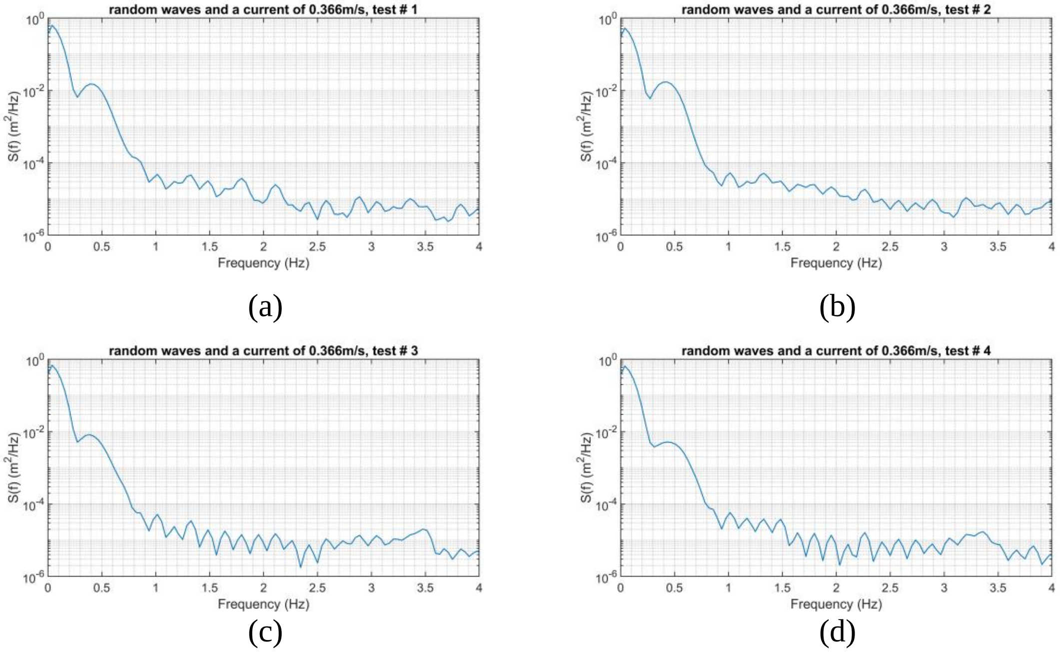

(a) (b)

(c) (d)

Fig. 4.9. Power spectral density of $\boldsymbol{X}(\boldsymbol{t})$ under random waves and a current of 0.366m/s, (a) test 1; (b) test 2; (c) test 3; (4) test 4.

Table 4.1. Statistical and spectral moments of mid-span displacement $\boldsymbol{X}(\boldsymbol{t})$

Parameters	μ	σ	α_3	α_4	$\mu^2+\sigma^2$	λ_0	$\bar{f}$	q	ε
	m	m	-	-	m^2	m^2	s^{-1}	-	-
Unidirectional random waves									
	0.0006	0.0484	0.382	3.505	0.0023	0.0023	0.475	0.364	0.979
Multi-directional random waves (20-degree spreading angle)									
	-0.0055	0.0164	-0.069	2.921	0.0027	0.0029	0.535	0.539	0.989
Random waves and a current of 0.244m/s									
Test # 1	-0.122	0.071	-0.156	2.431	0.0199	0.0181	0.150	0.820	0.997
Test # 2	-0.115	0.052	-0.330	2.887	0.0159	0.0144	0.097	0.867	0.999
Test # 3	-0.117	0.054	-0.738	3.329	0.0165	0.0159	0.102	0.877	0.999
Test # 4	-0.110	0.055	-0.692	3.418	0.0152	0.0144	0.094	0.877	0.999
Random waves and a current of 0.366m/s									
Test # 1	-0.273	0.0678	-0.339	2.787	0.0790	0.0708	0.091	0.822	1.000
Test # 2	-0.250	0.0682	-0.032	1.989	0.0671	0.0605	0.098	0.829	1.000
Test # 3	-0.280	0.0512	0.195	2.584	0.0812	0.0755	0.083	0.830	1.000
Test # 4	-0.276	0.0546	0.106	3.067	0.0793	0.0729	0.083	0.836	1.000

Initially the measured time series of the horizontal cylinder's mid-span displacement $X(t)$ and their power spectral density (PSD) calculated by Welch's method are shown in Fig. 4.2 through Fig. 4.9. Then both the statistical moments and the spectral moments of each test condition are calculated and presented in Table 4.1. In Table 4.1 the values of $\mu^2+\sigma^2$ are found to have a good agreement with the 0th spectral moment λ_0, which confirms that the calculated PSD are correct.

When the cylinder was only subjected to unidirectional random waves, one observes that the time series plotted in Fig. 4.2 is very similar to a stationary random process. This observation is confirmed by examining the value of the skewness α_3 and the kurtosis α_4 as presented in Table 4.1, which only show a small deviation from the Gaussian process. When the random waves were generated in multi directions with a 20-degree spreading angle, it is observed in Fig. 4.4 that the measured value of $X(t)$ exhibits significantly smaller amplitude while the statistical moments shown in Table 4.1 indicate that the process $X(t)$ is almost Gaussian.

When a steady current of 0.244m/s and 0.366m/s were respectively superposed to the random waves, one observes in Fig. 4.6 and Fig. 4.8 that the measured time series of $X(t)$ varies significantly from case to case. In Table 4.1 one can also notice the variations in the statistical moments. Although the calculated mean value of the four tests are relatively close, the higher-order statistical moments of each test show significant differences, especially when the current speed was increased to 0.366m/s. These discrepancies might be attributed to the short duration of the test time and the complexity of the interactive response behavior of the cylinder subject to random waves combined with a steady current. In addition, the calculated mean frequency $\bar{f}$ is found to decrease from around 0.5Hz to below 0.1Hz after the superposition of the current, which indicates that the energy from the current was dominant and the current was strong compared to the waves.

Considering the significant variations in the calculated values of the above parameters, one might conclude that it is extremely difficult to utilize a set of deterministic parameters to characterize the cylinder's flow-induced response behavior, which is stochastic in nature as addressed by Resvanis and Vandiver (2017). Thus, it becomes reasonable for one to acknowledge the stochastic nature of the cylinder's flow-induced motions and look for a general approach to investigate the statistical characteristics in the observed response behavior. In the following sections a statistical approach based on generalized extreme value (GEV) distribution is utilized to analyze the cylinder's mid-span displacement $X(t)$ of all the test scenarios listed in Table 4.1.

4.4.2 Analysis of the cylinder mid-span displacement under random waves

In Table 4.1 one observes that the mean value of $X(t)$ under random waves only is almost 0. Thus, the target variable of the statistical analysis is selected as the amplitude of the cylinder's mid-span displacement $X(t)$ normalized by the cylinder diameter D. Accordingly, the constructed block maxima $Z_{n,i}$ represents the cylinder's maximum mid-span response amplitude observed in a block length of $n\delta t$. To determine the initial block size n, this analysis follows the same iterative procedure presented in Chapter 3. Initially, both the complete and zoomed-in plots of the partial autocorrelation function (PACF) of $X(t)$ are examined in Fig. 4.10, where the time lag represents the number of data points recorded. For the cylinder placed in unidirectional random waves, one observes in Fig. 4.10 (a) that the PACF becomes small and remains stable after approximately 100 data points (2.5 sec). When the cylinder was subjected to multi-directional random waves, it is observed in Fig. 4.10 (b) that it takes approximately 150 data points (3.75 sec) for the PACF to fall within the 95% C.I. bounds of the white noise. Thus, it is reasonable to start the iterative process for the cylinder subjected to unidirectional random waves with an initial block size of 120 and include two additional block sizes of 180 and 240 for the sensitivity analysis. Similarly, block sizes of 160, 240, and 320 are selected for the multi-directional random wave case.

After determining the three block sizes for investigation, the corresponding PACF of the block maxima sequence $\{Z_{n,i}\}$, the quantile plots of the models and $\{Z_{n,i}\}$, and the histograms of $\{Z_{n,i}\}$ are presented in Fig. 4.11 and Fig. 4.12. When the incoming random waves were unidirectional, the Gumbel distribution is found to provide a better fit in the upper tail of the distribution. In Fig. 4.11, one observes that the PACF of $\{Z_{n,i}\}$ with a block size of 120 shows significant short-range dependence at a time lag of one block but no long-range dependence is detected. This temporal dependence decreases substantially as the block size becomes large, and the PACF is within the 95% C.I. of the white noise when the block size is raised to 240. Again, the model's performance to fit the data is observed to remain stable disregarding the change in block size. Excellent agreement between the model and the data are observed in both the quantile plots and the histograms at the three block sizes. In Table 4.2, the corresponding AD-test p-values presented only show mild variations between 0.729 and 0.833, which again represent an excellent fit. When the cylinder was subjected to multi-directional random waves, one observes in Fig. 4.12 that the PACF of $\{Z_{n,i}\}$ has siginificant short-range dependence and weak long-range dependence given a block size of 160. With the block size increased to 240 and 320, only a minor short-range dependence is observed in PACF and the long-range dependence becomes minimal. In the quantile plots there are notable deviations between the model and the data, but the discrepancies remain small and the models show a generally good agreement with the trend of the data. In Table 4.3, the calculated AD test p-value of 0.073 indicates that a block size of 240 might not be a good choice. However, one also observes in Table 4.3 that given a block size of 160 and 320, the AD test p-values illustrate that the GEV models could provide an excellent to good fit to the data. Thus, it is deemed appropriate to choose a block size of 160 or 320 for the cylinder subject to multi-directional random waves.

With the selected block sizes and the extremal statistical models, the threshold-crossing probabilities of the cylinder's maximum mid-span response amplitudes within a duration of the corresponding block length could be estimated. As an illustration, three predicted values are provided for each model at the selected block sizes in Table 4.4. The predicted probabilities are also found consistent with the time series in Fig. 4.2 and Fig. 4.4 that the cylinder subjected to unidirectional random waves experienced substantially larger response amplitudes. Here again this statistical methodology is shown to be an appropriate approach for capturing the characteristics of extreme flow-induced vibration response amplitudes of a slender horizontal cylinder subject to random wave excitation.

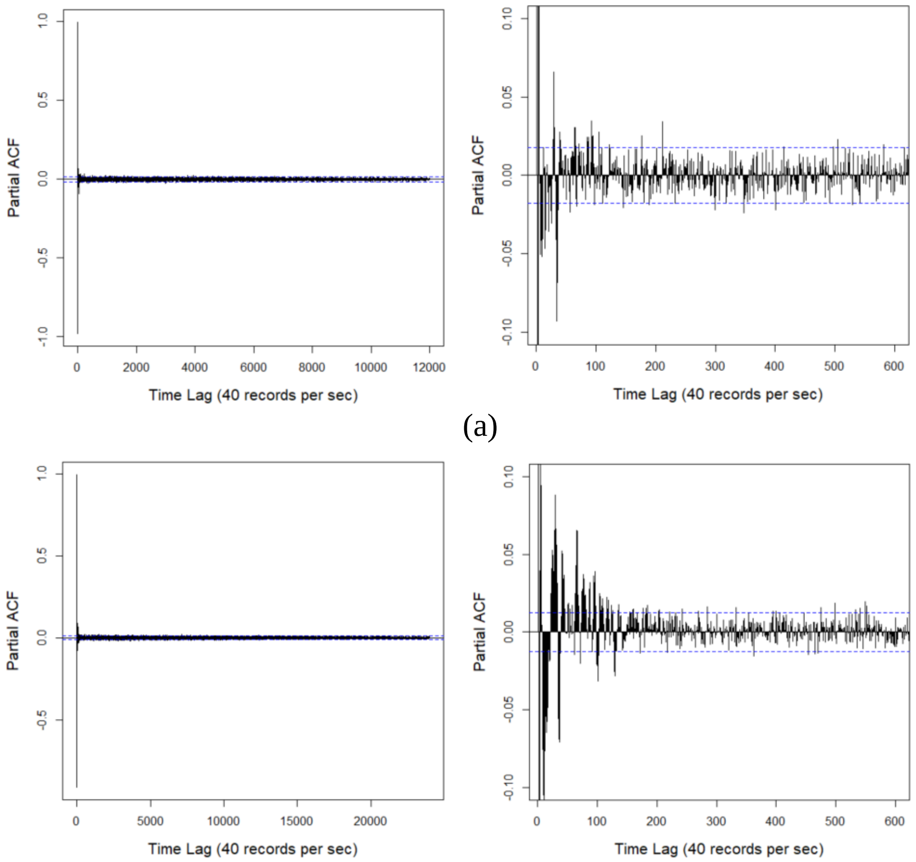

(a)

(b)

Fig. 4.10. PACF of the horizontal cylinder's vibration displacement, complete plot (left) and zoomed-in plot for the first 600 data points (right) under (a) unidirectional random waves; (b) multi-directional random waves.

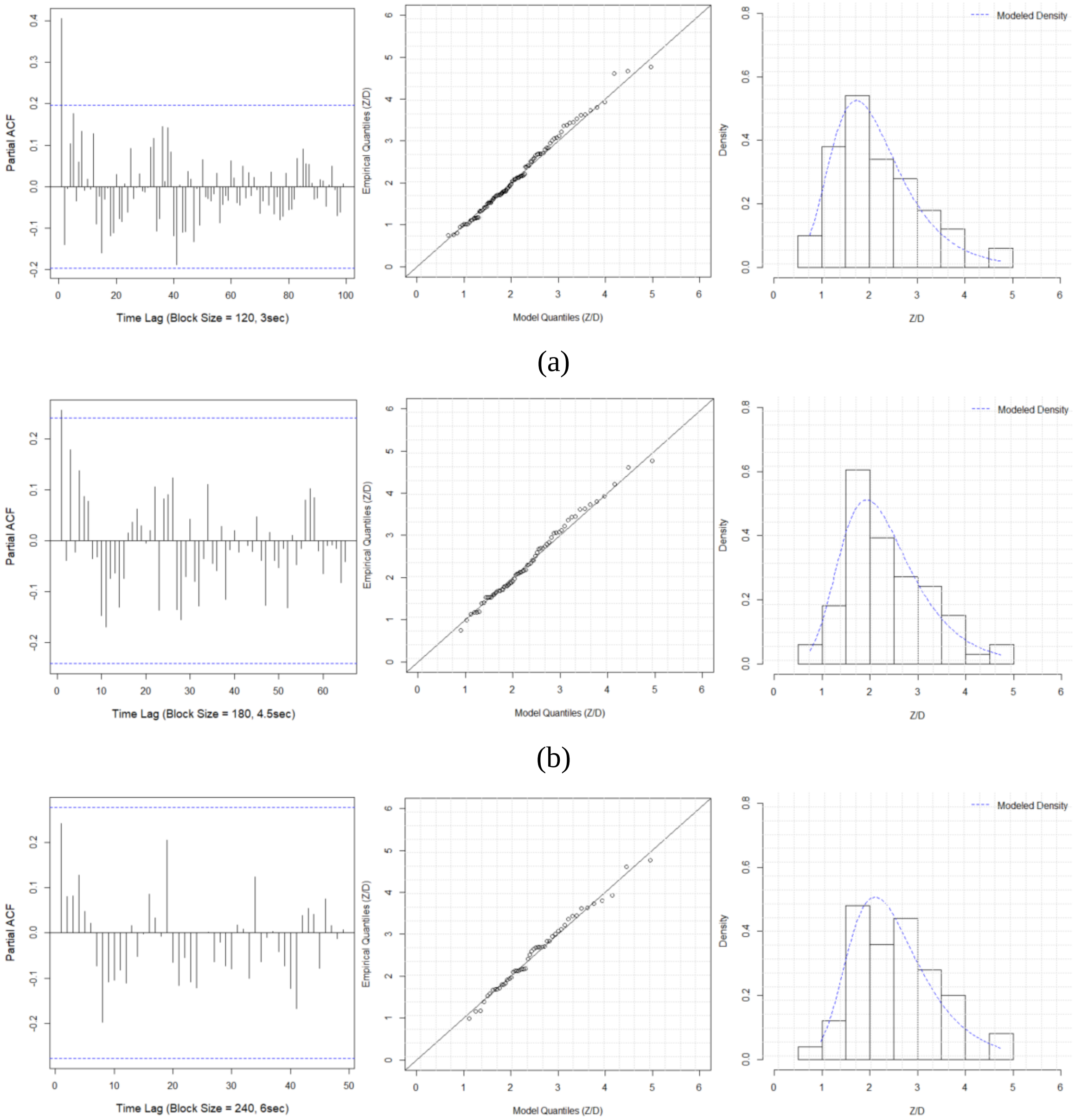

(a)

(b)

(c)

Fig. 4.11. PACF of the block maxima $\{\boldsymbol{Z_{n,i}}\}$ (left), quantile plots of the Gumbel model fitted to $\{\boldsymbol{Z_{n,i}}\}$ (right) for the horizontal cylinder's VIV amplitudes under unidirectional random waves, with a b} (middle), and density plot of the Gumbel model compared with the histograms of $\{\boldsymbol{Z_{n,i}}\}$ lock size of (a) n = 120; (b) n = 180; (c) n = 240.

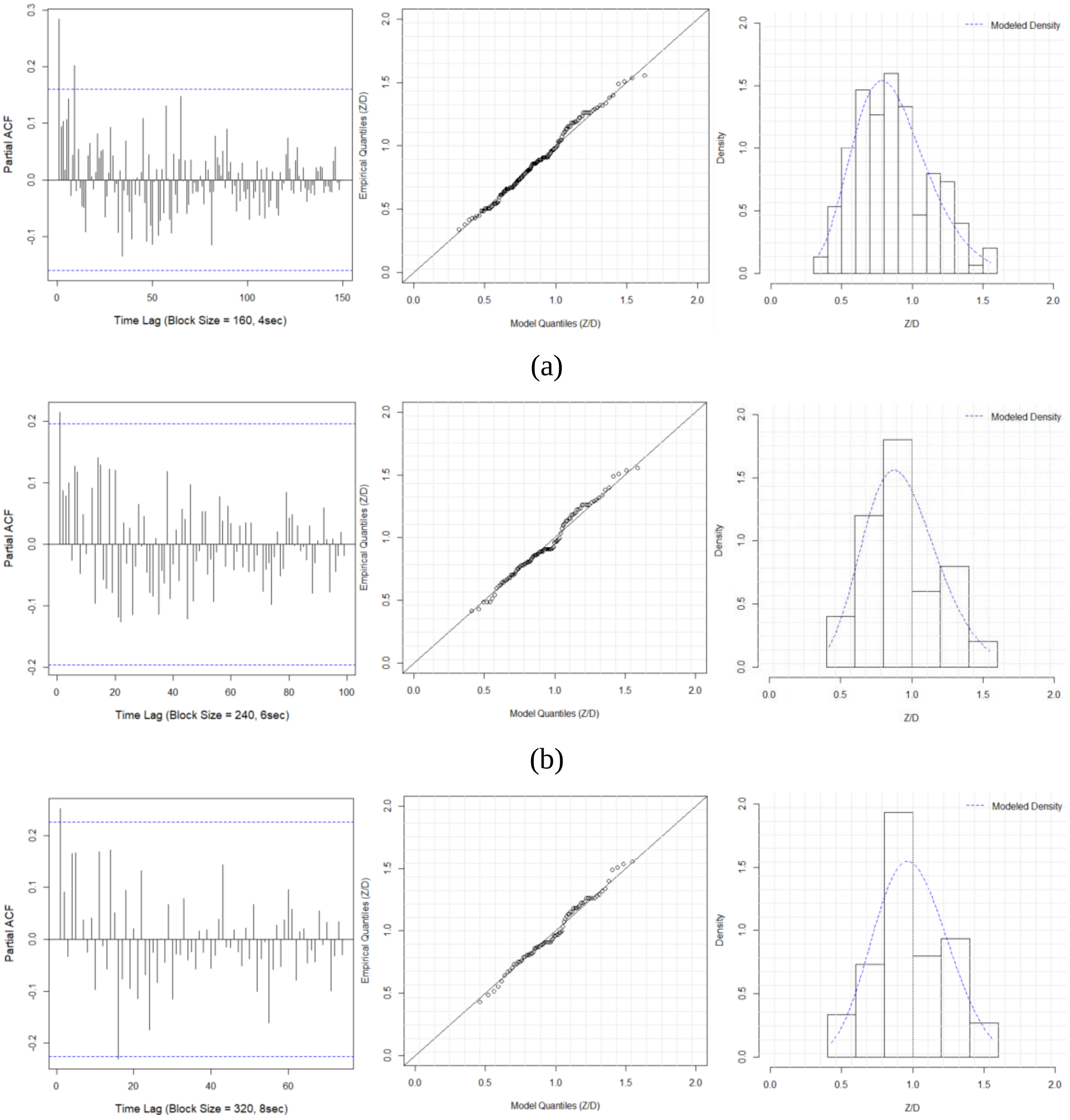

(a)

(b)

(c)

Fig. 4.12. PACF of the block maxima $\{\boldsymbol{Z_{n,i}}\}$ (left), quantile plots of the GEV model fitted to $\{\boldsymbol{Z_{n,i}}\}$ (middle), and density plot of the fitted GEV model compared with the histograms of $\{\boldsymbol{Z_{n,i}}\}$ (right) for the horizontal cylinder's VIV amplitudes under multi-directional random waves, with a block size of (a) n = 160; (b) n = 240; (c) n = 320.

Table 4.2. Comparison of statistical models for the cylinder's vibration amplitudes under unidirectional random waves at three block sizes

Unidirectional random waves	Block size **n=120**				Block size **n=180**				Block size **n=240**			
	$\hat{\mu}$	$\hat{\sigma}$	$\hat{\xi}$	AD p-value	$\hat{\mu}$	$\hat{\sigma}$	$\hat{\xi}$	AD p-value	$\hat{\mu}$	$\hat{\sigma}$	$\hat{\xi}$	AD p-value
Gumbel	1.7303	0.7008	-	0.759	1.9309	0.7186	-	0.833	2.1127	0.7252	-0.1014	0.729

Table 4.3. Comparison of statistical models for the cylinder's vibration amplitudes under multi-directional random waves at three block sizes

Multi-directional random waves	Block size **n=160**				Block size **n=240**				Block size **n=320**			
	$\hat{\mu}$	$\hat{\sigma}$	$\hat{\xi}$	AD p-value	$\hat{\mu}$	$\hat{\sigma}$	$\hat{\xi}$	AD p-value	$\hat{\mu}$	$\hat{\sigma}$	$\hat{\xi}$	AD p-value
GEV	0.7512	0.2411	-0.1365	0.310	0.8299	0.2397	-0.1760	0.073	0.8953	0.2462	-0.249	0.212

Table 4.4. Selected statistical models and predicted threshold-crossing probabilities for the cylinder's vibration amplitudes under random waves

	Optimal block size	Duration of block length	Model	$\hat{\mu}$	$\hat{\sigma}$	$\hat{\xi}$	AD p-value	$P(Z > 2D)$	$P(Z > 4D)$	$P(Z > 6D)$
Unidirectional random waves	120	3 sec	Gumbel	1.7303	0.7008	-	0.759	0.4937	3.845×10^{-2}	2.257×10^{-3}
	180	4.5 sec	Gumbel	1.9309	0.7186	-	0.833	0.5968	5.462×10^{-2}	3.468×10^{-3}
	240	6 sec	Gumbel	2.1127	0.7252	-	0.729	0.6891	7.141×10^{-2}	4.488×10^{-3}
Multi-directional random waves	Optimal block size	Duration of block length	Model	$\hat{\mu}$	$\hat{\sigma}$	$\hat{\xi}$	AD p-value	$P(Z > 1D)$	$P(Z > 1.5D)$	$P(Z > 2D)$
	160	4 sec	GEV	0.7512	0.2411	-0.1365	0.310	0.2802	1.743×10^{-3}	1.242×10^{-4}
	320	8 sec	GEV	0.8953	0.2462	-0.249	0.212	0.4716	2.217×10^{-3}	1.824×10^{-4}

4.4.3 Analysis of the cylinder mid-span displacement under random waves and a current

When the cylinder was simultaneously subjected to random waves and a steady current, one observes in Table 4.1 that the mean value of $X(t)$ became negative due to the current. Thus, the target variable of this analysis is determined to be the cylinder's mid-span displacement in the current direction. Accordingly, the block maxima $\{Z_{n,i}\}$ represents the maximum value of the displacement observed in a duration of $n\delta t$. Again the complete and zoomed-in plots of PACF of $X(t)$ are investigated for test 1 - 4 in Fig. 4.13 and Fig. 4.14 to determine the initial block size. In Fig. 4.13, one observes that when the cylinder was subject to random waves and a current of 0.244m/s, the PACF of $X(t)$ become small and stable after approximately 70 data points. When the current speed was increased to 0.366m/s, one observes in Fig. 4.14 that the PACF falls within the 95% C.I. of a white noise after about 50 data points. Thus, it is deemed reasonable to select an initial block size of 80 (block length = 2 sec) considering the convenience for comparison. However, the duration of each test is found to be relatively short in Fig. 4.6 and Fig. 4.8, which makes it difficult to obtain enough data points for extremal statistical analysis. To solve this problem, the block maxima $\{Z_{n,i}\}$ constructed for each of the four tests under the same flow condition are combined for the analysis, and only one additional block size of 120 is selected for sensitivity study.

To determine the most appropriate block size and the corresponding extremal statistical models, the PACF of $\{Z_{n,i}\}$ for test 1 – 4 are first examined in Fig. 4.15-Fig. 4.16 and Fig. 4.18-Fig. 4.19. Then, constructed block maxima $\{Z_{n,i}\}$ for the four tests are combined and the fitted models are examined in both the quantile plots and the histograms presented Fig. 4.17 and Fig. 4.20. The corresponding model parameters and the calculated AD test p-values are also presented in Table 4.5.

When the steady current speed was 0.244m/s, one observes in Fig. 4.15 that provided a block size of 80, the PACF of $\{Z_{n,i}\}$ illustrates moderate to significant short-range dependence for each of the tests while no long-range dependence is detected. With the block size increased to 120, only test 3 shows an extremely small short-range dependence while the PACF of $\{Z_{n,i}\}$ falls within the 95% C.I. bounds of a strict white noise for the other three tests. In the quantile plots presented in Fig. 4.17, the model is observed to follow the trend of the data pretty well and the discrepancies remain small. In Table 4.5, one observes that the AD test p-value of 0.088 for the model with a block size of 80 only represents a moderately good fit. With the block size increased to 120, the AD test p-value of 0.314 indicates that the model fits the data significantly better. Thus, considering only the AD test p-values might favor a larger block size of 120 for this flow condition. However, it is observed in Fig. 4.17 that the model with a smaller block size of 80 provides a better fit to the upper tail of the distribution while the model fitted for a larger block size of 120 is slightly unconservative in the upper tail. Since the focus of this study is to investigate the extreme events that correspond to the data points in the upper tail of the distribution, a smaller block size of 80 is deemed more appropriate for the data when the cylinder was subjected to random waves and a current of 0.244m/s.

When a stronger current of 0.366m/s was superposed to the random waves, one observes in Fig. 4.18 that given a block size of 80, only test 2 shows a minimal dependence at a time lag of 5 blocks, while the PACF of $\{Z_{n,i}\}$ for each of the other three tests are within the 95% C.I. of a white noise. When a larger block size of 120 is introduced to construct the block maxima, no temporal dependence is detected in the PACF of $\{Z_{n,i}\}$ for each test as presented in Fig. 4.19. In the quantile plots shown in Fig. 4.20, the models are found to have a generally good agreement with the data under both block sizes. However, one also observes in the quantile plots that introducing a larger block size of 120 could not only remove the outlier in the lower tail of the distribution, but also notably improve the model's performance in fitting the data points in the upper tail, which is the focus of extreme value analysis. In Table 4.5, the calculated AD test p-values are also observed to increase from 0.186 to 0.502 when a larger block size of 120 is given. Thus, the block size of 120 is considered more appropriate for the data under this flow condition.

Based on the selected optimal block size and the corresponding extremal statistical models, the threshold-crossing probabilities of the observed data could be assessed, and two predicted values are given in Table 4.6 for illustration. In Table 4.6, the calculated AD test p-values indicate that the GEV statistical model could give an at least moderately good fit to the whole data set, provided the upper tail of the distribution has already been satisfactorily captured by the model. These findings are noteworthy considering the complexity of the flexible cylinder's flow-induced response behavior when the cylinder was subjected to both random waves and a strong current simultaneously. The GEV statistical model is found capable of capturing the essential statistical characteristics of the extreme values observed in the cylinder's flow-induced response amplitude obtained in this model basin test program (Chitwood, Niedzwecki and Vandiver, 1998)

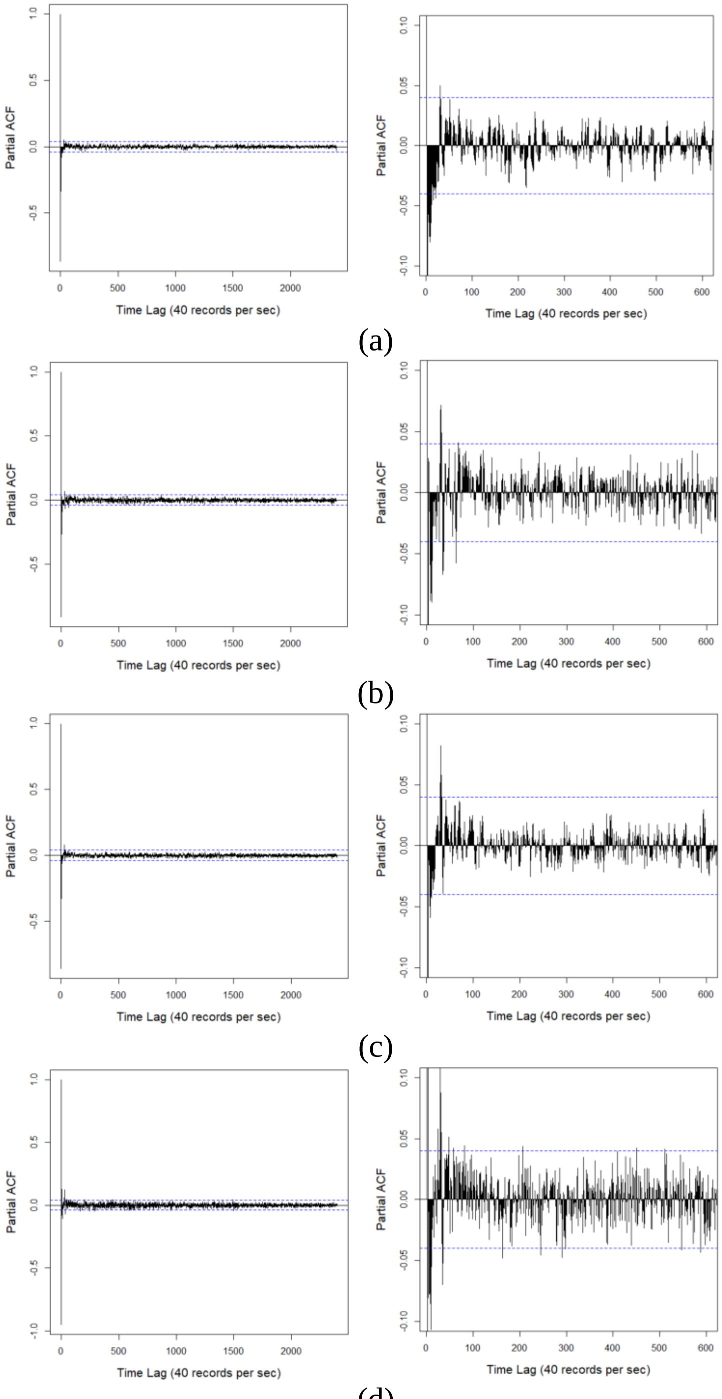

(a)

(b)

(c)

(d)

Fig. 4.13. PACF of the cylinder’s displacement, complete plot (left) and zoomed-in plot for the first 600 data points (right) under random waves and a current of 0.244m/s, (a) test #1; (b) test #2; (c) test #3; (d) test #4.

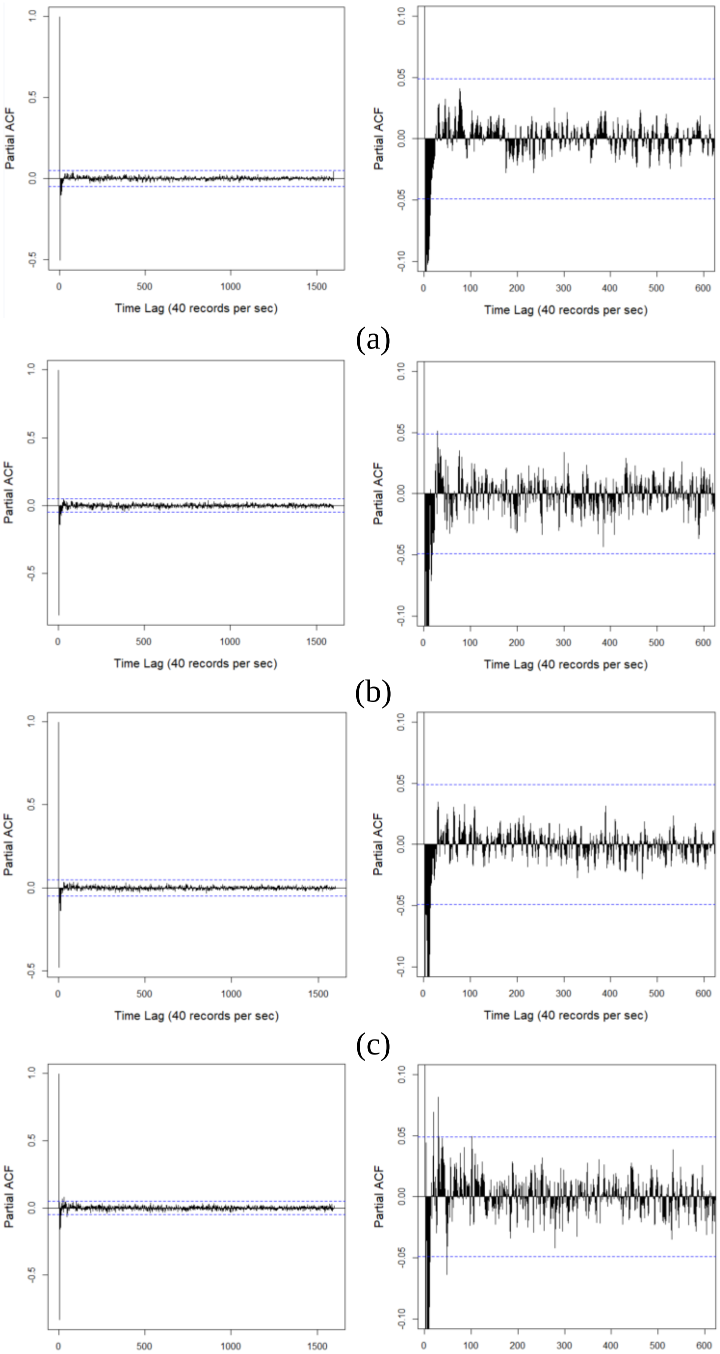

(a)

(b)

(c)

(d)

Fig. 4.14. PACF of the cylinder's displacement, complete plot (left) and zoomed-in plot for the first 600 data points (right) under random waves and a current of 0.366m/s, (a) test #1; (b) test #2; (c) test #3; (d) test #4.

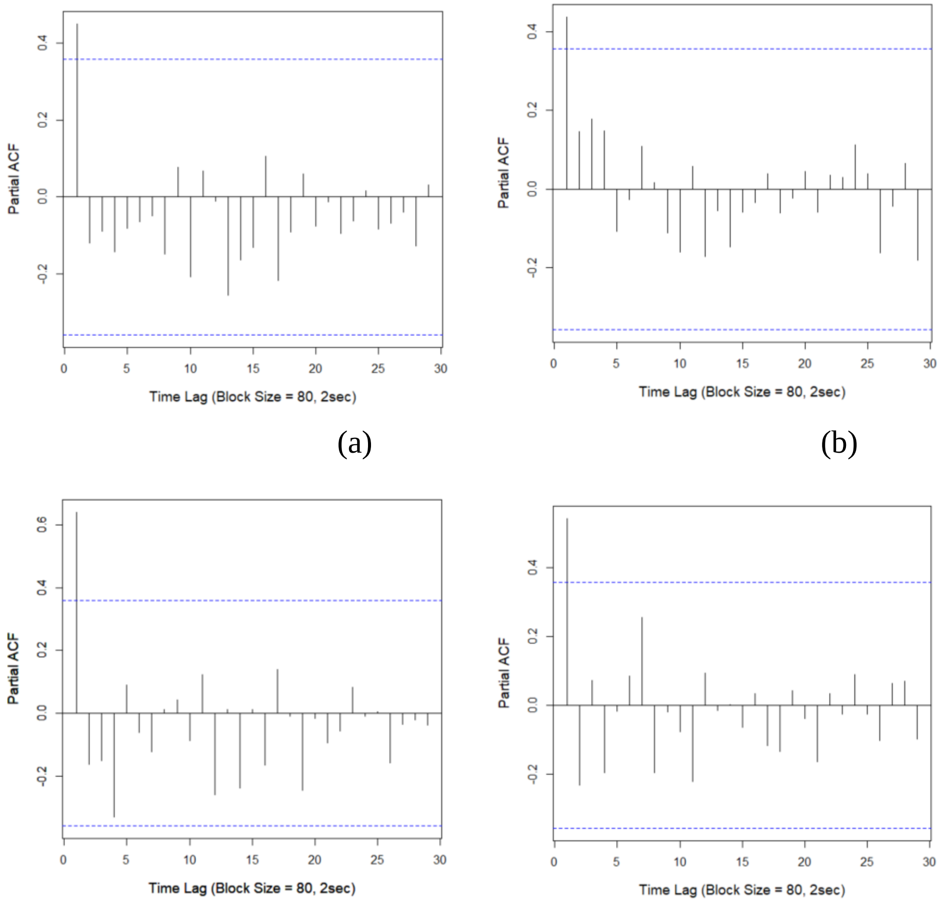

(a) (b)

(c) (d)

Fig. 4.15. PACF of the block maxima $\{\boldsymbol{Z_{n,i}}\}$ for the horizontal cylinder's vibration amplitudes under random waves and a current of 0.244m/s, with a block size of n = 80, for (a) test #1; (b) test #2; (c) test #3; (d) test #4.

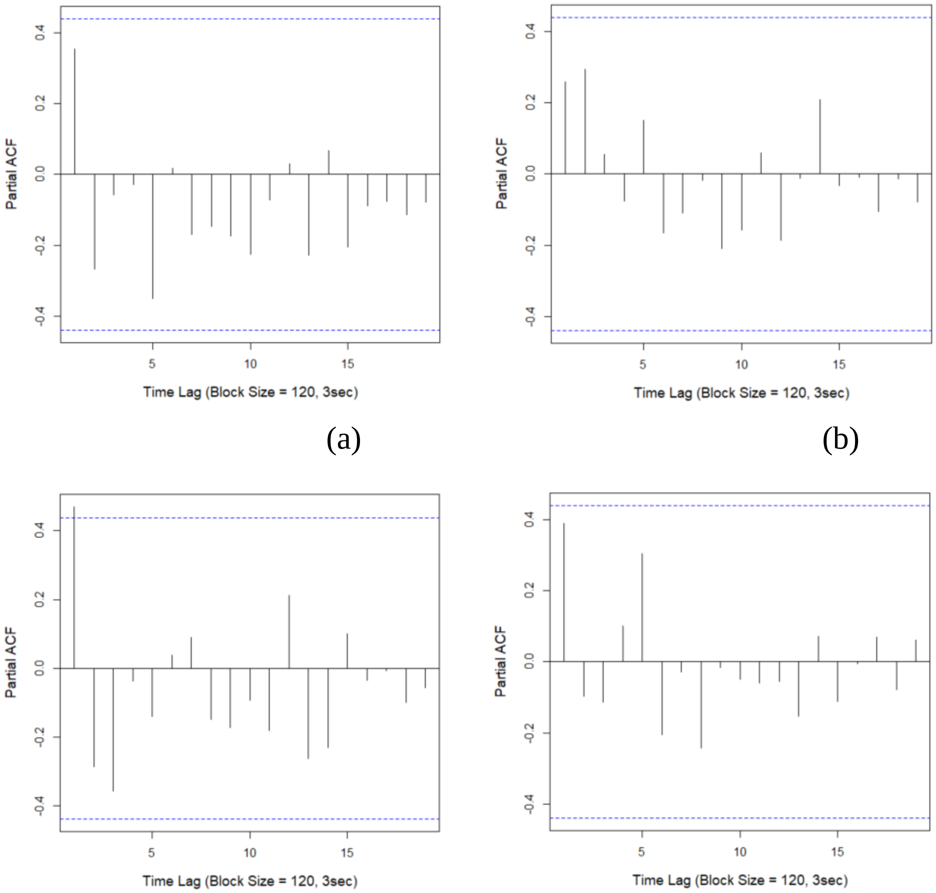

(a) (b) (c) (d)

Fig. 4.16. PACF of the block maxima $\{Z_{n,i}\}$ for the horizontal cylinder's vibration amplitudes under random waves and a current of 0.244m/s, with a block size of n = 120, for (a) test #1; (b) test #2; (c) test #3; (d) test #4.

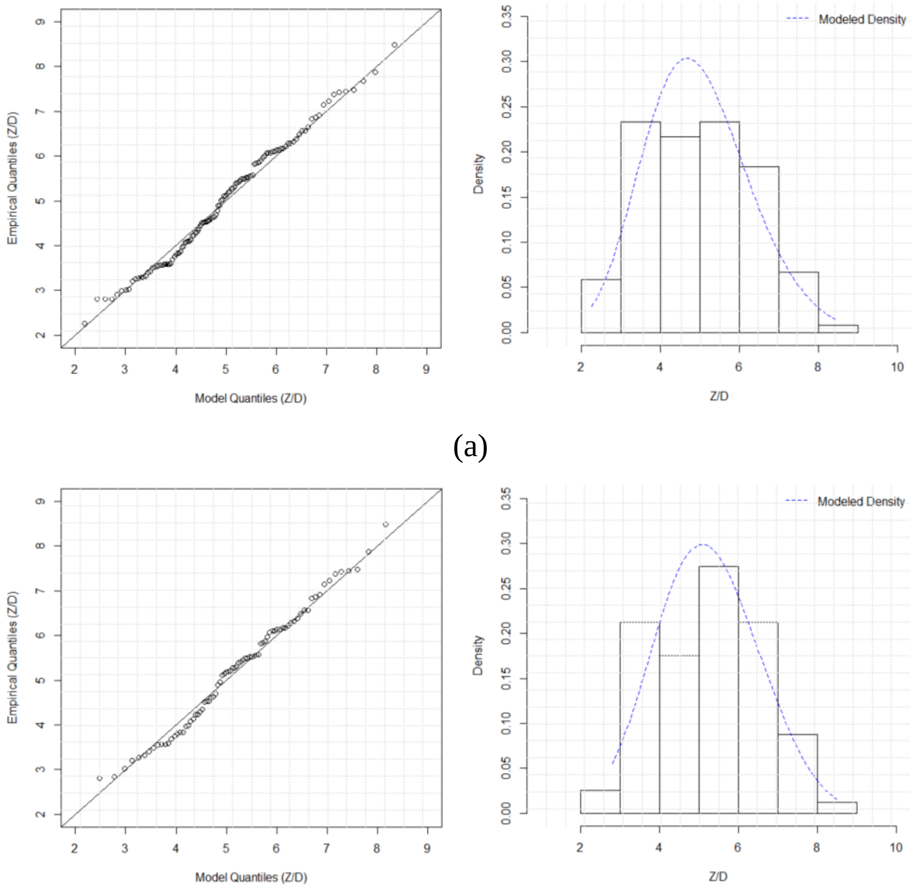

(a)

(b)

Fig. 4.17. Quantile plots of the GEV model fitted to $\{\boldsymbol{Z_{n,i}}\}$ (left), and density plot of the fitted GEV model compared with the histograms of $\{\boldsymbol{Z_{n,i}}\}$ (right) for the horizontal cylinder's vibration amplitudes under random waves and a current of 0.244m/s, with a block size of (a) n = 80; (b) n = 120, for the combined data of test #1-4.

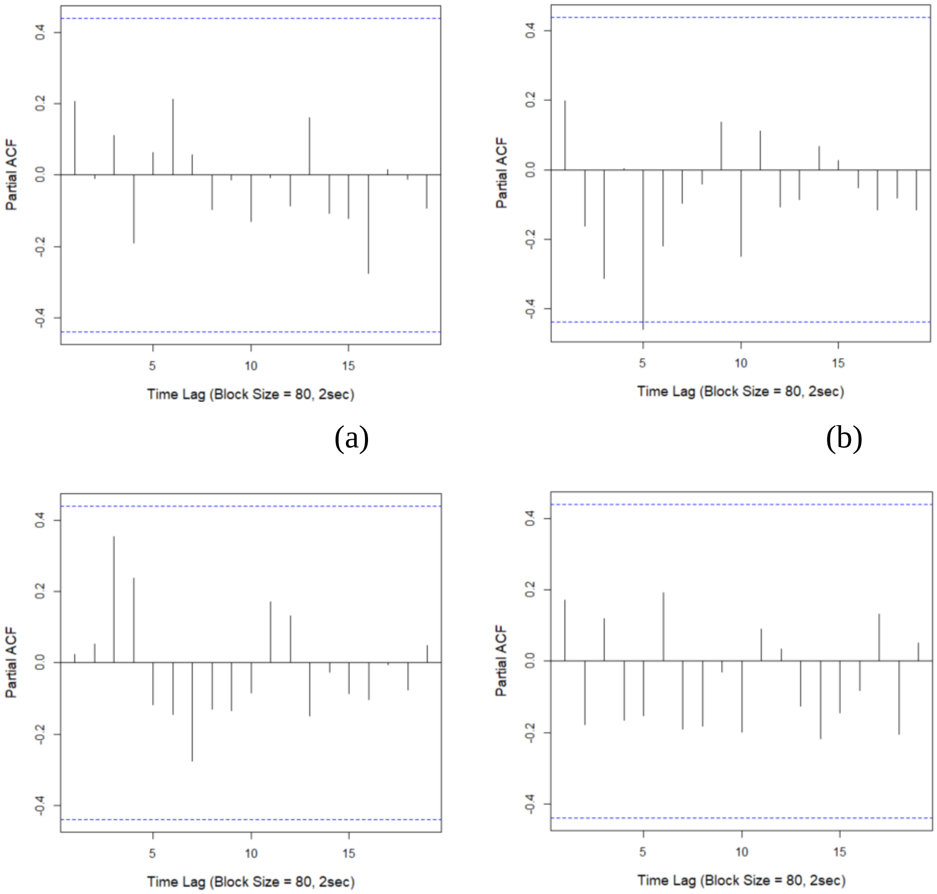

(a) (b)

(c) (d)

Fig. 4.18. PACF of the block maxima $\{\boldsymbol{Z_{n,i}}\}$ for the horizontal cylinder's vibration amplitudes under random waves and a current of 0.366m/s, with a block size of n = 80, for (a) test #1; (b) test #2; (c) test #3; (d) test #4.

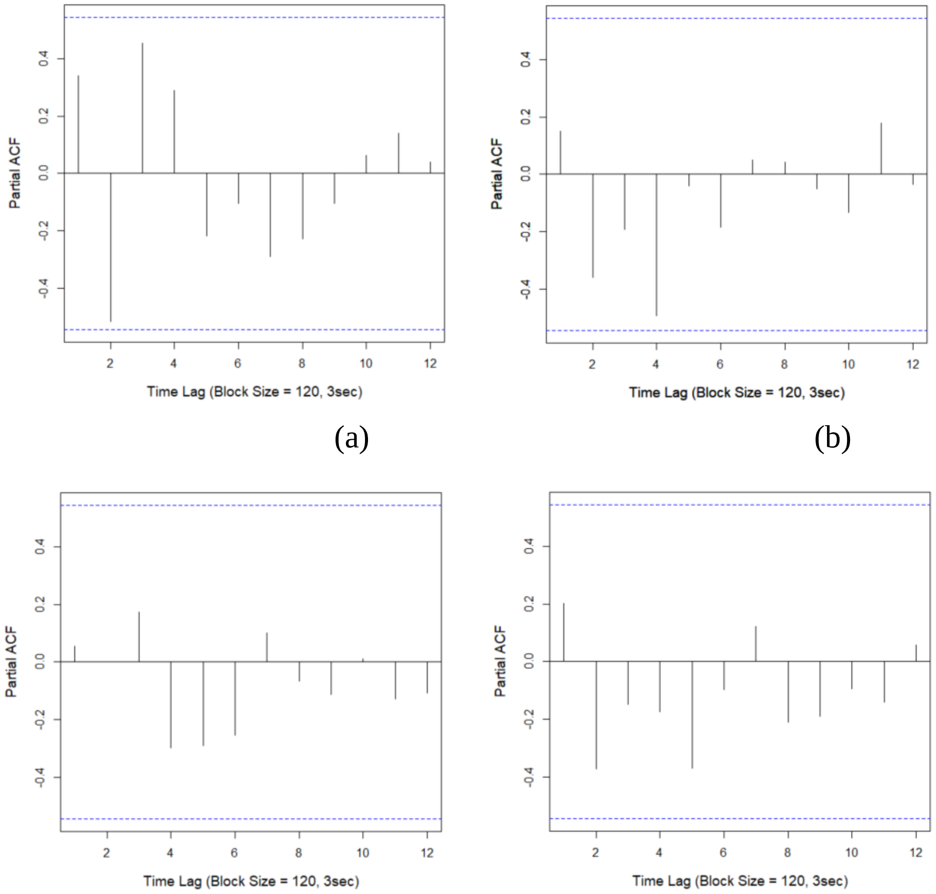

(a) (b)

(c) (d)

Fig. 4.19. PACF of the block maxima $\{\boldsymbol{Z_{n,i}}\}$ for the horizontal cylinder's vibration amplitudes under random waves and a current of 0.366m/s, with a block size of n = 120, for (a) test #1; (b) test #2; (c) test #3; (d) test #4.

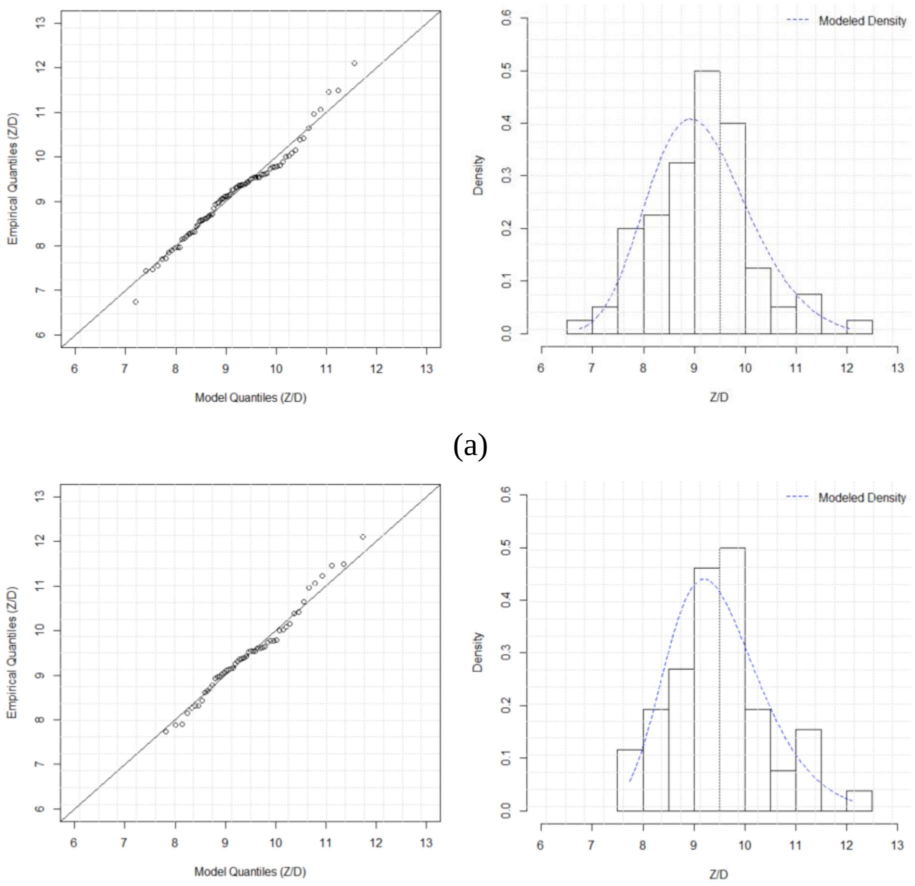

(a)

(b)

Fig. 4.20. Quantile plots of the GEV model fitted to $\{\boldsymbol{Z_{n,i}}\}$ (left), and density plot of the fitted GEV model compared with the histograms of $\{\boldsymbol{Z_{n,i}}\}$ (right) for the horizontal cylinder's VIV amplitudes under random waves and a current of 0.366m/s, with a block size of (a) n = 80; (b) n = 120, for the combined data of test #1-4.

Table 4.5. Comparison of statistical models for the cylinder's vibration amplitudes under random waves and a current at two block sizes

Random waves and 0.244m/s current	Block size **n=80**				Block size **n=120**			
	$\hat{\mu}$	$\hat{\sigma}$	$\hat{\xi}$	AD p-value	$\hat{\mu}$	$\hat{\sigma}$	$\hat{\xi}$	AD p-value
GEV	4.427	1.233	-0.1835	0.088	4.737	1.270	-0.2434	0.314
Random waves and 0.366m/s current	Block size **n=80**				Block size **n=120**			
	$\hat{\mu}$	$\hat{\sigma}$	$\hat{\xi}$	AD p-value	$\hat{\mu}$	$\hat{\sigma}$	$\hat{\xi}$	AD p-value
GEV	8.755	0.9167	-0.1759	0.186	9.087	0.8432	-0.1213	0.502

Table 4.6. Selected statistical models and predicted threshold-crossing probabilities for the cylinder's vibration amplitudes under random waves and a current

Flow conditions	Optimal block size	Duration of block length	Model	AD-test p-value	Goodness of fit	$\hat{\mu}$	$\hat{\sigma}$	$\hat{\xi}$	Threshold-crossing probabilities	
Random waves and 0.244m/s current	80	2 sec	GEV	0.088	Moderately good	4.427	1.233	-0.1835	$P(Z > 7D)$ 0.0695	$P(Z > 9D)$ 1.989×10^{-3}
Random waves and 0.366m/s current	120	3 sec	GEV	0.502	Excellent	9.087	0.8432	-0.1213	$P(Z > 10D)$ 0.269	$P(Z > 12D)$ 1.130×10^{-2}

4.5 Summary

This chapter utilizes the general extremal statistical approach to investigate the statistical characteristics of a flexible horizontal cylinder's flow-induced response amplitude observed in a model basin test program (Chitwood, 1998). The cylinder was tested under a combination of random waves and current loadings. Spectral analysis is first performed to the measured cylinder's mid-span displacement $X(t)$, of which both the spectral and the statistical moments are calculated to interpret the cylinder's response behavior and understand the roles of random waves and current in the energy input. In the next phase of the analysis a statistical approach based on extremal statistics methods is introduced. This approach requires the subdivision of the time series into a sequence of block maxima $\{Z_{n,i}\}$ to extract the extreme values in the measured data $X(t)$. The most appropriate block size is first determined by the iterative process presented in Chapter 3 and the corresponding GEV family of distribution is fitted to the constructed block maxima $\{Z_{n,i}\}$. The model's performance is assessed by both the Anderson-Darling (AD) test criterion and the use of quantile plots and histograms.

For the case when the cylinder was only subject to random waves, the mid-span displacement $X(t)$ is found to be weakly non-Gaussian. When a steady current was superposed on the random wave excitation, the current is found dominant in the energy input, even though the statistical moments illustrate significant variations among different tests even under the same flow condition. This scatter in the values of the parameters suggests that the flow-induced response behavior is too complicated to be adequately characterized by a set of deterministic parameters. These observations are consistent with the earlier research finding of Resvanis and Vandiver (2017), who concluded that the VIV response of flexible cylinders was stochastic in nature even in a steady flow, and they called for further research investigation into the observed response variability. A noteworthy finding is that the GEV distribution provides a good to excellent fit when the cylinder was subject to random waves alone, and it could at least provide a moderately good fit even with a strong current superposed to the random waves. These research findings based on the OTRC model basin data (Chitwood, 1998) indicate that the extremal methodology presented could also be useful to capture the essential characteristics of the stochastic flow-induced response behavior. This methodology enables engineers to utilize the information contained in the whole data set instead of trying to characterize a complex fluid-structure interaction with just a few deterministic parameters. It provides a means to choose the most appropriate block size and the corresponding statistical model for a specific design scenario. Having made the selection of the most appropriate block size and the extremal statistics model engineers would be able to make probabilistic predictions of exceedance over different design conditions for the system. The methodology is promising and merits further investigation of other laboratory and field data.

5 . SUMMARY AND CONCLUSIONS

Applications of flexible cylindrical structures such as closely spaced vertical risers and tendons, and long slender horizontal pipelines can be widely observed in the offshore oil and gas industry. These cylindrical structures are often subjected to random waves and current loadings and it is crucial to accurately model their response behavior in engineering design. This research study is focused on investigating both analytical and statistical methodologies to bound and characterize the complicated wave-cylinder interactive response behavior. Initially, this study examined the Huse-Muren (1987) wake flow model and Huse's modified model (1993) for its assumptions and approximations in the evaluation of the influence of wake effects on fluid drag force coefficients for a slender vertical cylinder. The focus of the analytical investigation is to explore and determine the valid range of applications where these analytical predictive methods could be used as a simple design approach to bound the drag coefficient correction ratio. Later, since it was observed that the analytical models appeared to have limited range of applications, this study investigated a general statistical approach based on generalized extreme value (GEV) distribution as an alternative to characterize and interpret the experimental data obtained in industrial scale model basin test programs. The statistical approach was found capable to provide an excellent fit to the extreme values of the in-line relative displacement between adjacent cylinders in a densely spaced deep-water cylinder array subject to random waves based on the OTRC model basin data. The fitted GEV models based on the selected optimal block sizes could then be used to characterize the impact of cylinder spacings and top tensions on the probability of collision. For a different design scenario of the flow-induced vibrations of a long slender horizontal cylinder subject to random waves and current loadings, this general statistical methodology was also found useful to capture the extremal statistical characteristics of the cylinder's mid-span displacement amplitude in the flow direction. The fitted statistical models were found to produce a good to excellent fit when the cylinder was subject to random waves alone, and an at least moderately good fit even with a strong current superposed to the random waves.

Huse and Muren (1987) developed their analytical models based on the earlier seminal research studies of Prandtl (1935) and Schlichting (1979) to address the amplification of the stationary flow drag coefficient for a slender cylinder to account for oscillatory flows and oscillatory flows with a cross current. Investigation of their wake flow models could potentially provide insight to the more complicated cylinder clashing phenomenon. It was shown in this study that the wake velocity profile in Huse and Muren's approximations only has slight deviations from Schlichting's classical models. However, a quite larger deviance could be observed in Huse's modified model (1993), especially when the wake profile was located less than two diameters downstream of the cylinder. This study then proceeded to identify and quantify the potential sources of errors in their analytical formulations. It was observed that their estimated wake velocity correction for in-line oscillatory flow was only valid for fully developed wake flows. In the crossflow formulation where a steady current coming from the transverse direction was superposed to the in-line oscillatory flow, Huse and Muren were found to utilize the concept of a "true" relative velocity to estimate the drag coefficient in the in-line direction even though it does not necessarily lie in this direction and consequently could be a source of error.

Based on Huse and Muren's models, new dimensionless expressions were developed for the drag coefficient correction ratio and the Keulegan-Carpenter parameter ratio for the cross-flow cases. To investigate whether these analytical formulations could be used to provide a bound on the experimental data, both DNV-RP recommended drag coefficients and Sarpkaya's U-tube measurements were utilized in the analysis. It was found that the bounding of the experimental data predicted by Huse and Muren's original model only agreed with Sarpkaya's measurements for a limited range of the dimensionless parameters. Unfortunately, no improvement was observed using Huse's modified model for the range of data considered. Later in the investigation of the crossflow formulation, a new dimensionless ratio N_{CF}/N_{KC} was identified from the variables in their original formulations, which was found helpful to better understand the impact of the steady cross current with respect to the inline oscillatory flow. The drag coefficient correction ratios C_{dc}/C_{ds} were predicted as a function of the cross-flow parameter N_{CF} and the standard Keulegan-Carpenter number N_{KC}. Interestingly, the values of the ratio C_{dc}/C_{ds} were found to converge as the ratio of N_{CF}/N_{KC} became large. This convergence was also noted in the numerical simulations. The simulated curves of the drag coefficient correction ratios for the pinned-end cylinders were found to have a similar shape and could be potentially developed to a family of design curves for offshore applications. However, future experimental data will be required for verification.

Having noted that the analytical wake flow models appeared to have a limited range of applications, an alternative approach was taken to investigate a general statistical methodology to capture the extreme interactive response behavior observed in the model basin data of cylindrical structures subject to random seaways. The methodology is based on the extremal types theorem, which leads to the development of the generalized extreme value (GEV) family of distributions. Initially, a sequence of block maxima $\{Z_{n,i}\}$ was generated from the time series $X(t)$ of the relative displacement between adjacent cylinders measured at an interval of δt. An iterative process based on Anderson-Darling (AD) goodness-of-fit test criterion together with quantile plots and histograms was introduced to identify the most appropriate block size n and the corresponding extremal statistical model for each data set, where special attention was paid to the quality of fit in the upper tail of the distribution. The selected models were then used to predict the threshold-crossing probabilities of $\{Z_{n,i}\}$, where each element $Z_{n,i}$ represents the maximum observed value in $X(t)$ in a duration of $n\delta t$.

Excellent agreement was observed between the selected models based on GEV family of distributions and the industrial scale model basin data of the densely spaced deep-water cylinder arrays subject to random waves. The predicted threshold-crossing probabilities for the paired cylinder data confirmed the experience that closely spaced cylinder arrays were more likely to collide while increasing the top tension could effectively reduce the risk of collision. For the test of triple cylinder arrays, the statistical models also successfully captured the unexpected phenomenon in the observed data that the second and the third cylinder were possible to experience to a higher risk of collision than the first and the second cylinder. These research findings indicated that the general extremal statistical methodology could be useful to capture the essential characteristics of the stochastic random wave-cylinder interactive response behavior.

The general statistical methodology was also found capable to characterize the model basin data of flow-induced vibration of a flexible horizontal cylinder subject to both random waves and constant current loadings. Initially, spectral analysis was performed to the measured cylinder's mid-span displacement to interpret the response behavior in terms of traditional deterministic parameters. For the case when the cylinder was only subject to random waves, the mid-span displacement $X(t)$ was found to be weakly non-Gaussian. However, when a strong constant current was superposed on the random wave excitation, significant variations were observed in the values of the statistical moments among different tests even under the same flow condition. These scatters in the values of parameters suggested that the flow-induced cylinder vibration response behavior might be too complicated to be adequately addressed by a set of traditional deterministic parameters. These observations of the scatter in parameters could also be found in a recent research study reported by Resvanis and Vandiver (2017), who underscored the stochastic nature of flexible cylinder's VIV response and addressed that further research effort was required to investigate the observed response variability. A noteworthy finding of the methodology was that the selected GEV models provided a good to excellent fit when the cylinder was subject to random waves alone, and it could at least provide a moderately good fit to the data even with a strong current superposed to the random waves. These observations further illustrated the promising applicability of the general extremal statistical methodology for the study of the stochastic flow-induced response behavior.

In sum, the main objective of this research study is to investigate analytical and statistical approaches to bound and characterize the interactive wave-cylinder response behavior using published DNV guidelines, U-tube data and industrial scale model basin data. It was found in this research that the traditional analytical wake flow models developed by Huse and Muren (1987) could be used to formulate a bounding on the data as a simple design approach when the cylinder is only subjected to in-line oscillatory flow. However, one should also note the limited range of parameters within which this estimated bounding is valid for application. When the cylinder is also subject to a steady current coming from the transverse direction, future experimental data is required to investigate the applicability of the Huse-Muren wake flow model in this crossflow formulation. Later, the general extremal statistical methodology was found to give promising results to capture the extreme interactive response behavior of two entirely different fluid-cylinder interactions in random seaways based on the measured data of OTRC model basin test programs (Rijken and Niedzwecki, 1998; Chitwood, 1998). This methodology could be used to investigate and interpret the information contained in the measured data directly instead of trying to describe a complex fluid-structure interaction with just a few deterministic parameters. It could potentially enable engineers to select the most appropriate statistical model for a specific design scenario and make probabilistic predictions of different extremal statistical events for the system. This statistical methodology is promising for offshore applications and future research investigation is highly recommended with other laboratory and field data.

REFERENCES

American Bureau of Shipping. (2017). Drilling Riser Analysis, p. 15-17.

American Petroleum Institute. (1993). API Recommended Practice for Design, Selection, Operation, and Maintenance of Marine Drilling Riser Systems, No. API-RP-16Q, p. 10.

American Petroleum Institute. (1998). API Recommended Practice for Design of Risers for Floating Production Systems (FPSs) and Tension-Leg Platforms (TLPs), p. 71-72.

Anderson, T. W. (1962). On the distribution of the two-sample Cramér-von Mises criterion. *Ann. Math. Statist*. 33, 1153.

Anderson, T. W. and Darling, D. A. (1954). A test for goodness of fit, *Journal of the American Statistical Association*, Vol 49, No. 268, 765-9

Blevins, R. D. (1977). Flow-Induced Vibration, Van Nostrand Reinhold Company New York.

Blevins, R. D. (2005). Forces on and stability of a cylinder in a wake, *Journal of Offshore Mechanics and Arctic Engineering*, Vol. 127.

Blevins, R., D., Saint-Marcoux, J-F., Wu, M. (2008). Experimental investigation of two dimensional motion of an elastically supported cylinder in a wake, *Journal of Offshore Mechanics and Arctic Engineering*, Vol. 130/044502-1

Bushnell, M.J. (1977). Forces on cylinder arrays in oscillating flow, *Offshore Technology Conference*, Houston

Cartwright, D.E., Longuet-Higgins M.S. (1956). The statistical distribution of the maxima of a random function. *Proc Royal Soc Lond A*, 237:212–232

Chitwood, J.S., Vortex-induced vibration of a slender horizontal cylinder in currents and waves, OTRC report No. 2/98-A9575, 1998

Coles S. (2001). An introduction to statistical modeling of extreme values, Spinger, Verlag London.

Cramér H. (1928). On the composition of elementary errors, *Skand. Aktuarietids*, Vol. 11, pp. 13-74, 141-180.

Det Norske Veritas. (2014). Environmental Conditions and Environmental Loads, p. 85, No. DNV-RP-C205.

Duggal, A.S. and Niedzwecki, J.M. (1994). Probabilistic collision model for a pair of flexible cylinders, *Applied Ocean Research*, 16, 165-175

Fu, P., Leira, B.J., and Myrhaug, D. (2017). Reliability analysis of wake-induced collision of flexible risers, *Applied Ocean Research*, 62, 49-56.

Govardhan, R.N., Williamson, C.H.K., (2006). Defining the Modified Griffin Plot in Vortex-Induced Vibration: Revealing the Effect of Reynolds Number Using Controlled Damping, *Journal of Fluid Mechanics* 561, 147-180

Griffin, O.M., Skop, R.A., Ramberg, S.E. (1975). Resonant, Vortex-Excited Vibrations of Structures and Cable Systems, *Offshore Technology Conference*, Houston.

Herfjord, K. and Bryndum, M. (2001). Hydrodynamic interaction between two cylinders in steady flow, *Proceedings of the 11th International Offshore and Polar Engineering Conference*, Stavanger, Norway, June 17-22.

Herfjord,K., Holmås,T., Leira, B.J., Bryndum, M, and Hanson, T. (2002). Computation of interaction between deepwater risers, Collision statistics and stress analysis, *Proceedings of the International Conference on Offshore Mechanics and Arctic Engineering*, OMAE2002-28152 Oslo.

Huse, E. and Muren, P. (1987). Drag in oscillatory flow interpreted from wake considerations, *Offshore Technology Conference*, Houston.

Hues, E. (1993). Interaction in deep-sea riser arrays, *Offshore Technology Conference*, Houston.

I.J. Fylling, C.M. Larsen, N. Sødahl, H. Ormberg, A. Engseth, E. Passano, K. Holthe, Riflex Theory Manual, SINTEF Report No. STF70 F 95219, 53, 1995.

Klamo, J.T, Leonard, A., Roshko, A. (2005). On the Maximum Amplitude of a Freely Vibrating Cylinder in Cross-Flow, *Journal of Fluids and Structures* 21, pp. 429-434.

Lambrakos, K.F., Chao, J.C., Beckmann, H. and Branon, H.R. (1987). Wake model of hydrodynamic forces on pipelines, *J. Ocean Engineering* 14(2), 117-136.

Leira, B.J, Holmås, T., Herfjord, K. (2001). A probabilistic design approach for riser collision based on time-domain response analysis, *Proc. ICOSSAR*, Newport Beach

Lu, J. and Niedzwecki, J.M. (2020). Statistical analysis of in-line interaction of closely spaced cylinder arrays in random waves, *Proceedings of the International Conference on Offshore Mechanics and Arctic Engineering*, OMAE 2020-18179.

Lu, J. and Niedzwecki, J.M. (in-press), Analysis of random wave interaction with cylinders using extremal statistical methods, *Applied Ocean Research*, APOR_2020_420R1.

MARINTEK, (2011). Shell Riser VIV Tests Main Report, No. 580233.00.0

Nigam, (1983). Introduction to Random Vibrations, The MIT Press, Cambridge, MA.

Prandtl, L. (1935). The mechanics of viscous fluids. In W.F.Durand, Aerodynamic Theory, III, 166.

R Core Team (2019). R: A language and environment for statistical computing. R Foundation for Statistical Computing, Vienna, Austria. URL https://www.R-project.org/.

R. B. D'Agostino and M. A. Stephens, eds. (1986), Goodness-of-fit techniques, Marcel Dekker, New York

Reichardt, H. (1942). "Gesetzmäßigkeiten der freien Turbulenz. VID-Forschungsheft", 414, Berlin.

Resvanis, T.L., Jhingran, V., Vandiver, J.K., Liapis, S. (2012). Reynolds number effects on the vortex-induced vibration of flexible marine risers, *Proceedings of the ASME 2012 31st International Conference on Ocean, Offshore and Arctic Engineering*, OMAE 2012-83565.

Resvanis, T.L., Vandiver, J.K. (2017). Response variability in flexible cylinder VIV model test data, *Proceedings of the ASME 2017 36th International Conference on Ocean, Offshore and Arctic Engineering*, OMAE 2017-61516

Rijken, O.R. (1997). Dynamic response of marine risers and tendons. Ph.D. Dissertation, Department of Civil Engineering, Texas A&M University.

Rijken, OR, and Niedzwecki, JM. (1998). Direct displacement measurements of submerged objects, *J. Ocean Engineering*, April/May, Vol.25, No.4-5, 309-321.

Sagatun, S.I, Herfjord, K., Nielsen, F.G., Huse, E. (1999). Participating mass in colliding risers, *Journal of Marine Science and Technology*, 4, 58-67.

Sarpkaya, T. *Vortex Shedding and Resistance in Harmonic Flow About Smooth and Rough Circular Cylinders at High Reynolds Numbers*, Naval Postgraduate School Technical Report, No. NPS-59SL76021, February 1976, Monterey, California.

Sarpkaya, T. (1979). Vortex induced oscillations, *Journal of Applied Mechanics*, 46, pp. 241-258.

Sarpkaya, T. (2004). A critical review of the intrinsic nature of VIV, *Journal of Fluids and Structures* 19 (4) pp. 389-447.

Schlichting, H. (1979). Boundary Layer Theory, Chapter XIX, McGraw Hill Book Company Inc., New York.

Soedigdo, I. R. Lambrakos, K.F., Billy L. E. (1997). Wake II Model for hydrodynamic forces on marine pipelines, Ph.D. dissertation, Texas A&M University, College Station, Texas.

Sumer, B.M. and Fredsøe, J. (1997). Hydrodynamics Around Cylindrical Structures, *Advanced Series on Ocean Engineering*, Volume 12. World Scientific Publishing Co. Pte. Ltd.

Swithenbank, S.B., Vandiver, J.K., Larsen, C.M., Lie, H. (2008). Reynolds Number Dependence of Flexible Cylinder VIV Response Data, *Proceedings of the International Conference on Offshore Mechanics and Arctic Engineering*, OMAE2008-57045.

Vandiver, J.K. (1993). Dimensionless parameters important to the prediction of vortex-induced vibration of long, flexible cylinders in ocean currents, *Journal of Fluids and Structures* 7, pp. 423-455.

Vandiver, J.K. (2012). Damping parameters for flow-induced vibration, *Journal of Fluids and Structures*, 35, pp. 105-119.

Vanem, E. (2015). Uncertainties in extreme value modelling of wave data in a climate change perspective. J. Ocean Eng. Mar. Energy 1, 339–359.

Welch, P. D. (1967). The use of Fast Fourier Transform for the estimation of power spectra: A method based on time averaging over short, modified periodograms, *IEEE Transactions on Audio and Electroacoustics*, AU-15 (2): 70–73.

Winterstein, S. R. (1988). Nonlinear vibration models for extremes and fatigue, *J. Engng. Mech*. 114, 1772-90

Zdravkovich, M.M. (1990). On origins of hysteretic responses of a circular cylinder induced by vortex shedding, *Zeitschrift fur Flugwissenschaften und Weltraumforschung* (*Journal of Flight Sciences and Space Research*) 14, pp. 47–58. Springer-Verlag.

APPENDIX A

WAKE VELOCITIES IN VARIOUS WAKE FLOW MODELS

A.1. *Reichardt and Goertler's (1942) solution of the wake velocity based on Schlichting's model and Prandtl's turbulent shearing stress hypothesis*

From the turbulent shearing stress hypothesis as shown in Eq. (2.7) and the governing equation as shown in Eq. (2.3), one obtains (Schlichting, 1979)

$$V\frac{\partial u_1}{\partial x} = \varepsilon_\tau \frac{\partial^2 u_1}{\partial y^2} \tag{A.1}$$

where, the virtual kinematic viscosity $\varepsilon_\tau = \kappa_1\, u_m\, b = \varepsilon_0$

Let $\eta = y\,\sqrt{V/\varepsilon_0 x}$, one obtains from Schlichting's solution to the steady-state boundary layer equations in the wake of a flat plate at zero incidence (Schlichting, 1979)

$$u_1 = V\,C'\,\left(\frac{x}{D}\right)^{-\frac{1}{2}} \exp\left(-\frac{1}{4}\,\eta^2\right) \tag{A.2}$$

where, the constant C' can be determined from the momentum integral

$$C' = \frac{C_{ds}}{4\sqrt{\pi}}\sqrt{\frac{V\,D}{\varepsilon_0}} \tag{A.3}$$

Finally, one obtains

$$\frac{u_1}{V} = \frac{1}{4\sqrt{\pi}}\sqrt{\frac{V\,C_{ds}\,D}{\varepsilon_0}}\;\sqrt{\frac{C_{ds}\,D}{x}}\;\exp\left(-\frac{1}{4}\eta^2\right) \tag{A.4}$$

where, Schilichting (1979) indicated that

$$b_{1/2} = 1.675 \cdot \sqrt{\frac{\varepsilon_0}{V \cdot C_{ds} \cdot d}} \cdot \sqrt{x \cdot C_{ds} \cdot D} \qquad \text{(A.5)}$$

Comparing the above formula with Schlichting and Reichardt's measurements one obtains

$$\frac{\varepsilon_0}{V\ C_{ds}\ D} = 0.0222 \qquad \text{(A.6)}$$

Schlichting did not give further derivations beyond this point. However, introducing his experimentally determined values as shown in Eq. (A.5) and Eq. (A.6) into the wake velocity expression shown in Eq. (A.4), one obtains

$$u_m = 0.947\, V \sqrt{\frac{C_{ds}\ D}{x}} \qquad \text{(A.7)}$$

And the following expression for η^2

$$\eta^2 = y^2 \frac{V}{\varepsilon_0 x} = y^2 \left(\frac{V\ C_{ds}\ D}{\varepsilon_0}\right) \frac{1}{x\ C_{ds}\ D} = y^2 \left(\frac{V\ C_{ds}\ D}{\varepsilon_0}\right) \frac{1.675^2\ \frac{\varepsilon_0}{V\ C_{ds}\ D}}{b_{1/2}^2}$$

$$= 2.8056 \left(\frac{y}{b_{1/2}}\right)^2$$

Finally, we have:

$$u_1 = u_m \exp\left(-\frac{1}{4}\eta^2\right) = u_m\ e^{-0.7014\left(\frac{y}{b_{1/2}}\right)^2} \qquad \text{(A.8)}$$

A.2. *Derivation of the exact wake velocity sum U_W in Huse-Muren wake flow model for a vertical cylinder subject to both an in-line harmonically oscillatory flow and a steady cross current coming from the transverse direction.*

After time $\Delta t = \frac{1}{2}\ i\ T$, the maximum velocity of the ith wake at the x axis behind the cylinder is:

$$u_{mi}(\Delta t) = u_{mi}\ e^{-0.693\left(\frac{y}{b_{1/2}}\right)^2} = V\sqrt{\frac{C_{ds}\ D}{x}}\ \frac{1}{\sqrt{i}}\ e^{-0.693\left(\frac{V_C\ T\ i}{2b_{1/2}}\right)^2} \tag{A.9}$$

where, the value of y is obtained as $y = V_C\ \Delta t = \frac{1}{2}\ V_C\ i\ T$.

Substituting the above expression into Eq. (2.14), also noting $x = 2A_0$we have

$$U_W = -\sum_{i=1}^{\infty}(-1)^i \cdot u_{mi}\ (\Delta t)$$

$$= V\sqrt{\frac{C_{ds}\ \ D}{2A_0}}\sum_{i=1}^{\infty} -(-1)^i\ \ \frac{1}{\sqrt{i}}\ \ e^{-0.693\left(\frac{V_C\ T\ i}{2b_{1/2}}\right)^2} \tag{A.10}$$

Introducing $N_{KC} = \frac{2\pi\ A_0}{D}$, $b_{1/2} = \frac{1}{4}\sqrt{C_{ds}\ \ D\ \ x}$, and $N_{CF} = \frac{V_C\,T}{D}$ into the above equation, we could derive the expression of U_W in Eq. (2.24) as follows

$$
\begin{aligned}
U_W &= V \sqrt{\frac{C_{ds}\ \ D}{2A_0}\ \frac{\pi}{\pi}} \sum_{i=1}^{\infty} -(-1)^i\ \ \frac{1}{\sqrt{i}}\ \ e^{-0.693\ \frac{V_C^2\ \ T^2\ \ i^2}{4\,\frac{1}{16}\ C_{ds}\ \ D\ \ 2A_0\ \frac{D}{D}} \cdot \frac{\pi}{\pi}} \\
&= V \sqrt{\frac{C_{ds}\ \ \pi}{N_{KC}}}\ \sum_{i=1}^{\infty} -(-1)^i\ \frac{1}{\sqrt{i}}\ e^{-2.772\frac{V_C^2\ \ T^2\ \ i^2\ \pi}{C_{ds}\ \ D^2\ \ 2A_0\,\frac{\pi}{D}}} \\
&= \ V \sqrt{\frac{C_{ds}\ \ \pi}{N_{KC}}} \sum_{i=1}^{\infty} -(-1)^i\ \ \frac{1}{\sqrt{i}}\ \ e^{-\frac{8.7085}{C_{ds}\ \ N_{KC}}\ \left(\frac{V_C\ \ T}{D}\right)^2\ i^2} \\
&= \ V \sqrt{\frac{\pi\ \ C_{ds}}{N_{\mathrm{KC}}}} \sum_{i=1}^{\infty} -(-1)^i\ \ \frac{1}{\sqrt{i}}\ \ e^{-\ \frac{8.7085\ N_{KC}}{C_{ds}}\ \ \left(\frac{N_{CF}}{N_{KC}}\right)^2\ i^2}
\end{aligned}
\tag{A.11}
$$

APPENDIX B

THREE FAMILIES OF EXTREME VALUE DISTRIBUTIONS

In applications, there are three families of extreme value distributions that are commonly used. They are the Gumbel, Fréchet, and Weibull distributions. To completement the discussion in the theoretical background of the statistical methodology, the Appendix presents the form for each of the three distribution functions in common variables for comparison. The Gumbel distribution is expressed as

$$G(z) = \exp\left\{-\exp\left[-\left(\frac{z-b}{a}\right)\right]\right\}, \quad -\infty < z < \infty \tag{B.12}$$

the Fréchet distribution is of the form

$$G(z) = \begin{cases} 0, & z \leq b \\ \exp\left\{-\left(\frac{z-b}{a}\right)^{-\alpha}\right\}, & z > b \end{cases} \tag{13}$$

and the Weibull distribution is of the form,

$$G(z) = \begin{cases} \exp\left\{-\left[-\left(\frac{(z-b)}{a}\right)^{\alpha}\right]\right\}, & z < b \\ 1, & z \geq b\,, \end{cases} \quad -\infty < z < \infty \tag{14}$$

where, a is the scale parameter, b is the location parameter, and α is the shape parameter. Note $a > 0$ and $\alpha > 0$. The above three distributions can be combined as the generalized extreme value (GEV) distribution as shown in Eq. (3.5).